

The potential of silica nanoparticles as oral drug carriers

Dissertation
zur Erlangung des Grades
des Doktors der Naturwissenschaften
der Naturwissenschaftlich-Technischen Fakultät III
Chemie, Pharmazie, Bio- und Werkstoffwissenschaften
der Universität des Saarlandes

von
Diplom-Biologin
Andrea Neumeyer
Saarbrücken
2010

Tag des Kolloquiums:	27. September 2010
Dekan:	Prof. Dr. Stefan Diebels
Berichterstatter:	Prof. Dr. Claus-Michael Lehr
	Prof. Dr. Ingolf Bernhardt
Vorsitz:	Prof. Dr. Rolf Hartmann
Akad. Mitarbeiter	Dr. Ulrich Schäfer

Table of contents

1	General introduction	1
1.1	Silica nanoparticles as novel drug carriers	1
1.2	Overcoming the intestinal barrier	5
1.3	Cytotoxicity and oxidative stress caused by nanoparticles	8
1.4	Aim of the thesis	10
2	Characterization of fluorescently-labelled silica nanoparticles in physiological buffers and cell culture media	12
2.1	Introduction	12
2.2	Aim of the study	13
2.3	Materials and methods	
2.3.1	Silica nanoparticles	14
2.3.2	Materials and buffers	15
2.3.3	Measuring principle of the Zetasizer Nano ZS	17
2.3.4	Size, ζ potential and stability of nanoparticles in different buffers and media	19
2.4	Results and Discussion	
2.4.1	Alteration in the sizes of silica nanoparticles in different buffers and media	20
2.4.2	Stability of nanoparticles in different buffers and media	22
2.5	Collection of used silica nanoparticles	25
3	Oxidative and cytotoxic potential of fluorescently-labelled silica nanoparticles	27
3.1	Introduction	28
3.2	Aim of the study	31
3.3	Materials and methods	
3.3.1	Materials	31

3.3.2	Caco-2 cell culture	32
3.3.3	SensorDish [®] Reader (SDR)	32
3.3.4	DCF-DA assay	34
3.3.5	LDH assay	35
3.3.5	MTT assay	35
3.4	Results	
3.4.1	Establishment of a method for the combined determination of oxidative stress and cytotoxicity via SDR measurements	36
3.4.1.1	Determination of oxidative stress via SDR	36
3.4.1.2	Determination of cytotoxicity via SDR	43
3.4.2	Oxidative and cytotoxic potential of silica nanoparticles	46
3.4.2.1	Determination of the oxidative potential of silica nanoparticles via SDR in comparison to DCF-DA measurements	46
3.4.2.2	Size-, time-, surface modification- and concentration-dependent nanoparticulate cytotoxicity	48
3.4.2.3	PI-labelled nanoparticles caused a size-, time-, concentration-dependent and non-reversible cytotoxic effect in Caco-2 cells	52
3.4.2.4	Nanoparticle-damaged Caco-2 cells do not regenerate	54
3.5	Discussion	56
3.6	Conclusion	63
4	Cellular binding, association and transport of rhodamine B-isothiocyanate-labelled silica nanoparticles	64
4.1	Introduction	65
4.2	Aim of the study	66
4.3	Materials and methods	
4.3.1	Materials	66
4.3.2	Caco-2 cell culture	67
4.3.3	Visualization of cellular association by confocal laser scanning microscopy (CLSM)	67
4.3.4	Quantification of cellular or nuclear association by flow cytometry (FACS)	68
4.3.5	Cell preparation protocols	69
4.3.6	Cell washing procedures	70

4.3.7	Transport studies	71
4.4	Results	
4.4.1	Size-, time- and surface modification-dependent association of RITC-labelled silica nanoparticles	73
4.4.2	Removal of nanoparticles adsorbed to the outer cell membrane	77
4.4.3	Transport properties of RITC-labelled silica nanoparticles	79
4.5	Discussion	82
4.6	Conclusion	86
5	Cellular uptake and localization of propidium iodide-labelled silica nanoparticles	87
5.1	Introduction	88
5.2	Aim of the study	90
5.3	Materials and methods	
5.3.1	Materials	91
5.3.2	Caco-2 cell culture	91
5.3.3	Stability of the binding between PI and silica nanoparticles.....	91
5.3.4	Determination of the cellular uptake of PI-labelled nanoparticles via flow cytometry	92
5.3.5	PI-labelled nanoparticles as carriers for PI	92
5.3.6	Determination of the cellular localization of PI-labelled silica nanoparticles via RNase	93
5.3.7	Determination of the cellular uptake mechanisms of silica nanoparticles	93
5.4	Results	
5.4.1	PI-labelling allows a clear distinction between adsorbed and internalized silica nanoparticles	94
5.4.2	Silica nanoparticles serve as drug carriers for free PI	96
5.4.3	Cellular uptake and localization of PI-labelled silica nanoparticles ...	98
5.4.4	Identification of the internalization mechanisms involved in the uptake of silica nanoparticles	100
5.5	Discussion	103
5.6	Conclusion	108

6	Summary	109
7	Outlook	112
8	References	115
9	Publications	130
10	Abbreviations	132
11	Acknowledgements	134
12	Curriculum vitae	135

Short summary

Silica nanoparticles show promising characteristics as oral drug delivery carriers. This application implies a close contact with biological systems, therefore it is essential to investigate the cellular binding, uptake and transport properties of nanoparticles. Furthermore, their oxidative and cytotoxic potential has to be evaluated. A novel non-invasive assay for the combined determination of cytotoxicity and oxidative stress exhibited that unmodified nanoparticles with a size up to 84 nm caused a size-, time- and concentration-dependent cytotoxic effect in Caco-2 cells. In contrast, larger and poly ethylene glycol-modified nanoparticles provoked no deleterious effects. However, none of these particles showed an oxidative potential. Cytotoxicity studies correlated with cell association, uptake and transport experiments: Nanoparticles, which demonstrated a cytotoxic effect, were also in a strong association with Caco-2 cells or were even internalized. Thereby, the novel labelling of nanoparticles with propidium iodide (PI) allowed a clear distinction between adsorbed and internalized nanoparticles in a quantitative way which facilitated the identification of cellular mechanisms involved in the uptake of nanoparticles. Furthermore, silica nanoparticles could function as drug carriers for the membrane-impermeable compound PI. Free PI molecules were not able to enter Caco-2 cells, whereas nanoparticle bound PI was internalized time-dependently.

Kurzzusammenfassung

Silika-Nanopartikel zeigen vielversprechende Eigenschaften als orale Arzneistoffcarrier. Diese Anwendung impliziert einen engen Kontakt zwischen Partikeln und biologischen Systemen. Daher ist es unerlässlich die Assoziierung und Aufnahme von Partikeln zu untersuchen sowie ihr zytotoxisches und oxidatives Potential zu bewerten. Eine innovative Methode zur kombinierten Detektion von Zytotoxizität und oxidativem Stress zeigte, dass unmodifizierte Nanopartikel bis zu einer Größe von 84 nm einen größen-, zeit- und konzentrationsabhängigen zytotoxischen Effekt auf Caco-2 Zellen aufwiesen. Größere sowie Polyethylenglykol-modifizierte Partikel hatten dagegen keine zellschädigende Wirkung. Ein oxidatives Potential konnte von keinem der Partikel verzeichnet werden. Diese Toxizitätsstudien korrelierten mit zellulären Assoziierungs- und Aufnahmeexperimenten. Nanopartikel, die einen zytotoxischen Effekt zeigten, demonstrierten auch eine starke Assoziierung mit Caco-2-Zellen oder wurden sogar in diese aufgenommen. Die Markierung der Partikel mit Propidiumiodid (PI) ermöglichte dabei eine deutliche Unterscheidung zwischen adsorbierten und aufgenommenen Nanopartikeln. Die Identifizierung der zellulären Mechanismen, die in der partikulären Aufnahme involviert sind, wurde dadurch erleichtert. Silika-Nanopartikel fungierten zudem als Carrier für das membran-impermeable PI. Freies PI wurde nicht in Caco-2-Zellen aufgenommen, wohingegen partikelgebundenes PI zeitabhängig internalisiert wurde.

1

General introduction

1.1 SILICA NANOPARTICLES AS NOVEL DRUG CARRIERS

The intensive research and discovery of novel drugs such as peptides, proteins, plasmids, antibodies and nucleic acids require new drug delivery technologies. Thereby, the usage of nanomaterials allows various creative applications. They can improve the bioavailability of poorly water-soluble drugs, prolong the half-life of drug systemic circulation, release drugs at a sustained rate, deliver drugs in a targeted manner and therefore, minimize side effects. Furthermore, this new technology allows the administration of two or more drugs with e.g. different water solubilities simultaneously in combinatory therapy and thus suppresses drug resistance. In addition, nanoparticles as drug carrier offer the usage of more effective and convenient routes of administration (e.g. the oral route), minimize therapeutic toxicity, extend the product life cycle and reduce health-care costs (Zhang et al., 2008). Numerous nanoparticle-based drug formulations and diagnostic agents had been already developed, e.g. for the treatment of cancer, diabetes, pain, asthma, allergy and infections (Brannon-Peppas & Blanchette, 2004; Kawasaki & Player, 2005). Besides therapy, nanomaterials can be also used as diagnostic tools. They allow the detection of disease markers in the molecular scale and identify abnormalities such as virus fragments or cancerous cells (Zhang et al., 2008). All these applications can be summarized in the term nanomedicine (Figure 1.1). Thereby, nanoparticles show various therapeutic potentials in different medical fields such as oncology or immunology (Farokhzad & Langer, 2006). Hitherto, about 20 nanoparticle-based formulations are in clinical use referring to the promising properties of these novel materials (Danson et al., 2004; Gabizon et al., 2006; Gradishar, 2006; Valle et al., 2010). Therefore, nanomedicine is expected to become a well-established term in modern medicine.

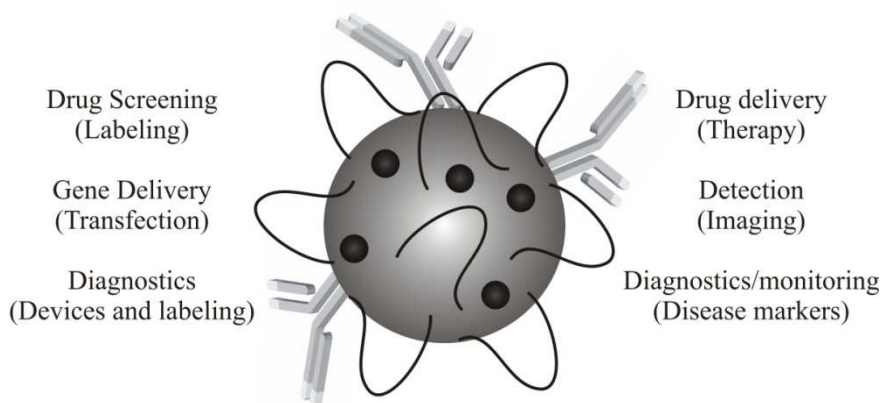


Figure 1.1: Applications and research aims in nanomedicine (modified from Liu et al., 2007).

In this regard, silica nanoparticles exhibit various advantages and show a great promise in many medical and pharmaceutical applications. Silica is a non-toxic compound which is already used as food additive or as carrier material in tablets (Barbé et al., 2004). Silica nanoparticles can be easily surface modified with several molecules to improve and target the cellular uptake over surface chemistry (Chung et al., 2007; Kneuer et al., 2000; Kneuer et al., 2000). A surface modification of nanoparticles, e.g. with poly ethylene glycol (PEG) extends the residence time of these carriers in the blood. Thereby, the effect of PEG is based on the defilade of nanoparticles over surface chemistry, hence avoiding a clearance by the phagocytic system (Owens & Peppas, 2006; Roberts et al., 2002). Furthermore, PEG shows stabilizing properties on the nanoparticle surface due to a steric barrier formed by PEG chains (Behrens et al., 2002; Tobio et al., 2000). Further advantages of silica nanoparticles are their high hydrophilicity and insensitivity to microbial attack. In addition, they do not show any swelling or porosity changes within alteration in pH which becomes very important with regard to an oral application (Jain et al., 1998). Silica nanoparticles can be easily labelled with fluorescence dyes, which is essential for the investigation of their behaviour in cell culture systems. Dye-doped silica nanoparticles can be prepared by two general synthetic routes: the Stöber and microemulsion process. The Stöber synthesis was introduced in 1968 by Stöber and Fink. It is a one-pot synthesis that is performed under alkaline conditions in an ethanol/water mixture. Therefore, potentially toxic organic solvents or surfactants can be avoided (Rossi et al., 2005; Stöber & Fink, 1968). The method allows a controlled generation of spherical silica particles with uniform sizes ranging from 50 to 2000 nm in diameter. During microemulsion preparation, silica nanoparticles were prepared using a water in oil emulsion system that employs a water-soluble amine as catalyst and tetraethylorthosilicate (TEOS) as a silica source.

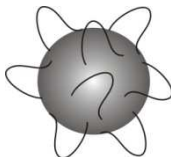

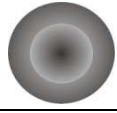


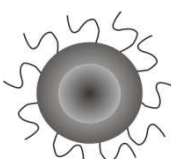
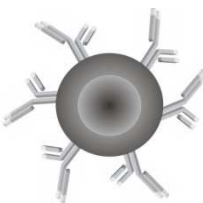
In recent years various studies proved the properties of silica nanoparticles as oral drug or gene carrier (Bharali et al., 2005; Fuller et al., 2008; Gemeinhart et al., 2005; Manzano et al., 2009; Moulari et al., 2008; Simovic et al., 2010; Slowing et al., 2008; Tan et al., 2010). Hollow mesoporous silica nanoparticles had been used as drug carriers for fluorescein isothiocyanate (FITC), which served as a model substance. FITC encapsulated in silica nanocapsules was released more slowly than free FITC indicative for a controlled release of the dye (Liu et al., 2007). Further studies showed that silica nanoparticles are also useful as gene carriers. Plasmids bound to amino-functionalized silica nanoparticles were completely protected from enzymatic digestion in human epithelial cancer cells (Kneuer et al., 2000; Roy et al., 2005). Furthermore, it was shown that organically modified silica nanoparticles can be effectively used to introduce genes into neuronal cells *in vivo* (Bharali et al., 2005). Silica nanoparticles could also serve as carriers for anticancer drugs such as doxorubicin. It was reported, that mesoporous silica nanoparticles (MSN) release the drug over a period of 20 days in a constant rate (Barbé et al., 2004). Furthermore, MSN were able to enhance the delivery of the hydrophobic anticancer drug paclitaxel to pancreatic cancer cells (Xia et al., 2009) and allowed a target delivery of the chemotherapeutic agent methotrexate (MTX). Free MTX caused apoptosis in cancer cells as well as in healthy cells. In contrast, MTX bound to nanoparticles induces cell death only in cancer cells but not in normal tissue (Rosenholm et al., 2010).

To evaluate silica nanoparticles as oral drug delivery system, it is important to determine their cellular uptake and localization. Especially, their distribution within the cell is an essential indication for the future application spectrum. Unmodified silica nanoparticles sized between 40 and 5000 nm were able to enter human epithelial cells in a size-dependent way. The qualitative analysis via confocal laser scanning microscopy (CLSM) demonstrated a clear penetration into the cytoplasm. For silica nanoparticles sized between 40 and 70 nm a nuclear localization was observed as well (Chen & Mikecz von, 2005). In the field of gene delivery the uptake of nanoparticles into the cell nucleus becomes very important because the cell nucleus contains the gene expression machinery and monitors the genetic material of a cell. Thus, it represents the target for delivered genetic material such as plasmids or antisense oligonucleotides (Bharali et al., 2005; Gemeinhart et al., 2005; Slowing et al., 2008). These results in fundamental research underline the high potential of silica nanoparticles as oral drug or gene carrier.

Another frequently discussed topic is the application of nanoparticles to inflamed tissue in inflammatory bowel disease (IBD) (Lamprecht et al., 2001; Lamprecht et al., 2005; Moulari et al., 2008; Nakase et al., 2000; Nakase et al., 2001). Most drugs which are used for the treatment of IBD are delivered also to non-inflamed tissue. A targeted delivery exclusively to the inflamed tissue would decrease side effects and improve the therapeutic success. Polystyrene micro- and nanoparticulate carrier were shown to accumulate size-dependently in inflamed colonic mucosa (Lamprecht et al., 2001). Also silica nanoparticles exhibit a sixfold higher accumulation in inflamed tissue than in the healthy control tissue. The successful delivery of a drug to inflamed colonic cells could be demonstrated using 5-Amino salicylic acid (5ASA) loaded silica nanoparticles. 5ASA is used to treat inflammation in ulcerative colitis and Crohn's disease. 5ASA-loaded silica nanoparticles with a concentration of 25 and 50 mg/kg caused a higher decrease in inflammatory than free 5ASA at a concentration of 100 mg/kg (Moulari et al., 2008).

The design of silica nanoparticles as drug or gene carriers has to follow several requirements. The composition of the particles must be biodegradable, biocompatible and nontoxic, so that they can be used in human therapy. The particle size must be suitable for the administration via different routes to enter the body and reach the biological target site. Furthermore, also the biodistribution should adjust to the therapeutic application. Finally, silica nanoparticles must be loaded with drug molecules, whereby the drug should be released in a controlled manner once it reaches the target organ e.g. a tumour (Vauthier & Couvreur, 2007; Zhang et al., 2008). Further developments lead to more complex oral delivery systems such as silica-lipid hybrid (SLH) microcapsules for the improved delivery of poorly soluble drugs. The system combined the solubilising effect of lipids with the stabilising effect of silica nanoparticles. This novel drug carrier was able to increase the oral availability of the model drug celecoxib from 62% to 93-100% when bound to SLH microcapsules (Tan et al., 2009). In this context various other silica-based formulations exist to control and facilitate drug dissolution (Sanganwar & Gupta, 2008). Table 1.1 summarizes the composition of silica nanoparticles as drug carriers.

Table 1.1: Summary of different types of nanoparticulate drug carriers (modified from Vauthier & Couvreur, 2007; Liu et al., 2007; Tan et al., 2009).

Nanoparticulate drug carrier	Definition	Schematic illustration
Carrier nanoparticles	Drug molecules are adsorbed to the surface of the nanoparticles.	
Oil-containing nanocapsules	Nanoparticles with an encapsulated oil droplet surrounded by a silica shell.	
Water-containing nanocapsules	Nanoparticles with an encapsulated water droplet surrounded by a silica shell.	
Mesoporous nanocapsules	Hollow mesoporous nanocapsules with encapsulated drugs.	
Silica-lipid hybrid microcapsules	Silica-lipid hybrid microcapsules with an internal porous matrix structure with encapsulated drugs.	
Stealth carriers	Modification of the nanoparticle surface with e.g. PEG will reduce recognition by the immune system and increase plasma stability.	
Targeted carriers	Drug-targeted system with a targeting ligand (e.g. antibodies) on the nanoparticle surface.	

1.2 OVERCOMING THE INTESTINAL BARRIER

Oral drug delivery is the most convenient route for the administration of drugs because it has the advantage of avoiding discomfort, pain and infections which can be caused by injectable dosage forms. However, most drugs are difficult or unable to be delivered orally because of their low bioavailability due to their poor stability in the gastrointestinal tract and their low

membrane permeation over the intestinal barrier. For systemic absorption it is indispensable that drug molecules resist the acid ($\sim\text{pH } 3$) and enzymatic environment of the stomach and finally cross the intestinal epithelial cells to reach the general circulation and the target sites (Figure 1.2).

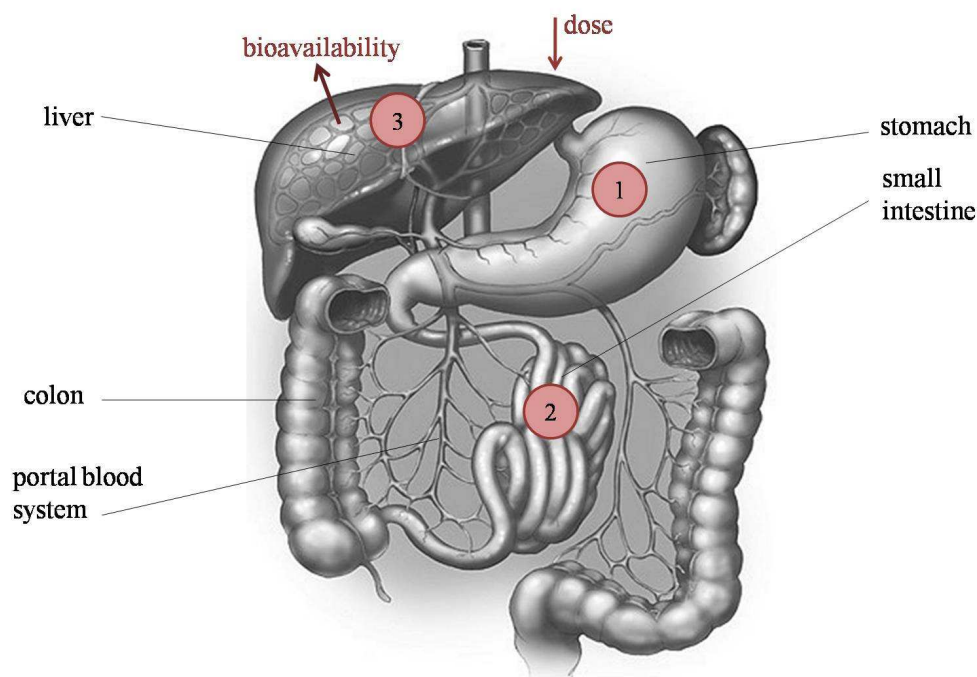


Figure 1.2: Biological barriers that influence oral bioavailability. Orally administered drugs have to be soluble and stable in the acid and enzymatic environment of the stomach (1) and have to cross the epithelium of the small intestine via an active or passive uptake to reach the blood circulation (2). Thereby efflux systems such as P-gp and enzymes (CYPs) hinder the passage. The first pass mechanism of the liver that eliminates xenobiotic substances is another critical obstacle (3). Figure was modified from Dave Carlson Illustration, Colorado, USA.

This process, however, is limited by various physical and biochemical barriers which normally protect the organism from toxins, antigens and microorganisms. The membrane of the intestinal epithelium builds a tight physical barrier which is composed of a single layer of columnar cells that are connected by tight junctions to form a tight membrane. Drug molecules or drug carriers such as nanoparticles can cross the gastrointestinal barrier via different pathways using paracellular passage and endocytotic or lymphatic uptake. The uptake between intestinal epithelial cells is mostly the preferred way of very small nanoparticles of up to 50 nm. Larger particles of sizes up to 500 nm are absorbed by intestinal enterocytes through endocytosis whereas microparticles ($<5\ \mu\text{m}$) are taken up by M cells of the Peyer's patches (Florence, 2005; Hamman et al., 2005; LeFevre et al., 1978; Liu et al.,

2007; Sanders & Ashworth, 1961; Venkatesan et al., 2005) (Figure 1.3). Efflux systems such as the P-glycoprotein (P-gp) demonstrate a further barrier function. P-gp is localized in the apical membrane and pumps compounds from within the cell back into the intestinal lumen. Substrates of P-gp are various chemical molecules such as cytostatics, HIV protease inhibitors, immunosuppressors and antibiotics (Gottesman et al., 2002; Hunter et al., 1993).

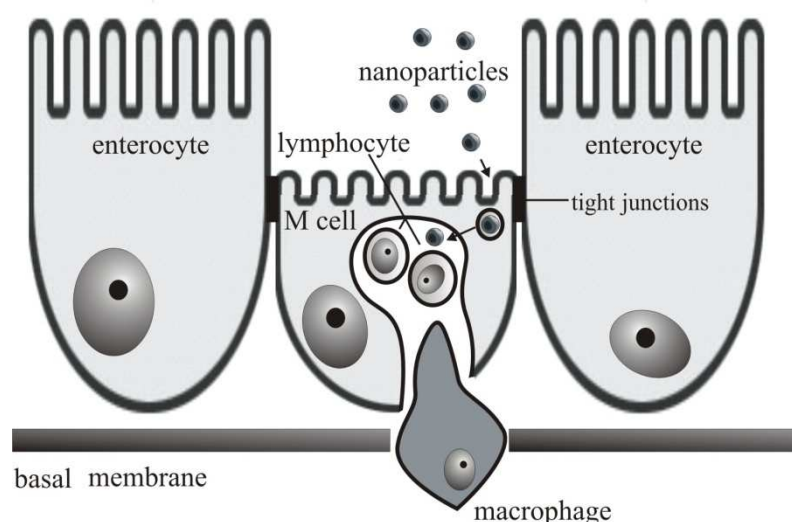


Figure 1.3: Uptake of nanoparticles at the intestinal epithelium. This epithelium consists of specialised antigen sampling M cells which possess a reduced number of microvilli and a pocket staying in contact with lymphocytes and macrophages. Nanoparticles are largely prevented from passing between epithelial cells by tight junctions. After the adherence to the apical membrane of M cells, nanoparticles cross the apical membrane and are delivered into the cells and subsequently are disseminated by the lymphatics (modified from Clark et al., 2001).

In recent years, the term “chemotherapy at home” presents a new concept of chemotherapy and purpose for the development of orally bioavailable cytostatics. This innovation would improve the life quality of cancer patients remarkably (Ajani & Takiuchi, 1999; Bottomley, 2002; DeMario et al., 1999; Feng, 2004). The difficulties are that most anticancer drugs are orally not or just minimally bioavailable, e.g. the oral bioavailability of the cytostatic paclitaxel is less than 1% of the administered concentration. This low absorption in the gastrointestinal tract is based on the first-pass elimination by the cytochrome P450 and the high affinity of paclitaxel to P-gp. The role of P-gp in that context was demonstrated in a study using wild-type and P-gp knockout mice. As a result, an increased oral uptake of paclitaxel could be observed in mice lacking P-gp (Sparreboom et al., 1997). The additional application of the P-gp inhibitor cyclosporine resulted in a 10-fold higher oral absorption of paclitaxel (Meerum Terwogt et al., 1999). In this context, further experiments showed that

doxorubicin and paclitaxel-loaded lipid-based nanoparticles overcome multidrug resistance by inhibiting P-gp (Dong et al., 2009). The application of TPGS, a water soluble vitamin E derivative, which is able to inhibit the P-gp mediated drug transport, represented a further improvement of drug delivery into intestinal cells (Collnot et al., 2006; Win & Feng, 2005). These findings exhibit the high demand of new strategies for the oral delivery of various drug molecules with low stability and bioavailability. However, the delivery of anticancer drugs to tumours is still a challenge. In this context, silica nanoparticles provide innovative and promising characteristics as drug carriers and present an attractive drug delivery system. Tumours contain a high density of abnormal blood vessels that are poorly differentiated with an aberrant branching. Furthermore, these tissues have an enhanced permeability and retention effect due to a decreased rate of clearance caused by the lack of functional lymphatic vessels in the tumour. Therefore, an increased accumulation of macromolecules as well as nanoparticles could be demonstrated (Allen & Cullis, 2004; Conti et al., 2006).

A widespread *in vitro* model for the investigation of oral bioavailability is the human colon adenocarcinoma cell line Caco-2. These cells form a polarized monolayer with an apical brush border morphologically comparable to that of the human small intestinal epithelium. Caco-2 cell express tight junctions, microvilli and a number of enzymes and transporters that are characteristic for enterocytes (e.g. P-gp). When cultured on permeable filter membranes, Caco-2 cells form a polarized epithelial cell monolayer that provides a physical and biochemical barrier to the passage of ions and small molecules. Caco-2 cells are widely used as an *in vitro* model to predict the absorption of orally administered drugs. The *in vitro/in vivo* correlation is well established and shows a high accordance (Artursson et al., 1997; Artursson et al., 2001; Chen et al., 2002; Hidalgo et al., 1989; Hughes et al., 1987).

1.3 CYTOTOXICITY AND OXIDATIVE STRESS CAUSED BY NANOPARTICLES

Silica-based materials with defined structures and surface properties are known to be biocompatible. Silica is used to enhance the biocompatibility of various drug delivery systems such as magnetic nanoparticles, biopolymers and micelles (Allouche et al., 2006; Arruebo et al., 2006; Huo et al., 2006). Microscopic analysis showed normal cell morphology after an

uptake of mesoporous silica nanoparticles. Furthermore, growth rates of cells exposed to silica nanoparticles demonstrated no difference to the ones of control cells grown in the absence of silica nanoparticles (Slowing et al., 2006; Slowing et al., 2008). A long-term biocompatibility study exhibited that silica implants caused no toxic effects within a period of 42 days (Kortesuo et al., 1999).

However, the growing biomedical and pharmacological applications of silica nanoparticles call for the importance to investigate their influence on cells as their uptake implies a close contact between nanoparticles and the biological systems. Therefore, a detailed evaluation of the cytotoxic potential of nanomaterials is required. In this course, nanotoxicology is a rising sector in nanotechnology. Institutions such as the European Commission or the European Food Safety Authority published scientific opinions about the potential risk of nanomaterials in cosmetics or food which suggest treating nanomaterials as new chemicals from a risk-point of view (EFSA, 2009; SCCP, 2007).

Hitherto, the molecular mechanism of nanoparticulate induced cytotoxicity is not fully understood. It is assumed that cytotoxicity is caused by cellular injuries through a variety of mechanism such as membrane peroxidation, glutathione depletion, mitochondrial dysfunction and DNA damage (Tao et al., 2009). Especially nanoparticulate induced oxidative stress raises suspicion affecting all types of biological molecules including lipids, proteins, carbohydrates and nucleic acids. Therefore, oxidative stress is one of the most important toxicity mechanism related to the exposure of nanoparticles (Eom & Choi, 2009; Green & Howman, 2005; Shvedova et al., 2003).

In various studies an increase in reactive oxygen species (ROS) could be detected simultaneously with a decrease in cell viability after incubation with silica nanoparticles (Eom & Choi, 2009; Park et al., 2008; Wang et al., 2009). A rising amount of ROS is often associated with a decrease in glutathione and an enhanced activity of antioxidant enzymes such as superoxide dismutase or heme oxygenase-1, which indicated an oxidative potential of silica nanoparticles. Inflammation signal and apoptosis markers can be increased as well. Further studies supposed that the acute cytotoxicity is primarily originated from the cellular internalization of nanoparticles rather than physical damage on cellular membranes (Yang et al., 2009). Furthermore, it is expected that the smaller the size, the stronger the observed toxicity is (Oberdorster et al., 2005). In a study of Wang et al., nanoparticles with a size of

20 nm showed a higher decrease in cellular viability than 50 nm particles with a simultaneously higher increase of ROS in human embryonic kidney cells (Wang et al., 2009). However the relationship between the physico-chemical properties of nanoparticles and their toxicities seems to be much more complicated than just a matter of their size and surface area (i.e. shape, charge, concentration, etc), but the debate is still ongoing (Hussain et al., 2005; Sayes et al., 2005).

1.4 AIM OF THE THESIS

The aim of this thesis was to investigate the interaction between silica nanoparticles and the human intestinal epithelial cell line Caco-2. Thereby, the cytotoxic and the oxidative potential as well as the uptake and transport characteristics of these particles should be explored.

One focus was stressed on the establishment of novel alternatives to standardized method for the detection of oxidative stress and cytotoxicity *in vitro*. The measurement principles of the standardized techniques often interfere with nanoparticles and prohibited their usage for these applications. In their role as potential drug carriers, silica nanoparticles are supposed to come into close contact with biological systems, thus it is essential to have a dependable assay to evaluate the toxicity of nanoparticles.

Another aim of this thesis was to allow a quantification of the cellular uptake of nanoparticles. Hitherto, the nanoparticulate uptake was mostly determined via microscopic techniques such as confocal laser scanning microscopy or transmission electron microscopy, which makes a comparison between single studies very difficult. Therefore, a quantitative assay for the determination of the quantification of nanoparticles should be established.

Based on this novel experimental design, the uptake behaviour of silica nanoparticles with different sizes and surface modifications should be explored. Furthermore, the endocytotic mechanisms involved in the uptake of these nanoparticles should be identified (Figure 1.4).

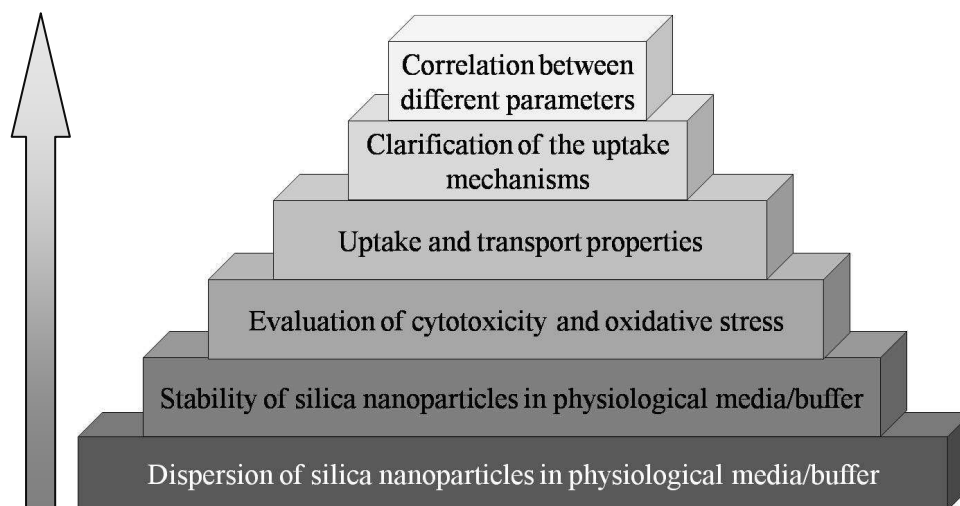


Figure 1.4: Working flow chart of the present thesis.

2

Characterization of fluorescently-labelled silica nanoparticles in physiological buffers and cell culture media

Fluorescently-labelled silica nanoparticles were prepared by the Leibniz Institute of New Materials (INM, Saarbrücken, Germany) and were stored highly concentrated in an aqueous solution stabilized with acetic acid to a pH of ~5. For their use in *in vitro* cell culture experiments, these nanoparticles had to be dispersed in physiological buffers or cell culture media. The tendency of nanoparticles to agglomerate is sensitive to ingredients such as bivalent ions (e.g. Ca^{2+} or Mg^{2+}). Therefore, the dispersion of nanoparticles in these isotonic solutions as well as their stability had to be explored before performing *in vitro* experiments. The alteration in size and ζ potential of a nanoparticle gives information about the nanoparticulate behaviour in physiological media and were determined via dynamic light scattering or electrophoretic light scattering using the Zetasizer Nano Zs (Malvern Instruments, Herrenberg, Germany).

2.1 INTRODUCTION

The upcoming usage of nanostructured biomaterials in pharmaceutical or medical purposes requires an improved knowledge of the biological interaction of nanomaterials with cells or tissues. Therefore, *in vitro* experiments are essential. These assays require the compatibility

and stability of nanoparticles in physiological buffers or media. As a consequence, nanoparticles have to be dispersed in isotonic solutions with a pH of 7.4, where they interfere with bivalent ions (typically magnesium or calcium) and protein mixtures. Due to their large surface area/volume ratio, nanoparticles show a strong tendency to agglomerate and to adsorb proteins. The knowledge of protein adsorption is very important because the adsorption of blood proteins *in vivo* will affect the cellular uptake and biochemical activity (Patil et al., 2007; Schulze et al., 2008).

Recent studies already demonstrated aspects of nanoparticle dispersion and protein adsorption. The addition of proteins such as bovine serum albumin (BSA) to nanoparticles reduced the ζ potential from ~ 55 mV to ~ 18 mV indicative for a strong protein adsorption to the particle surface. Furthermore, a binding to proteins resulted in an accelerated clearance by macrophages which avoid nanoparticles from reaching their biological target sites (Patil et al., 2007). For this purpose, besides unmodified silica nanoparticles, poly ethylene glycol (PEG)-modified silica nanoparticles were characterized in this study as well. Thereby, it could be possible to increase the circulation time of nanoparticles in the blood stream by minimizing and eliminating protein adsorption due to the characteristics of PEG. PEG is a polyether compound which is known to reduce reticuloendothelial clearance, the uptake by macrophages, recognition by the immune system and the degradation by proteolytic enzymes. It shows stabilizing properties due to a steric stabilization as well (Roberts et al., 2002; Behrens et al., 2002; Tobio et al., 2000).

2.2 AIM OF THE STUDY

In the present study, fluorescently-labelled nanoparticles with different sizes and surface modifications were characterized concerning their behaviour in different media or buffer over time by investigation of their variation in size and ζ potential. The absorption of BSA as model protein was explored as well. For a better comprehensibility and clarity only exemplary results are presented, especially because nanoparticles with analogue characteristics behaved similarly.

The aim of this study was to determine the size alteration and the stability of fluorescently-labelled silica nanoparticles in physiological buffers and cell culture media (+/- proteins). Furthermore, the ζ potential as well as the adsorption of BSA should be investigated. The characterization of the nanoparticles should help to establish a catalogue of different nanoparticles for various experimental approaches and questions.

2.3 MATERIALS AND METHODS

2.3.1 Silica nanoparticles

Amorphous silica nanoparticles were received from the Leibniz Institute of New Materials (INM, Saarbrücken, Germany) where they had been prepared by Stöber synthesis. Synthesized nanoparticles were either unmodified or additionally surface-modified with amino-ethyl-3-aminopropyl-trimethoxysilan (DIAMO) or poly ethylene glycol (PEG) chains with a molecular weight of 750 g/mol. Transmission electron microscopy (TEM) measurements were performed as a visual control. Figure 2.1 shows exemplary TEM images of unmodified and PEG-modified silica nanoparticles with different sizes.

For fluorescence detection, nanoparticles were matrix-loaded with the fluorescent dye rhodamine B-isothiocyanate (RITC). Thereby, the silica matrix served as a protective shell limiting the effect of the outer environment to the fluorescent molecules. For further experiments, nanoparticles were surface-loaded with propidium iodide (PI). The choice of the fluorescence dyes was reasoned in different experimental approaches, which will be discussed in detail in the different chapters (compare to chapter 4 and 5). Nanoparticle names are composed of the particle size in HBSS, the surface modifications (D=DIAMO or P=PEG) and the fluorescence dye (RITC or PI).

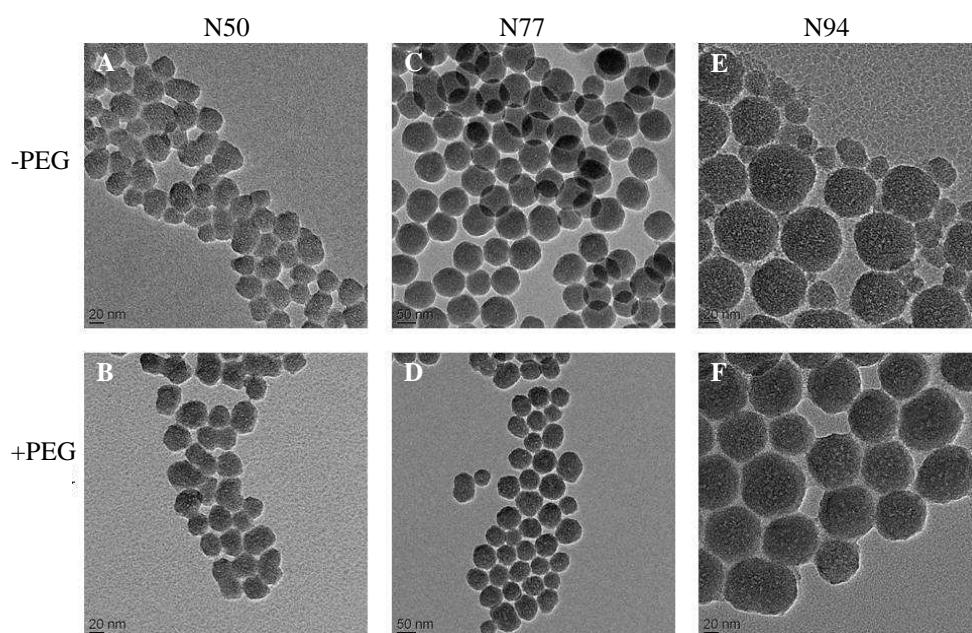


Figure 2.1: TEM micrographs of silica nanoparticles with and without PEG-modification. **(A)** Unmodified nanoparticles, N50-RITC, 50 nm. **(B)** PEG-modified nanoparticles, N50-P-RITC, 55 nm. **(C)** Unmodified nanoparticles, N77-RITC, 77 nm. **(D)** PEG-modified nanoparticles, N77-P-RITC, 87 nm. **(E)** Unmodified nanoparticles, N94-RITC, 94 nm. **(F)** PEG-modified nanoparticles, N94-P-RITC, 97 nm. Bars=20 nm (A, B, E and F) or 50 nm (C and D).

2.3.2 Materials and buffers

Different silica nanoparticles were dispersed in phosphate buffered saline (PBS) (Table 2.1), Hank's balanced salt solution (HBSS) (Table 2.2) with and without addition of 1% bovine serum albumin (BSA) or in Dulbecco's modified eagle medium (DMEM) from Gibco (Karlsruhe, Germany) (Table 2.3). All buffers were adjusted to pH 7.4 by means of NaOH. Acrylic cuvettes for the determination of particles' sizes were purchased from Sarstedt (Nümbrecht, Germany). Zeta folded capillary cuvettes for the measurement of the ζ potential were obtained from Malvern (Herrenberg, Germany).

Table 2.1: Composition of phosphate buffered saline (PBS). PBS were adjusted to pH 7.4 by means of NaOH.

Ingredient	Concentration
NaCl	129.00 mM
KCl	2.50 mM
Na ₂ HPO ₄ *7H ₂ O	7.00 mM
KH ₂ PO ₄	1.30 mM

Table 2.2: Composition of Hank's balanced salt solution (HBSS). HBSS were adjusted to pH 7.4 by means of NaOH.

Ingredient	Concentration
NaCl	136.90 mM
KCl	5.40 mM
NaHCO ₃	4.26 mM
Na ₂ HPO ₄ *7H ₂ O	0.34 mM
KH ₂ PO ₄	0.35 mM
Glucose	5.50 mM
HEPES	10.00 mM
CaCl ₂	1.26 mM
MgCl ₂ *6H ₂ O	0.50 mM
MgSO ₄ *7H ₂ O	0.40 mM

Table 2.3: Composition of Dulbecco's modified eagle medium (DMEM).

Ingredient	Concentration
CaCl ₂ *2H ₂ O	1.80 mM
Fe(NO ₃) ₃ *9H ₂ O	0.00025 mM
MgSO ₄ *7H ₂ O	0.81 mM
KCl	5.33 mM
NaHCO ₃	44.05 mM
NaCl	110.34 mM
NaH ₂ PO ₄ *2H ₂ O	0.92 mM
D-Glucose	25.00 mM
Phenol red	0.40 mM
Amino acids	10.64 mM
Vitamins	0.15 mM

2.3.3 Measuring principle of the Zetasizer Nano ZS

The Zetasizer Nano ZS allows the determination of the average hydrodynamic diameter by dynamic light scattering (DLS) and the ζ potential of nanoparticles by electrophoretic light scattering (ELS). DLS is a technique to characterize the diffusion of particles in solution. It measures Brownian motion and relates this to the size of the particles. Brownian motion is the random movement of particles due to forces resulted from the solvent molecules that surrounded them. The larger the particle, the slower is its Brownian motion because smaller particles move more rapidly. The size of a particle is calculated from the translational diffusion coefficient by using the Stokes-Einstein equation. Thereby, the measured hydrodynamic diameter refers to how a particle diffuses within a fluid. The principle of this measurement technique is based on a monochromatic laser beam that passes through a cuvette with a colloidal dispersion. Some of the light is uniformly scattered by the particles in all directions via Rayleigh scattering. The changing distances of the particles due to their Brownian motion causes interferences of the light scattered by neighbouring particles. The analysis of these occurred time-dependent fluctuations in the scattering intensity gives information about the speed of the particles in the solution. Using a diffusion coefficient, the hydrodynamic diameter of a nanoparticle could be determined (Malvern Technical Note).

The ζ potential is a physical property which is exhibited by any particle in suspension and is determined via ELS. It is the potential difference between the dispersion solution and the stationary layer of fluid attached to the particle, thereby it is measured at the slipping plane of particles. The liquid layer which surrounds a particle consists of two parts: an inner region (Stern layer) where the ions are strongly associated and an outer diffuse region, where ions are loosely bound. Within the diffuse layer there is a fictive boundary inside which the ions and particles form a stable unit. That would mean, if a particle moves, ions within the boundary move it. The potential at this boundary (=surface of hydrodynamic shear) is the ζ potential (Figure 2.2). The ζ potential is a measure for the degree of stability of a colloidal system. If all particles in suspension have a high negative or positive ζ potential, there will be no tendency for the particles to come together and so they repel each other. In contrast, if the particles have a low ζ potential, there will be no forces preventing the agglomeration of particles. The ELS measurement principle is based on the application of an electric field to the dispersed particles. By alternating the charge between the electrodes, the particles move back and forth between the electrodes at a velocity relative to their surface charge and the potential of the electrode (Malvern Technical Note).

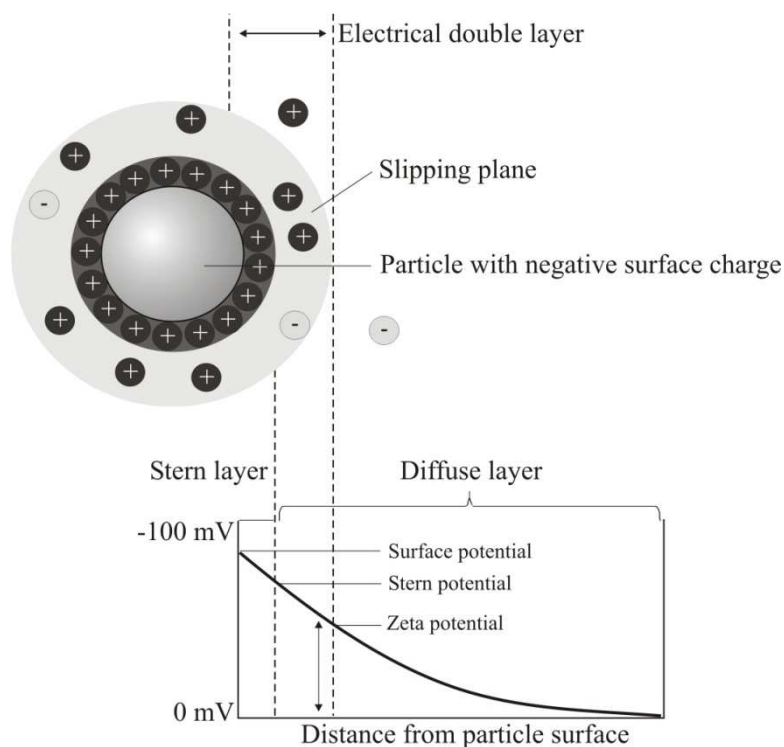


Figure 2.2: Schematic illustration of the ζ potential (modified from Malvern Technical Note).

2.3.4 Size, ζ potential and stability of nanoparticles in different buffers and media

Stock solutions from the used fluorescently-labelled silica nanoparticles had concentrations ranging from 3.7 to 12.5 mg/ml. For the determination of the particles size as well as the ζ potential, particles were diluted in the respective dispersion buffer or media to a concentration of 100 $\mu\text{g/ml}$. Size measurements were performed at 37°C with an equilibration time of 120 seconds in disposable sizing cuvettes at the automatic mode. Every measurement was performed three times at different time points. For stability measurements, nanoparticle dispersions were stored at 37°C between the single measurements. For determination of the ζ potential, automatic measurements (10-100 runs) were performed at a temperature of 37°C and with an equilibration time of 120 seconds using the calculation model of Smoluchowski.

2.4 RESULTS AND DISCUSSION

2.4.1 Alteration in the sizes of silica nanoparticle in different buffers and media

Due to the alteration in the complexity of buffers and media, silica nanoparticles exhibited different behaviours. Thereby, unmodified RITC-labelled silica nanoparticles with different sizes could be dispersed in H₂O as well as in PBS and HBSS. The dispersion in a cell culture medium e.g. DMEM with a very high complexity could be also performed without any agglomeration of nanoparticles (Figure 2.3).

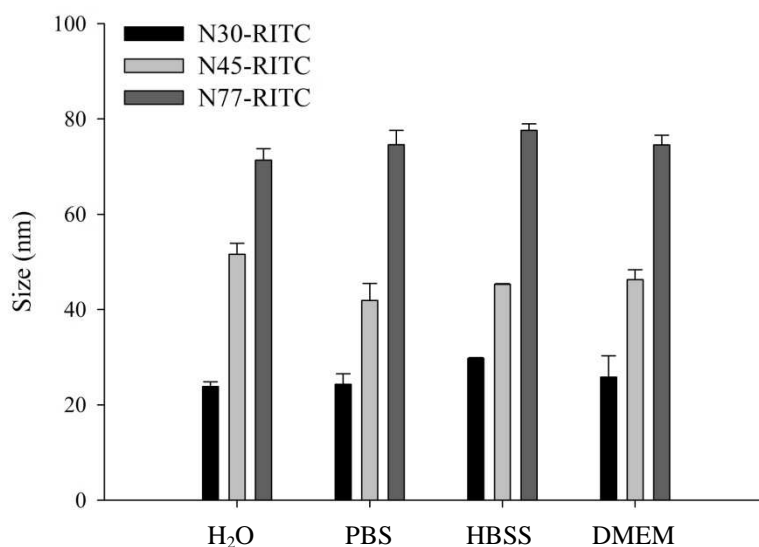


Figure 2.3: Dispersion of three unmodified RITC-labelled silica nanoparticles with different sizes (N30-RITC, N45-RITC and N77-RITC) in H₂O, PBS, HBSS and DMEM. Bars present the mean \pm SD of three measurements.

Difficulties could be observed in the dispersion behaviour of nanoparticles with modified surfaces. Silica nanoparticles with adsorbed aminosilanes (DIAMO) showed a strong agglomeration in HBSS due to an interaction with bivalent ions in the buffer (Figure 2.4). The resulting aggregation was due to an electrostatic destabilization described by the Derjaguin-Landau-Verwey-Overbeek theory (DLVO theory). This theory explains that the stability of colloidal systems is based on steric, electrostatic or van der Waals interactions between dispersed particles. A surface in an aqueous milieu is charged by dissociation of surface groups or by adsorption of charged molecules from the surrounding liquid. This arrangement results in the development of a wall surface potential which attract counterions from the environment and exclude ions with the same charge. Stable dispersions consist of a wall surface potential balanced by an equal but opposite charge of counterions. This potential can

be decreased via the adsorption of specific ions which results in a reduction of the interspace between single particles and a consequently agglomeration of the particles (Zhang et al., 2009). DIAMO-modified nanoparticles exhibited a positive ζ potential of 21.8 mV. The addition of bivalent cations such as Mg^{2+} and Ca^{2+} which are ingredients of HBSS caused a strong agglomeration of these particles due to an excess of positive charged molecules and a consequently reduced charge balance. In contrast, nanoparticles with the same size but without a DIAMO-modification could be dispersed in HBSS. Due to their negative ζ potential of -22.9 mV, unmodified silica nanoparticles were still in a balance with the surrounding milieu.

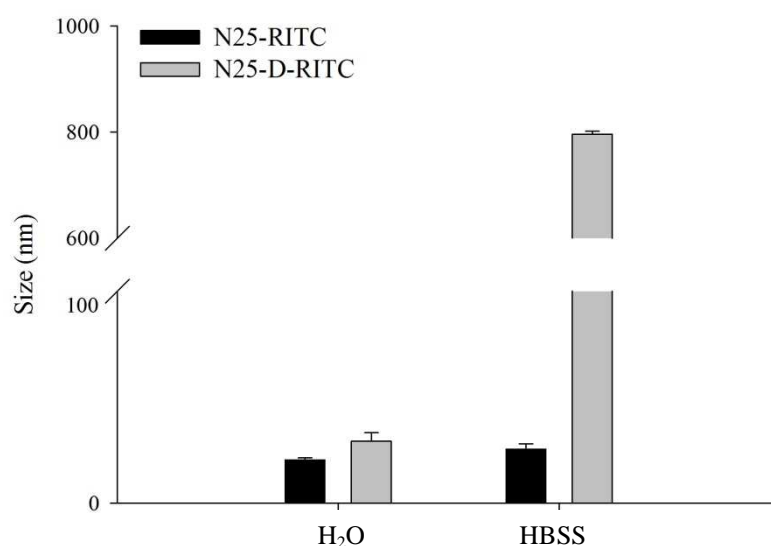


Figure 2.4: Dispersion of RITC-labelled unmodified silica nanoparticles (N25-RITC; -22.9 mV) and DIAMO-modified silica nanoparticles (N-25-D-RITC; +21.8 mV) in H₂O and HBSS. Bars present the mean \pm SD of three measurements.

In contrast, PEG-modified nanoparticles could be dispersed in the same way as the corresponding unmodified nanoparticles. Thereby, the addition of PEG on the outer particle surface caused an increase in size of 0.7 nm to 10 nm (Figure 2.5). Furthermore, PEG-modified nanoparticles showed no altered ζ potential.

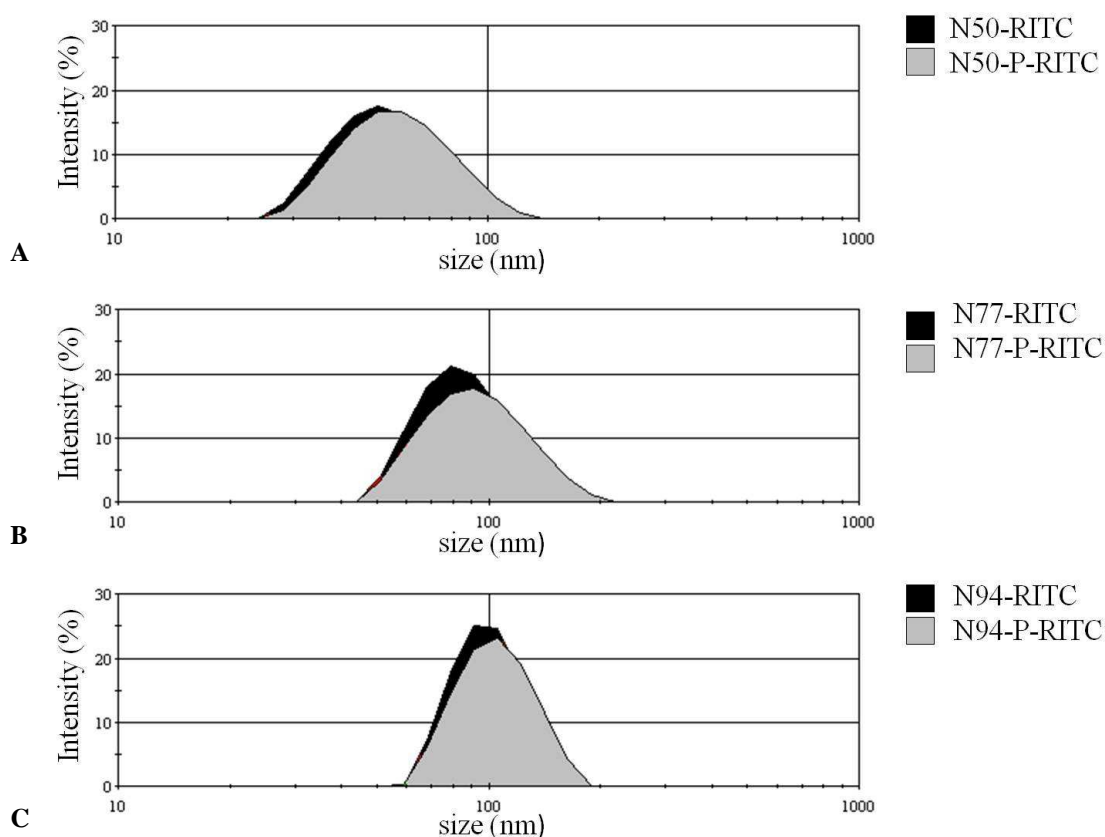


Figure 2.5: Size histograms of unmodified (black peaks) and the corresponding PEG-modified RITC-labelled nanoparticles (grey peaks). Particles were dispersed in HBSS buffer. **(A)** Unmodified nanoparticles N50-RITC, 50 nm and PEG-modified nanoparticles N50-P-RITC, 55 nm. **(B)** Unmodified nanoparticles N77-RITC, 77 nm and PEG-modified nanoparticles N77-P-RITC, 87 nm. **(C)** Unmodified nanoparticles N94-RITC, 94 nm and PEG-modified nanoparticles N94-P-RITC, 97 nm.

2.4.2 Stability of nanoparticles in different buffers and media

For *in vitro* experiments a long-term incubation of cells with particles is sometimes necessary. Therefore, nanoparticles have to be dispersed in a cell-friendly milieu. Physiological buffers such as HBSS sustain the viability of cells for about 24 hours. If long-term experiment with longer incubation times should be performed, further supplements such as proteins, amino acids or vitamins are essential. All used RITC-labelled nanoparticles except DIAMO-modified nanoparticles (Figure 2.4) were stable in HBSS over 24 hours (data not shown). The core-bound fluorescence dye RITC had no contact to the surrounding medium and therefore caused no interactions. In contrast, stability experiments with PI-labelled nanoparticles demonstrated that these nanoparticles often show no stability in HBSS over that period. PI-labelled silica nanoparticles with different sizes (62 and 74 nm) could be dispersed in HBSS but showed a high agglomeration rate after a 24-hour-incubation (Figure 2.6). This

agglomeration effect could be based again on the presence of bivalent ions in the buffer and their interaction with surface adsorbed PI molecules. Apparently, the charge balance could not be sustained for such a long period. However, time kinetic measurements of N21-PI, N34-PI and N84-PI nanoparticles demonstrated that these particles were stable for this period (Figure 2.6).

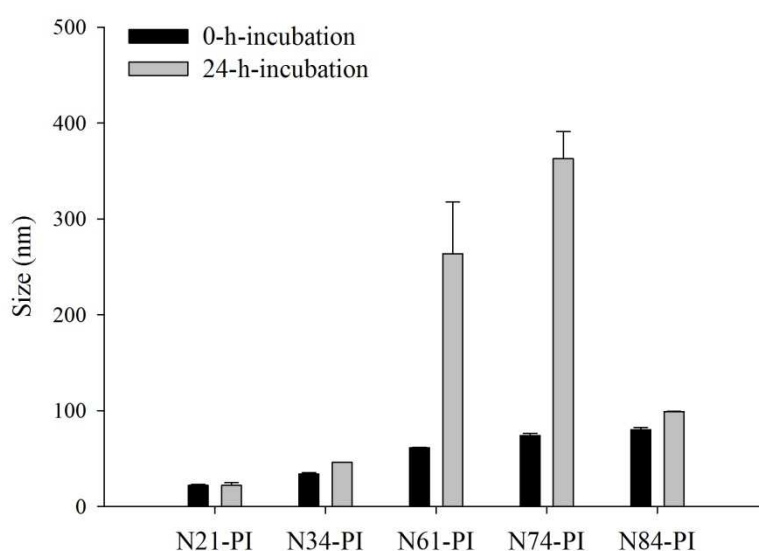


Figure 2.6: Stability of PI-labelled unmodified nanoparticles with different sizes over 24 hours. Samples were measured directly after dispersion (0-h-incubation, black bars) or after an incubation of 24 hours at 37°C under standard cell culture conditions (24-h-incubation, grey bars). Bars present the mean \pm SD of three measurements.

A method for the solution of this stability problem was the application of ultrasonic which allows a separation of nanoparticles. Experiments showed that ultrasonic was able to separate agglomerated nanoparticles but did not help to stabilize these dispersions. Ultrasonic-treated nanoparticles even showed a higher agglomeration rate as untreated samples. The usage of ultrasonic with nanoparticles labelled with fluorescence dyes presents a further difficulty as these labellings can be released via this treatment.

A further approach to stabilize nanoparticles is the stabilization via addition of bovine serum albumin (BSA). Various studies investigated the aspects of nanoparticle dispersion and protein adsorption including the binding enthalpy of proteins and the change of the ζ potential (Limbach et al., 2005; Patil et al., 2007; Schulze et al., 2008). The supplement of BSA to buffers or media resulted in a detectable size peak at ~ 8.4 nm which was based on BSA monomers (Figure 2.7, black peak). The measured diameter of nanoparticles was increased as well due to BSA monomers adsorbed to the particle surface creating a protein corona.

Unmodified N77-RITC nanoparticles exhibited a diameter of $108 \text{ nm} \pm 34.5$ when dispersed in HBSS supplemented with 1% BSA (Figure 2.7, grey peak). In contrast, N77-RITC nanoparticles dispersed in HBSS without any addition of BSA showed a size of $77.2 \text{ nm} \pm 0.53$ (Figure 2.5 B). A further indication of a BSA coating was the alteration in ζ potential. N77-RITC nanoparticles dispersed in HBSS demonstrated a ζ potential of -28 mV . The addition of BSA into the medium caused a reduction of the ζ potential to -7.8 mV .

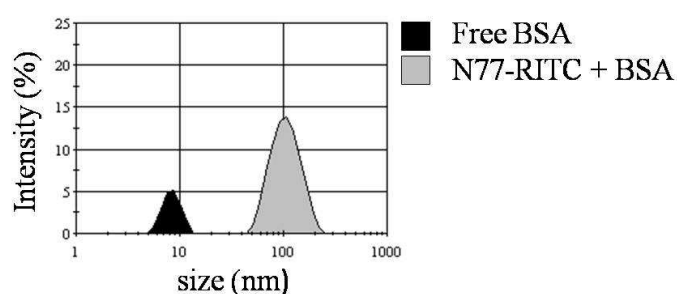

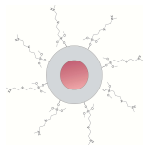




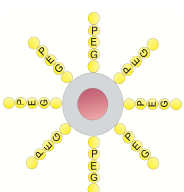


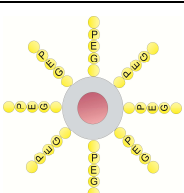



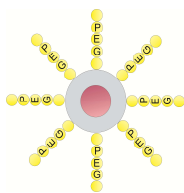
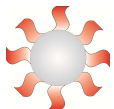
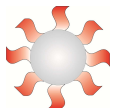
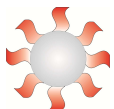
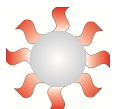
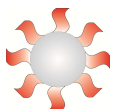
Figure 2.7: Adsorption of BSA to the nanoparticle surface. Unmodified N77-RITC nanoparticles were dispersed in HBSS supplemented with 1% BSA. The grey peak demonstrated the size of N77-RITC nanoparticles coated with BSA. The black peak showed the size of free BSA in the solution. Bars present the mean \pm SD of three measurements.

The protein coating led to a sterical stabilization of the nanoparticle dispersions, which resulted in a reduction of particle agglomeration. Such a steric stabilization due to a coating with BSA had already been shown for gold, polymer and aluminium hydroxide nanoparticles, whereby these particles could be dispersed in media containing bivalent ions (Cedervall et al., 2007; Deschaume et al., 2006; Lucocq & Baschong, 1986). The disadvantage of such a binding to proteins is that such particles are quickly cleared by macrophages *in vivo* and are not allowed to reach their target cells. Approaches to increase the particle circulation time, therefore try to eliminate protein adsorption. This approach would stay in contrast with the stabilization issue and lead to the point that particle stabilization via BSA or other proteins is not the best solution. However, an adsorption of proteins to the particle surface is not avoidable when nanoparticles, without a special surface modification, enter cells. As shown in figure 2.7 unmodified nanoparticles exhibited a strong BSA absorption which resulted in an increase in particle size of 30.8 nm. In contrast, nanoparticles modified with poly ethylene glycol (PEG) demonstrated only an increase in size of 6.15 nm (data not shown). The PEG-modification avoids an adsorption of proteins to the outer particle surface. The characteristics of PEG will be discussed in depth in chapter 4.

2.5 COLLECTION OF USED SILICA NANOPARTICLES

Table 2.4: Characterization of silica nanoparticles used in this thesis. Size was determined via dynamic light scattering. ζ potentials were determined via electrophoretic light scattering. Nanoparticle names are composed of the particle size, surface modification (P=PEG, D=DIAMO) and the fluorescence dye (RITC or PI).

Name	Design	Surface modification	Fluorescence labelling	Size in HBSS (nm)	ζ potential (mV)
N25-RITC		-	RITC	25.4 ± 2.51	-22.9
N25-D-RITC		DIAMO	RITC	795.9 ± 5.3	+21.8
N30-RITC		-	RITC	29.8 ± 0.18	-32.0
N37-RITC		-	RITC	37.2 ± 3.70	-35.0
N45-RITC		-	RITC	45.3 ± 0.16	-29.0
N50-RITC		-	RITC	49.7 ± 0.06	-42.7
N50-P-RITC		PEG	RITC	54.6 ± 0.86	-27.5
N62-RITC		-	RITC	61.6 ± 0.07	-31.4
N77-RITC		-	RITC	77.2 ± 0.53	-28.0
N77-RITC		PEG	RITC	87.2 ± 2.42	-25.0
N94-RITC		-	RITC	93.7 ± 4.19	-37.6

N94-P-RITC		PEG	RITC	97.4 ± 3.03	-35.4
N21-PI		-	PI	21.1 ± 0.48	-33 mV
N34-PI		-	PI	34.0 ± 1.40	-0.17*
N61-PI		-	PI	61.4 ± 0.54	-12.1*
N74-PI		-	PI	73.8 ± 2.40	-0.48*
N84-PI		-	PI	84.0 ± 0.21	-5.55*

* The surface modification with the fluorescence dye PI caused interactions with the measurement principle for determination of the ζ potential.

Oxidative and cytotoxic potential of fluorescently-labelled silica nanoparticles

Parts of this chapter have been submitted for publication as journal articles:

1. A. Neumeyer, C.-M. Lehr & N. Daum. Novel method for the non-invasive determination of reactive oxygen species *in vitro*. Submitted to *Toxicology In Vitro*
2. A. Neumeyer, M. Bukowski, M. Veith, C.-M. Lehr & N. Daum. Non-invasive determination of the cytotoxic effect caused by fluorescently-labelled silica nanoparticles. In preparation

Nanomaterials are innovative tools in the field of drug delivery. Thereby, inorganic nanoparticles such as silica particles provide promising characteristics as novel drug carriers. Since silica exposure has also been associated with the generation of reactive oxygen species, it is essential for a thorough risk assessment to analyze the cytotoxic and oxidative potential of nanoparticles. Recent opinions of the Scientific Committee on Consumer Products (SCCP) of the European Commission and the European Food Safety Authority (EFSA) underlined this approach, suggesting the validation of *in vitro* methodologies for nanomaterials. Furthermore, nanoparticles often interfere with various standardized assays revealing again the importance for the development of alternatives for already commercially available techniques. Therefore, a novel method for the combined detection of oxidative stress and cytotoxicity was established. This assay is based on the automated non-invasive online monitoring of the oxygen concentration in solution (SensorDish[®] Reader). Silica nanoparticles with different sizes and surface modifications were investigated with this novel method concerning their

oxidative and cytotoxic potential. Thereby, size, time, concentration as well as surface modification of nanoparticles affected cellular viability but not oxidative stress levels.

3.1 INTRODUCTION

Silica nanoparticles have to be investigated concerning their oxidative and cytotoxic potential, particularly with regard to a pharmaceutical or medical application where particles come in close contact with biological systems. Recent studies described that silica nanoparticles can cause oxidative stress (Eom & Choi, 2009; Park & Park, 2009; Wang et al., 2009) which is in turn associated with deleterious effects resulting in several serious diseases such as autoimmune diseases and cancer (Avalos et al., 2007; Gonsette, 2008; Rice-Evans & Burdon, 1993; Sayre et al., 2008). These findings reveal that the validation of the oxidative and cytotoxic potential of nanomaterials is of great interest. To exclude potential harmful effects, these new materials have to undergo a thorough risk assessment. Referring to this, the European Food Safety Authority (EFSA) and the Scientific Committee on Consumer Products (SCCP) of the European Commission recently published opinions on the safety of nanomaterials in cosmetic products or food (EFSA, 2009; SCCP, 2007). It is suggested that nanomaterials should be treated as new chemicals from a risk point of view. For this purpose, various *in vitro* assays already exist. However, the use of standardized assays for the detection of oxidative stress and cytotoxicity with these new kinds of materials pose specific challenges. Because of their material properties, nanomaterials often cause interactions with many standardized assays revealing the importance for the development of useful alternatives for already commercially available techniques (Laaksonen et al., 2007; Ulukaya et al., 2008; Wahl et al., 2008; Worle-Knirsch et al., 2006).

Oxidative stress arises with an imbalance of the generation and the decomposition of reactive oxygen species (ROS). Normally, cells are able to defend themselves against ROS damage, using their antioxidant defence mechanism which includes enzymes such as superoxide dismutases (SOD) and catalases (Johnson & Giulivi, 2005; Lavrovsky et al., 2000; Sies, 1993). However, after exposure to oxidants the ROS levels can increase dramatically which results in damages affecting all types of biological molecules including lipids, proteins,

carbohydrates and nucleic acids. This can lead to protein oxidation and fragmentation, lipid peroxidation, membrane damage, mutagenesis and carcinogenesis (Sies, 1986).

ROS are either free radicals, reactive anions containing oxygen atoms or molecules containing oxygen atoms. They can produce free radicals or are chemically activated by themselves, e.g., the hydroxyl radical (OH^\bullet), superoxide anion radical ($\text{O}_2^{\bullet-}$) and hydrogen peroxide (H_2O_2) all result from molecular oxygen (O_2) (Figure 3.1). *In vivo* the main amount of ROS is generated in mitochondria during the aerobic respiration (Fernandez-Checa et al., 1998). In addition to this endogenous oxidative stress, exogenous factors including UV- or X-rays, ozone, smog and the exposure to chemicals such as nicotine are much more hazardous and result in an increased generation of ROS (Baier et al., 2007; Barr et al., 2007; Bertram & Hass, 2008; Rugo & Schiestl, 2004; Wang et al., 2006). A well known method for the detection of oxidative stress is the 2', 7'-dichlorofluorescein diacetate (DCF-DA) assay (Rosenkranz et al., 1992; Wang & Joseph, 1999). This method is based on a fluorescence assay first described by Keston and Brandt (Brandt & Keston, 1965) who employed DCF-DA to measure hydrogen peroxide in aqueous solution.

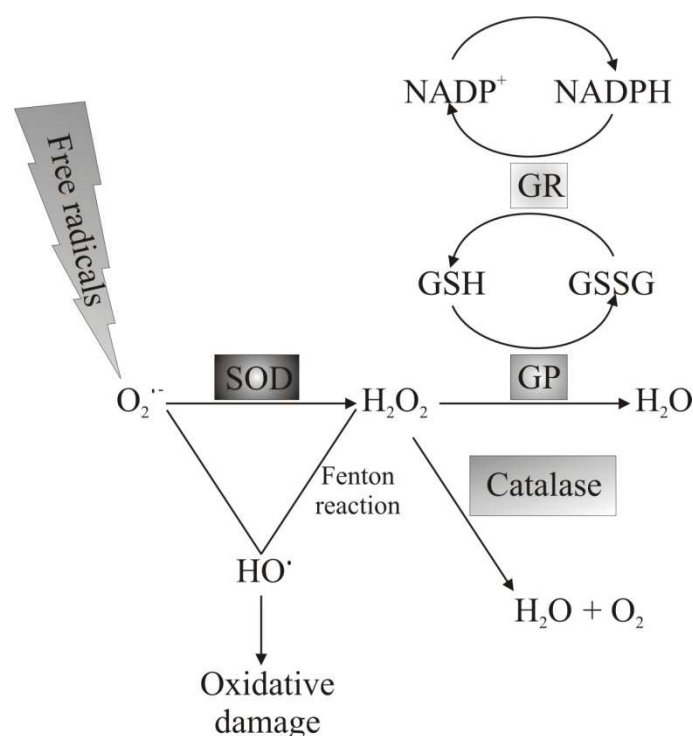


Figure 3.1: Summary of the antioxidant defence mechanism. Superoxide anion ($\text{O}_2^{\bullet-}$) is scavenged by the antioxidant superoxide dismutase (SOD). Glutathione peroxidase (GP) uses hydrogen peroxide (H_2O_2) to convert reduced glutathione (GSH) to oxidized glutathione (GSSG). Glutathione reductase (GR) reduces GSSG to GSH via nicotinamide adenine dinucleotide phosphate (NADPH) oxidation, while catalase decomposed H_2O_2 into water and molecular oxygen (Maier & Chan, 2002).

Oxidative stress can result in cytotoxicity, wherefore the cytotoxic potential of nanoparticles have to be investigated as well. Assays for the detection of cytotoxicity address many cellular parameters as cytotoxicity can occur in nearly all parts of the cell and in every cell organelle. Exposure to cytotoxic molecules can result in a loss of membrane integrity, cell lysis and necrosis. In consequence of these damages, cell growth and division are arrested, which can be detected as a decrease in cellular viability. Furthermore, apoptosis can be activated, which is characterized by well defined events including shrinkage of the cytoplasm and nuclear condensation. Cytotoxicity assays detect either the damage of cell membranes (mechanical cytotoxicity) or the mitochondrial metabolism (metabolic cytotoxicity). One common measured parameter in cell death and cell lysis determination is lactate dehydrogenase (LDH) which is released from the cytosol of damaged cells into the supernatant. For the measurement of cellular proliferation and viability, MTT assay is a well known example. All these assays are easy to perform but they detect only high-specific alterations of one cellular or metabolic parameter at one selected time point and they are mostly invasive methods (Fotakis & Timbrell, 2006; Weyermann et al., 2005).

As an alternative to standardized and commonly-used assays such as DCF-DA, LDH or MTT, a novel assay using the SensorDish[®] Reader (SDR) was established. This method allows an automated and combined online detection of ROS generation and cytotoxicity *in vitro*. This method was so far applied for the monitoring of cell cultivation, bacterial respiration and the validation of cytotoxicity caused by several drugs (Beckers et al., 2009; Kensy et al., 2005; Noor et al., 2009). The measurement principle is based on the automated online monitoring of the molecular oxygen concentration in a microtiter plate format (Kocincova et al., 2008). Cellular respiration is associated with a consumption of oxygen and therefore serves as an indicator for cytotoxicity. Cytotoxicity can be determined measuring the long-term cellular consumption of oxygen during cell incubation. An increase in air saturation caused by decreased cellular consumption of oxygen is a very early indication for cytotoxicity before other toxicity markers such as mitochondrial dysfunction or destruction of the cell membrane can be detected. The generation of ROS as an indication for oxidative stress was determined indirectly measuring the conversion of oxygen radicals via superoxide dismutase.

3.2 AIM OF THE STUDY

Aim of this study was to evaluate an alternative to standardized assays for the detection of cytotoxicity and oxidative stress *in vitro*. For this purpose the SensorDish[®] Reader (SDR) was used. In this study, a first-time combined non-invasive method for the detection of ROS and cytotoxicity *in vitro* based on the cellular consumption of molecular oxygen was established. Therefore, the SDR assay had to be adjusted for the detection of ROS in cellular systems, as the method had never been used before for this application. For this establishment H₂O₂ served as a model substance for the generation of ROS causing oxidative stress. The involvement of the SOD during exposure to H₂O₂ was investigated as well. Furthermore, the novel assay was evaluated by comparison with well known standardized assays for the detection of ROS (DCF-DA) and cytotoxicity (LDH and MTT).

This new established assay allows the evaluation of the oxidative and cytotoxic potential of different silica nanoparticles with various sizes and surface modifications.

3.3 MATERIALS AND METHODS

3.3.1 Materials

Dulbecco's modified eagle medium with high glucose (4.5 g/l) and L-glutamine was obtained from Gibco (Karlsruhe, Germany), fetal bovine serum was purchased from PAN-Biotech (Aidenbach, Germany), non-essential amino acids were obtained from PAA (Cölbe, Germany). 2', 7'-dichlorofluorescein diacetate (97%), 2', 7'-dichlorofluorescein (~90%), sodium diethyldithiocarbamate trihydrate, hydrogen peroxide (30%), thiazolyl blue tetrazolium bromide, bovine serum albumin and polyethylenimine (PEI) (25 kDa) were purchased from Sigma (Munich, Germany). Composition of Hank's balanced salt solution was as follows: 136.9 mM NaCl, 5.4 mM KCl, 4.26 mM NaHCO₃, 0.35 mM KH₂PO₄, 5.5 mM glucose, 10 mM HEPES, 1.26 mM CaCl₂, 0.5 mM MgCl₂*6H₂O, 0.4 mM MgSO₄*7H₂O. Hank's balanced salt solution was adjusted to pH 7.4 by means of NaOH. Cytotoxicity detection kit for lactate dehydrogenase was purchased from Roche Applied Science (Mannheim, Germany), OxoDish[®] plates were obtained from PreSens (PreSens

Precision Sensing GmbH, Regensburg, Germany). BreathSeal[®] foils were obtained from Greiner bio-one (Essen, Germany).

3.3.2 Caco-2 cell culture

The human colon adenocarcinoma cell line, Caco-2, clone C2Bbe1, was purchased from American Tissue Culture Collection (ATCC, Manassas, VA) and used at passages 60-80. Cells were cultured in Dulbecco's modified eagle medium (DMEM) with high glucose (4.5 g/l) and L-glutamine, supplemented with 10% fetal calf serum (FCS) and 1% non-essential amino acids and were maintained under standard culture conditions at a temperature of 37°C and in a humidified atmosphere of 5% CO₂. The culture medium was changed three times a week. For oxygen measurements with the SensorDish[®] Reader (SDR), Caco-2 cells were cultured in 24-well OxoDish[®] plates at a density of 1×10^5 cells per well in 1 ml culture medium and were allowed to attach and proliferate for 96 hours. For the determination of the conversion of DCF-DA into DCF (DCF-DA assay), Caco-2 cells were plated into 96-well plates at a density of 2×10^4 cells per well in 0.2 ml culture medium and allowed to attach and proliferate for 96 hours as well. For MTT assay Caco-2 cells were cultured also in 96-well plates in a density of 2×10^4 cells per well and were cultivated for 8 days.

3.3.3 SensorDish[®] Reader (SDR)

The SensorDish[®] Reader (SDR) is an innovative system for the measurement of the molecular oxygen concentration (O₂) in solution. For this purpose special 24-well plates (OxoDish[®] plates) were used. These sterile multidishes contain sensor spots on the bottom of each well, which consist of an oxygen-sensitive fluorescent dye embedded in a tissue compatible polymer (Figure 3.2). The fluorescence lifetime of this dye depends on the amount of oxygen in solution. The emitted sensor signal is read out non-invasively through the bottom of the OxoDish[®] plates by the SDR and is converted automatically to e.g., oxygen air saturation (%) or oxygen concentration (mg/L) using calibration parameters provided in the corresponding software (SDR_V37). A decrease in air saturation refers to an increase in oxygen consumption which is indicative for viable cells, whereas an increase in air saturation indicates a loss of cellular activity. The calculated alteration in air saturation results from the difference between the value for air saturation under normal culture conditions (buffer control) and the value of the top of an amplitude which develops e.g., after application of

H₂O₂. Measurements can be performed in user-defined time intervals. To avoid evaporation effects in the 24-well plates, all dishes were sealed with an air- and gas-permeable foil (BreathSeal[®] foils).



A
Figure 3.2: Assembling of the SensorDish[®] Reader (SDR). **(A)** SDR with an OxoDish[®] plate on top. Sensor spots are immobilised at the bottom of each well. **(B)** Measurement principle of the SDR. The sensor is excited by the reader non-invasively through the transparent bottom of the OxoDish[®] plates. Its emission is detected from the bottom side as well. Images were received from PreSens (Regensburg, Germany).

For the detection of oxidative stress, Caco-2 cells were cultured for 96 hours in OxoDish[®] plates. Alterations in air saturation were documented every hour during cell cultivation. After the cell culture medium was removed, H₂O₂ in different concentrations (75, 150, 300, 1000 and 2000 µM) diluted in DMEM was added to the cells. To analyse the involvement of the SOD in the course of the assay establishment, cells were pre-incubated for 24 hours with the SOD inhibitor diethyldithiocarbamate trihydrate (DDC). This hydrophobic chelating agent removes Cu (II) ions from the active site and thus inactivating the SOD (Fridovich, 1986; Khazaei et al., 2009). Cells were treated with different concentrations (20, 100 and 200 µM) of DDC before 2000 µM H₂O₂ were applied as described before. MTT experiments demonstrated no cytotoxic effect of the used DDC concentrations (data not shown). For the evaluation of the oxidative potential of nanoparticles, cells had been additionally washed with HBSS, whereupon various nanoparticles in different concentrations (10, 50, 100, 200 and 500 µg/ml) were added to the cells. H₂O₂ in a concentration of 1000 µM served as a positive control. After addition of the test substance measurements were performed every minute for 1 hour.

For detection of cytotoxicity, Caco-2 cells were treated as described in the paragraph above. Triton-X (0.000001-1%), polyethylenimine (PEI) (0.01-100 µg/ml) or different nanoparticles

in different concentrations (10-500 $\mu\text{g/ml}$) (dispersed in HBSS) were added to the cells. The consumption of molecular oxygen, indicative for the cell growth behaviour, was detected over 24 hours every hour. Triton-X served as a positive control for cytotoxicity. To investigate, if the cytotoxic effects are reversible, Caco-2 cells were cultured for 48 hours as described before. Afterwards cells were treated for 4, 8 and 24 hours with nanoparticles dispersed in HBSS or with HBSS alone. After these incubation times (4, 8 and 24 hours), cells were rinsed with HBSS and were cultured in DMEM for further 72 hours.

To exclude the detection of chemical reactions due to H_2O_2 or nanoparticles, all experiments were additionally performed in a cell-free milieu as well. Therefore, OxoDish[®] plates were incubated with DMEM under standard cell culture conditions in the absence of cells. Afterwards H_2O_2 or nanoparticles were added as described before.

3.3.4 DCF-DA assay

The production of intracellular ROS was measured using 2', 7'-dichlorofluorescein diacetate (DCF-DA). DCF-DA is a non-ionic, non-polar and non-fluorescent fluorescein derivative which is able to cross cell membranes and is hydrolyzed enzymatically by intracellular esterases. In the presence of ROS DCF-DA is oxidized to the highly fluorescent dichlorofluorescein (DCF). A 10 mM DCF-DA stock solution (in dimethyl sulfoxide, DMSO) was diluted in Hank's balanced salt solution (HBSS) with 1% bovine serum albumin (BSA) to obtain a working solution with a concentration of 20 μM . Final DMSO concentration was kept below 0.2%. After cell cultivation, Caco-2 cells were washed twice with HBSS supplemented with 1% BSA, followed by an incubation of DCF-DA at 37°C for 30 minutes. After that period DCF-DA was removed and H_2O_2 in different concentrations (75-1000 μM) or nanoparticle dispersions (10-500 $\mu\text{g/ml}$) were added and incubated at 37°C for 180 minutes. This time point had been determined in previous time kinetic experiments, where an increase in fluorescence over time had been shown (data not shown). HBSS with 1% BSA served as negative control. To investigate the suitability of different buffers and media, the above described experiment was performed with HBSS, DMEM and DMEM without phenol red, respectively. Emission of the developed fluorescence was analyzed with a fluorescence plate reader (Infinite M200, Tecan, Crailsheim, Germany) using a 485 nm extinction filter and a 530 nm emission filter. Measurements were performed immediately after addition of H_2O_2 or after a 180-minute-incubation.

3.3.5 LDH assay

The release of lactate dehydrogenase (LDH) from damaged cells was detected in a two-step enzymatic reaction. In the first step LDH catalyzes the conversion of lactate to pyruvate, which results in the reduction of NAD^+ to NADH/H^+ . In a second step the catalyst transfers H/H^+ from NADH/H^+ to the tetrazolium salt INT which is reduced to a water-soluble formazan dye. The absorbance of this formazan dye was measured at an absorbance of 492 nm (Infinite M200, Tecan, Crailsheim, Germany). Caco-2 cells were treated with different concentrations of triton-X (0.000001%-1%) or different nanoparticles (N50-RITC and N50-P-RITC) in different concentrations (100-500 $\mu\text{g}/\text{ml}$). The release of LDH into the supernatant was analyzed after 2, 4, 6 and 8 hours. An interference of the used nanoparticles with the LDH assay was excluded performing substance control tests beforehand (data not shown).

3.3.6 MTT assay

Cells were treated with N50-RITC and N50-P-RITC particles in a concentration of 200 $\mu\text{g}/\text{ml}$ in HBSS and were incubated for 4, 8 or 24 hours. The MTT reagent was subsequently added for further 4 hours. Cytotoxicity was determined by measuring the reduction of the yellow tetrazolium salt thiazolyl blue tetrazolium bromide (MTT) to water-insoluble purple formazan crystals by metabolic active cells. Formazan crystals were extracted with DMSO and their absorbance was measured at 550 nm (Infinite M200, Tecan, Crailsheim, Germany). An interference of the used nanoparticles with the MTT assay was excluded performing substance control tests beforehand (data not shown).

3.4 RESULTS

3.4.1 Establishment of a method for the combined determination of oxidative stress and cytotoxicity via SDR measurements

3.4.1.1 Determination of oxidative stress via SDR

3.4.1.1.1 *Cell concentration- and H₂O₂ concentration-dependent increase in molecular oxygen*

The SDR had previously been used for the monitoring of cell cultivation and the non-invasive determination of cytotoxicity based on cellular O₂ consumption. For its application in the detection of oxidative stress in human cell culture systems, a new assay had to be established. For this purpose, H₂O₂ served as a model substance to generate ROS resulting in oxidative stress in Caco-2 cells. After cells were cultivated for 96 hours under standard cell culture conditions, H₂O₂ in different concentrations, (75-2000 µM) diluted in cell culture medium (DMEM), was added to the cells. Measurements of the resulting oxygen concentration were performed directly after addition of H₂O₂. Figure 3.3 A shows exemplarily a typical SDR run of control cells (treated with DMEM alone) (black circles) and cells treated with 1000 µM H₂O₂ (open circles). Immediately after the addition of H₂O₂ (Figure 3.3 A, arrow) a strong increase in air saturation ($+55.50\% \pm 0.54$) and consequently in the concentration of molecular oxygen was documented. This effect reached a maximum after 1 hour, followed by a short stagnation with a subsequent decrease of molecular O₂. Control cells also showed a low increase in air saturation ($+6.35\% \pm 0.93$) due to variations in temperature. Within about six hours, control cells reached nearly their basic value ($-3.77\% \pm 0.80$), whereas cells which were incubated with 1000 µM H₂O₂ exhibited a great difference between the amount of air saturation before application of H₂O₂ and after the reaction ($+14.34\% \pm 2.11$) (Figure 3.3 A). This observed effect was associated with the amount of cells as can be shown in Figure 3.3 B. H₂O₂ in a concentration of 1000 µM was added to Caco-2 cells, which were cultured for 48, 72 or 96 hours. Cells which were cultured for 48 or 72 hours exhibited a reduced reaction to H₂O₂ when compared to cells cultivated for 96 hours. The air saturation was increased by $+23.28\% \pm 2.53$ for Caco-2 cells cultured for 48 hours and by $+33.67\% \pm 2.7$ for cells cultured for 72 hours (Figure 3.3 B).

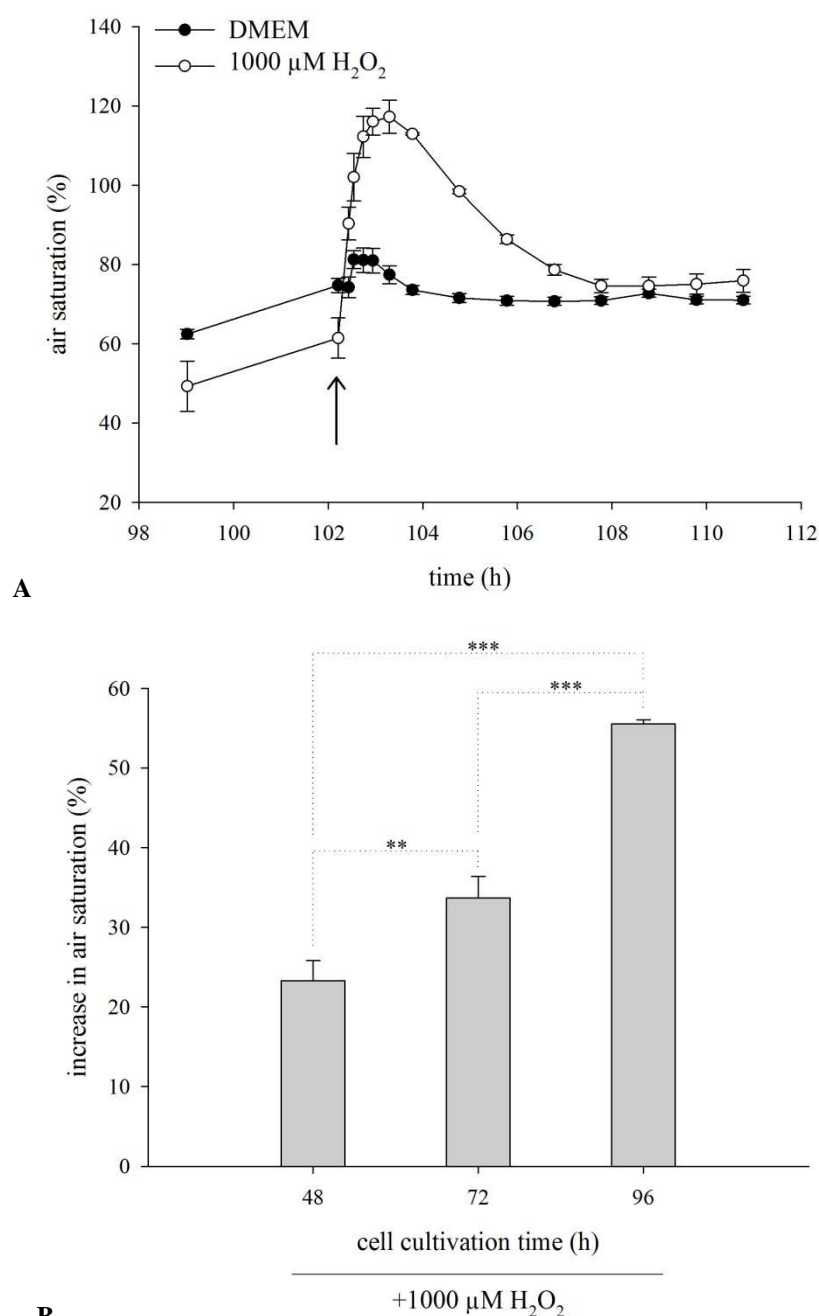


Figure 3.3: Influence of H_2O_2 on Caco-2 cells. **(A)** Run of an SDR experiment to measure indirectly the generation of oxygen radicals in Caco-2 cells cultivated for 96 hours under standard cell culture conditions. Measurements were performed every minute after application of DMEM as control or H_2O_2 (arrow). For clarification not all time points were plotted. Data represent the mean \pm SD of three wells. **(B)** Cell concentration-dependent increase in air saturation after application of H_2O_2 . Caco-2 cells were cultivated for 48, 72 and 96 hours under standard cell culture conditions. Afterwards 1000 μM H_2O_2 was added to the cells. Plotted data were calculated by subtracting the starting air saturation from the maximal occurred air saturation. Data represent the mean \pm SD of three wells. The asterisks depict significant differences between different cell cultivation times ($p \leq 0.01$ **, $p \leq 0.001$ ***).

The results of three independent experiments with different concentrations of H_2O_2 (75-2000 μM) are presented in Figure 3.4 A, where a concentration-dependent increase of oxygen concentration could be detected. H_2O_2 in a concentration of 75 μM did not increase the air saturation compared to the DMEM control, while 2000 μM H_2O_2 resulted in a highly significant increase ($p \leq 0.00058$). The used concentrations of H_2O_2 and the resulting increase in air saturation exhibited a very strong correlation with a coefficient of determination of 0.9636 (Figure 3.4 B).

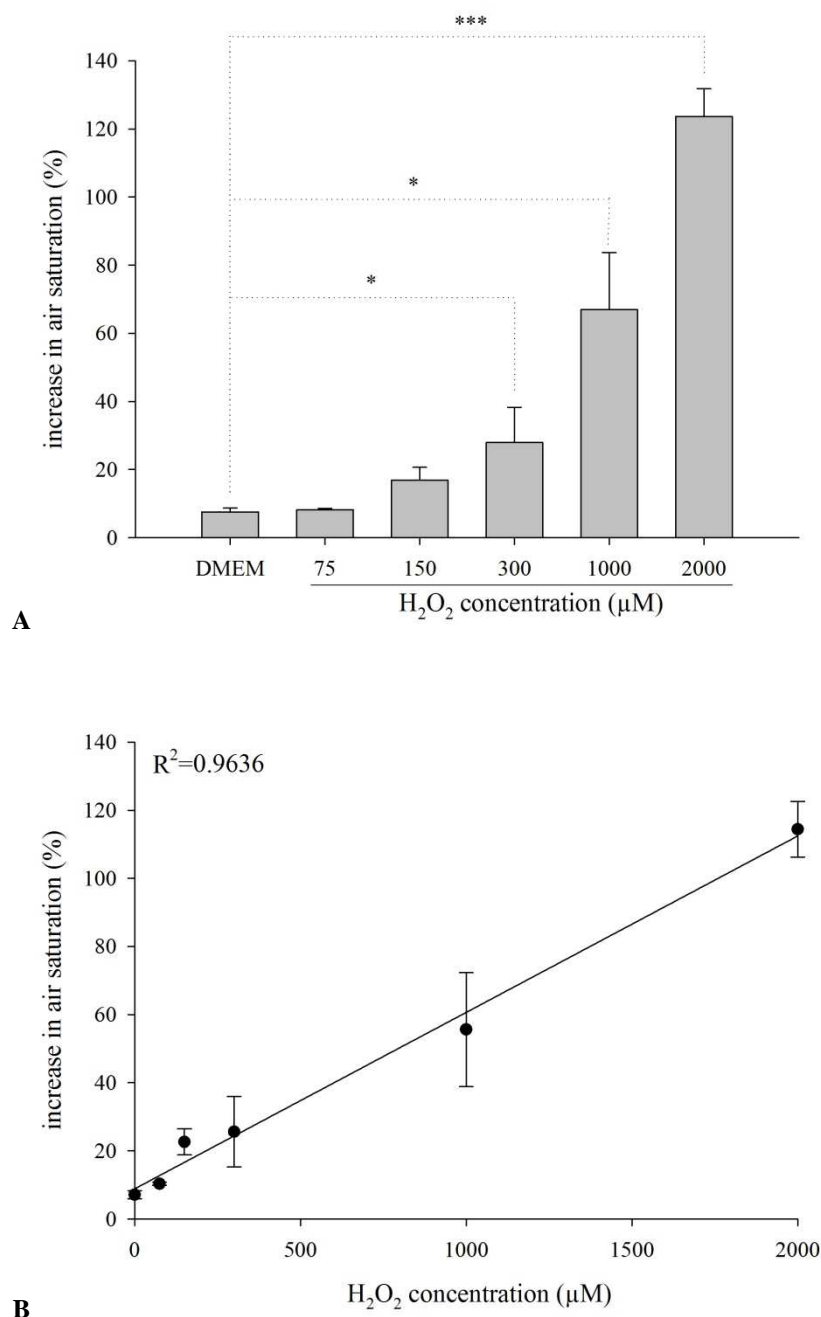


Figure 3.4: Increase in air saturation due to the application of H₂O₂. **(A)** H₂O₂ in different concentrations (75-2000 μM) was added to Caco-2 cells cultured for 96 hours. Plotted data were calculated by subtracting the starting air saturation from the maximal occurred air saturation. Data represent the mean ± SD of three independent experiments. The asterisks depict significant differences between the control and H₂O₂ treated cells ($p \leq 0.05$ *, $p \leq 0.001$ ***). **(B)** Correlation between H₂O₂ concentration and the increase in air saturation. Data represent the mean ± SD of three independent experiments.

As the degradation product of H₂O₂ is O₂ as well, it was necessary to investigate the behaviour of H₂O₂ in a milieu without any cells to exclude a chemical effect only. Directly after the addition of H₂O₂, this cell-free experiment showed a decrease in air saturation

(Figure 3.5, black bars). The rising of the oxygen concentration during the experiment was similar to that of control cells treated with DMEM alone (Figure 3.5, grey bars). These results confirmed a cellular and therefore biological answer to H_2O_2 and excluded a chemical reaction.

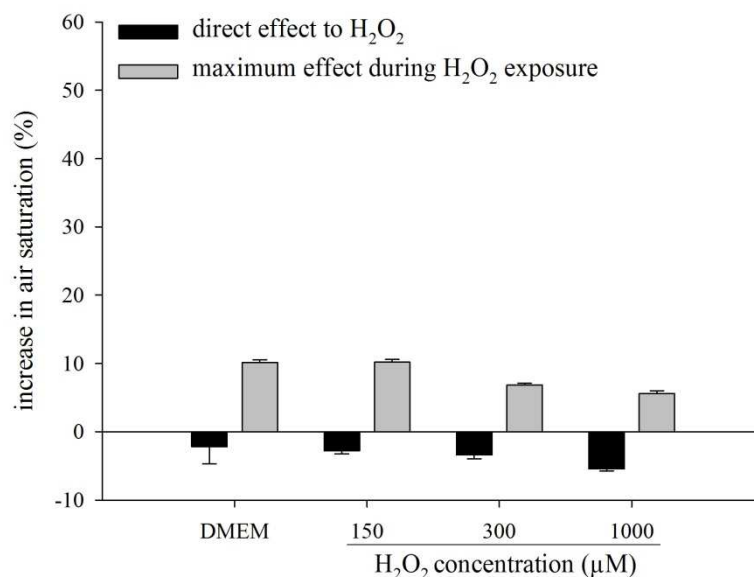


Figure 3.5: SDR experiments in absence of cells. OxoDish[®] plates were incubated with DMEM under normal cell culture conditions but in absence of cells. H_2O_2 in different concentrations (150-1000 μM) was added to the DMEM medium. The direct effect (black bars) as well as the maximum effect during H_2O_2 exposure (grey bars) were determined. Data represent the mean \pm SD of three independent experiments.

3.4.1.1.2 Involvement of the SOD in the H_2O_2 -induced effect

The observed H_2O_2 -induced effect of Caco-2 cells was supposed to be caused by the SOD. To prove the involvement of the SOD, an enzyme of the antioxidant defence mechanism, Caco-2 cells were pre-incubated with DMEM or the specific SOD-inhibitor DDC (20-200 μM) for 24 hours. After this pre-incubation cells were treated with 2000 μM H_2O_2 . Samples which were not pre-incubated with DDC showed a strong increase in molecular oxygen ($+125.99\% \pm 7.81$) as could be detected already in previous experiments. The pre-incubation with 20 μM DDC caused a reduction in air saturation of 73.57% compared to control cells incubated with DMEM without DDC. DDC in a concentration of 100 μM exhibited a further reduction of the H_2O_2 induced effect ($+2.57\% \pm 0.42$) or even resulted in a decrease of air saturation when using 200 μM DDC ($-15.98\% \pm 0.33$) (Figure 3.6) which is an indication for a complete inhibition of the SOD. Previous MTT experiments demonstrated no cytotoxic effect of the used DDC concentrations (data not shown).

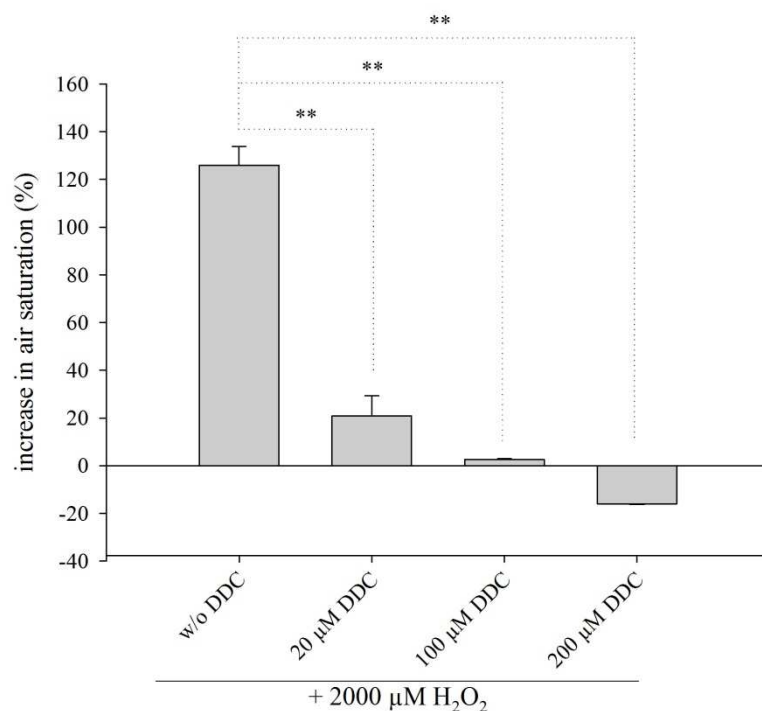


Figure 3.6: Influence of DDC on the H_2O_2 -induced effect. Caco-2 cells were cultured for 96 hours. Cells were pre-incubated for 24 hours with DDC in different concentrations (20-200 μM) followed by the addition of 2000 μM H_2O_2 . Bars show the alteration in air saturation after H_2O_2 application by subtracting the starting air saturation from the maximal occurred air saturation. Data represent the mean \pm SD of three independent experiments. The asterisks depict significant differences between control and DDC treated cells ($p \leq 0.01$ **).

3.4.1.1.3 Comparison with the DCF-DA assay

The authenticity of experiments with this novel technique was confirmed with a conventional fluorimetric assay for the detection of oxidative stress using 2', 7'-dichlorofluorescein diacetate (DCF-DA). Furthermore, the comparability of the SDR assay with a standardized method should be clarified. Caco-2 cells were pre-incubated with DCF-DA followed by a three-hour-incubation with different concentrations of H_2O_2 diluted in DMEM or HBSS with 1% BSA. The resulting emission values, based on the conversion of DCF-DA into the fluorescent dichlorofluorescein (DCF), were documented every hour over a 3-hour-incubation (data not shown). The occurred fluorescence is a parameter for the presence of ROS. The usage of the standard cell culture medium (DMEM) was not possible, because the medium interfered with the fluorescent measuring system. DMEM without addition of phenol red caused problems with the measurements technique as well (Figure 3.7 A). Thereupon, DCF-DA experiments were performed in HBSS supplemented with 1% BSA. Similar to the results of the SDR measurements, H_2O_2 caused a concentration-dependent increase in the

conversion of DCF-DA after three hours indicative for the generation of ROS (Figure 3.7 B). Thereby, the DCF-DA assay had a lower detection limit than the SDR assay.

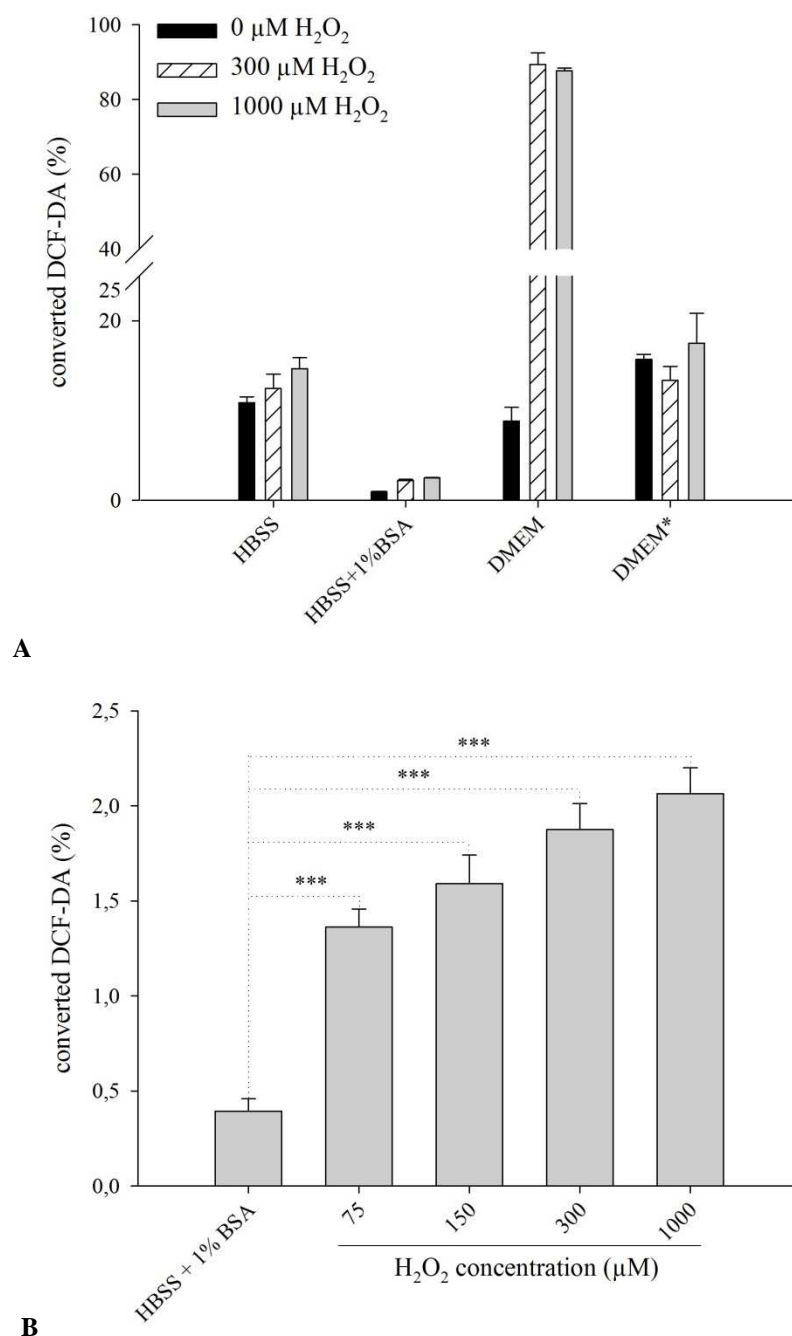


Figure 3.7: Standard DCF-DA assay for the detection of oxidative stress. **(A)** Fluorescence measurements of converted DCF-DA in HBSS, HBSS supplemented with 1% BSA, DMEM and DMEM without phenol red (DMEM*) after addition of H_2O_2 in different concentrations (0, 300 and 1000 μM). **(B)** Caco-2 cells were cultured for 96 hours and were pre-incubated with DCF-DA in HBSS+1% BSA for 30 minutes. Afterwards H_2O_2 in different concentrations (75-1000 μM) was added to Caco-2 cells followed by a 3-hour-incubation. Data represent the mean \pm SD of three independent experiments. The asterisks depict significant differences between the control and H_2O_2 treated cells ($p \leq 0.001$ ***).

Measurements were also performed directly after addition of H_2O_2 without a 3-hour-incubation step. No difference between several H_2O_2 concentrations and the HBSS + 1% BSA control could be observed (data not shown) which indicates that the conversion of DCF-DA into DCF seems not to be an immediate process and requires a longer incubation time.

3.4.1.2 Determination of cytotoxicity via SDR

To prove the correlation between the amount of cells and the consumption of molecular oxygen, Caco-2 cells were seeded with different cell numbers (6 300 – 78 900 cells per cm^2) in OxoDish[®] plates. The variation of the air saturation was measured every 30 minutes over 16 hours. Measurements were started with a delay of 1 hour, because the system needs about 1 hour to equilibrate (temperature and pH) after seeding the cells. Already 2 hours after seeding the cells a concentration-dependent decrease in air saturation was visible (Figure 3.8). The SDR run clarified that there is a strong correlation between the amount of seeded cells and the consumption of oxygen. A high cell concentration (79 000 cells per cm^2) showed a decrease in air saturation of $12.92\% \pm 4.16$ over 16 hours, whereas lower concentrated cells (6 300 cells per cm^2) caused a reduction in air saturation of $5.11\% \pm 0.56$. Cell-free samples showed no variation in air saturation during the whole experiment.

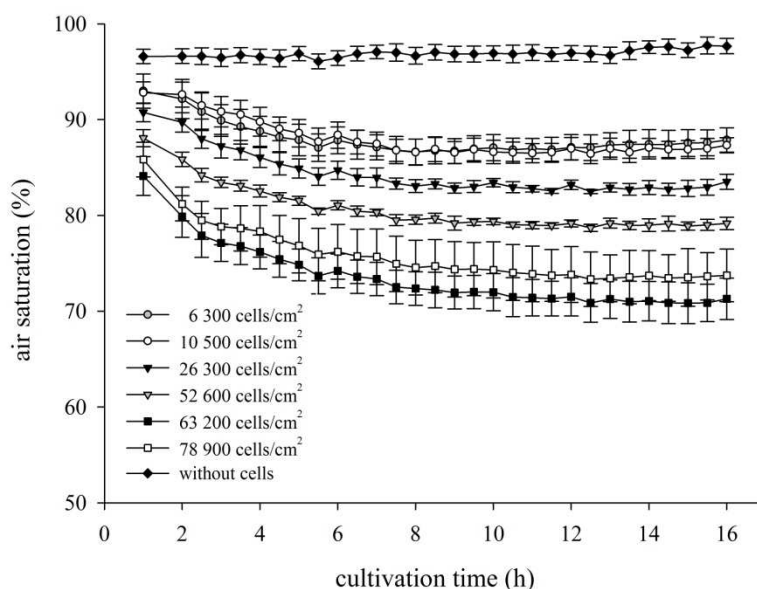


Figure 3.8: Alteration in air saturation correlates with the cell number. Air saturation profiles of several seeding densities of Caco-2 cells. Cells were seeded in different concentrations in OxoDish[®] plates and were cultured for 16 hours under normal cell culture conditions. Measurements were performed every 30 minutes. Data represent the mean \pm SD of three wells.

The cytotoxic potential of an added reagent is reflected by the decrease in cellular consumption of O_2 . For this purpose, triton-X served as a model substance causing cytotoxicity due to permeabilization of the cell membranes. Therefore, Caco-2 cells were treated with different concentrations of triton-X (0.000001%-1%) solved in DMEM. Samples incubated with the highest triton-X concentration (1%) showed a clear increase in air saturation directly after addition of triton-X. Air saturation values of samples with lower triton-X concentrations (0.0001%-0.1%) showed a concentration-dependent approximation to the highest triton-X concentration. However, control cells, cultivated in DMEM during the whole experiment, caused a decrease in air saturation over time which suggests a high consumption of molecular oxygen by viable cells (Figure 3.9 A). These results were proved with a standardized assay detecting the LDH release from damaged cells which is a commonly used and standardized marker for cell membrane integrity and cytotoxicity. Supernatants of all samples were collected simultaneously to the SDR measurements and analyzed concerning their LDH leakage over 8 hours. No clear concentration-dependent release of LDH could be detected for triton-X during the experiment. For the lower triton-X concentrations (0.000001%-0.01%) no increased LDH release could be detected when compared to the medium control, while the treatment with 0.1% and 1% triton-X showed already after two hours a very strong LDH release (Figure 3.9 B). In contrast to the SDR assay, where a clear concentration-dependent effect could be observed, the LDH assay exhibited either no or the maximal cytotoxic effect without any intermediate steps.

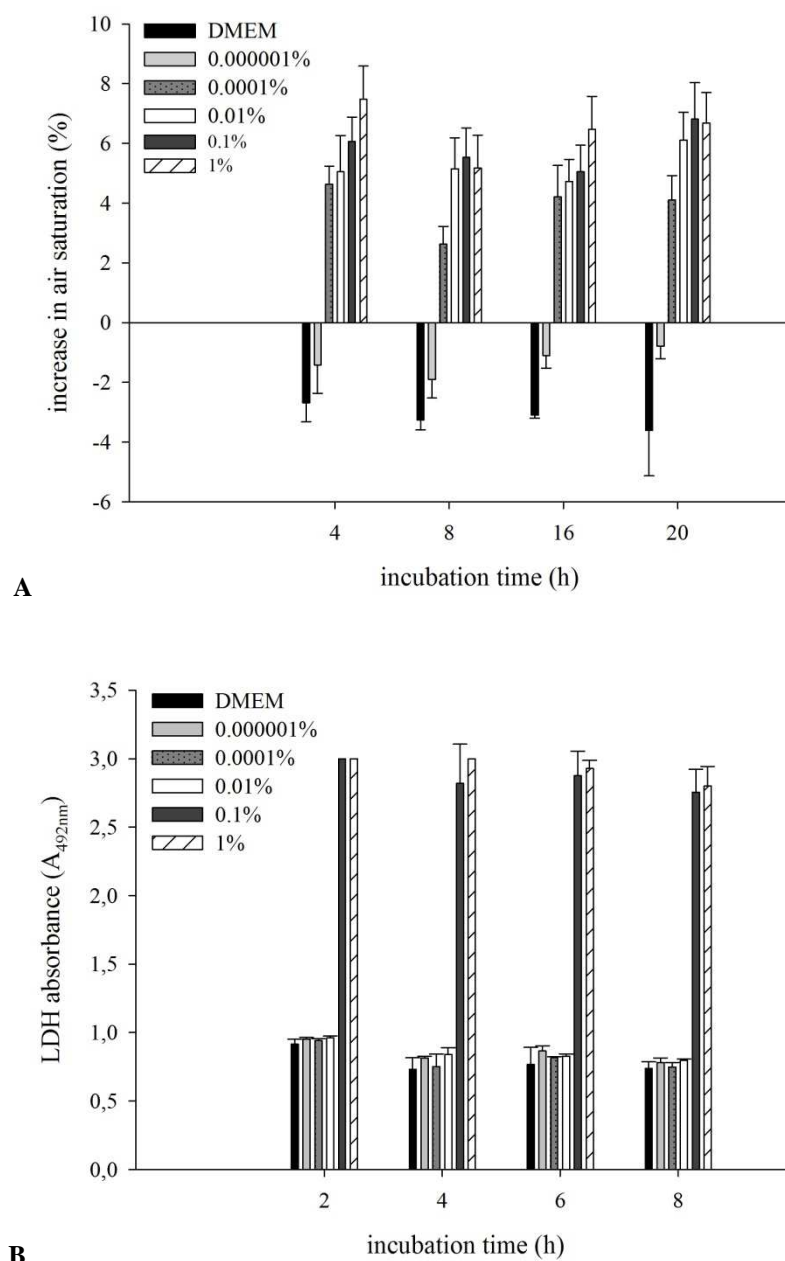


Figure 3.9: Air saturation correlates with occurred cytotoxicity. **(A)** Determination of triton-X-induced cytotoxicity via SDR measurements. Increase in air saturation due to the application of triton-X over time. Cells were incubated with different concentrations of triton-X solved in DMEM for 4, 8, 16 and 20 hours, respectively. **(B)** Determination of the triton-X-induced effect via LDH assay. Caco-2 cells were incubated with different concentrations of triton-X solved in DMEM. Supernatants were collected and analyzed concerning LDH leakage after 2, 4, 6 and 8 hours. Measurements were performed with an absorbance plate reader. Data represent the mean \pm SD of three independent experiments.

After finishing these establishment experiments, this novel assay could apply for the determination of oxidative stress and cytotoxicity in particulate systems such as silica nanoparticles.

3.4.3 Oxidative and cytotoxic potential of silica nanoparticles

3.4.3.1 Determination of the oxidative potential of silica nanoparticles via SDR in comparison to DCF-DA measurements

For determination of nanoparticulate-induced ROS generation, Caco-2 cells were plated for 96 hours in OxoDish[®] plates. Nanoparticles (N50-RITC, N50-P-RITC, N94-RITC and N94-P-RITC) were diluted in HBSS in different concentrations (10, 100, 200 and 500 µg/ml) and were added to the cells. H₂O₂ in a concentration of 1000 µM served again as a positive control for generation of ROS. Measurements were performed every minute after addition of nanoparticles. H₂O₂ with a concentration of 1000 µM showed a high increase in air saturation of $32.16\% \pm 5.83$ compared to the buffer control, while nanoparticles caused no significant increase in air saturation (Figure 3.10 A). This result could be also confirmed with a DCF-DA assay. Caco-2 cells plated in a 96-well plate were incubated with DCF-DA for 30 minutes, followed by addition of nanoparticles for further 180 minutes. H₂O₂ caused a conversion of DCF-DA into DCF of $3.05\% \pm 0.77$, whereas all tested nanoparticles showed no increased DCF-DA conversion compared to the buffer control ($0.93\% \pm 0.06$) (Figure 3.10 B).

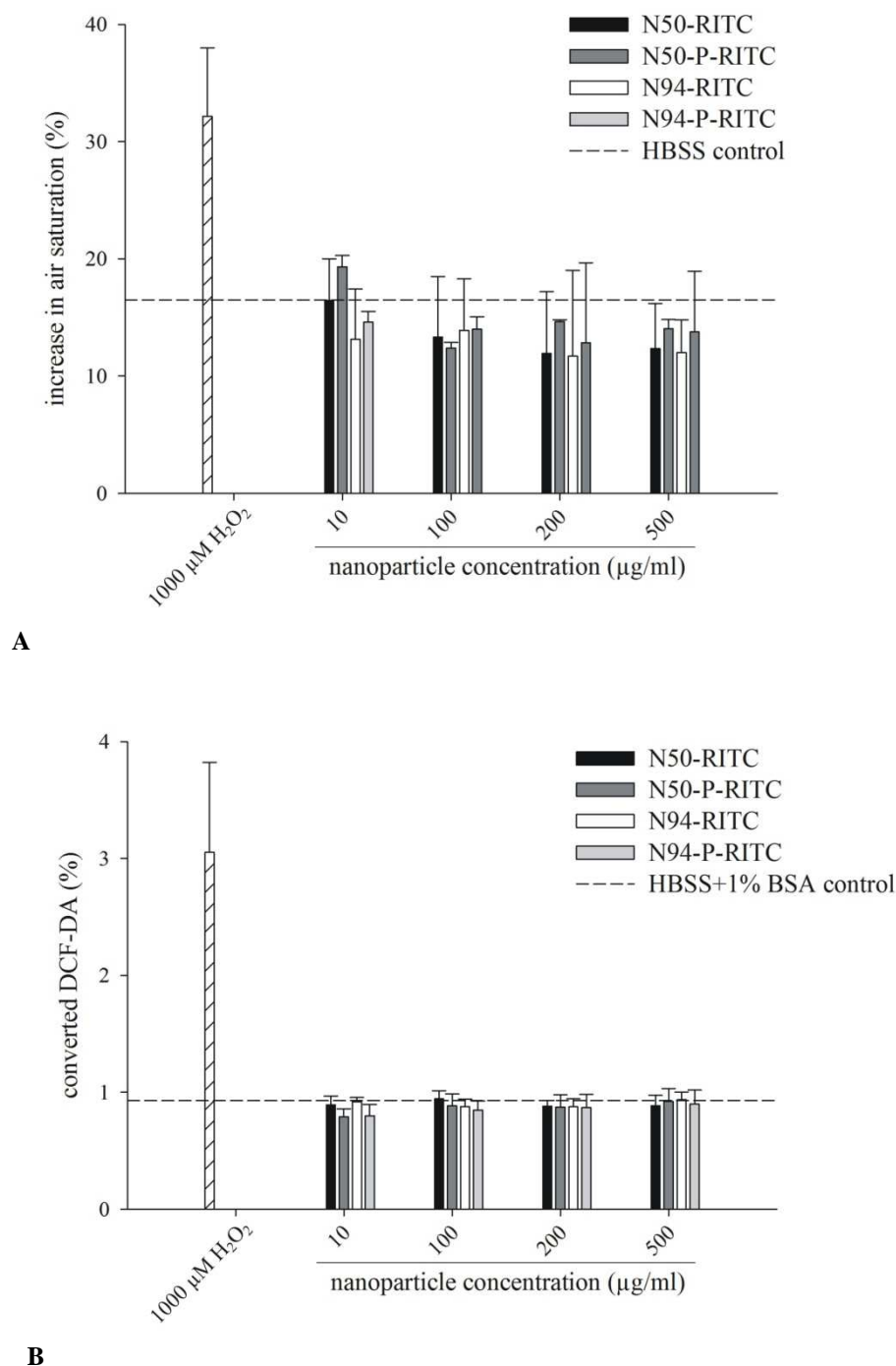


Figure 3.10: Determination of the oxidative potential of nanoparticles via SDR and DCF-DA measurements. **(A)** Detection of ROS generation via alteration in air saturation by SDR measurements. Different nanoparticles (N50-RITC, N50-P-RITC, N94-RITC and N94-P-RITC) in different concentrations (10-500 µg/ml) were added to Caco-2 cells plated in OxoDish® plates. H₂O₂ served as a positive control. **(B)** Detection of ROS generation via conversion of DCF-DA into DCF. Caco-2 cells were pre-incubated with DCF-DA for 30 minutes. Afterwards, different nanoparticles (N50-RITC, N50-P-RITC, N94-RITC and N94-P-RITC) in different concentrations (10-500 µg/ml) were added to the cells followed by a 3-hour-incubation. The buffer control (HBSS or HBSS + 1% BSA) is displayed by the dashed line. Data represent the mean ± SD of three independent experiments.

3.4.3.2 Size-, time-, surface modification- and concentration-dependent nanoparticulate cytotoxicity

Long-term determination of nanoparticulate cytotoxicity was measured on the basis of the consumption of oxygen over 24 hours. Caco-2 cells were plated for 96 hours in OxoDish® plates. For the cytotoxic evaluation of a particulate model substance, Caco-2 cells were incubated with PEI in different concentrations (0.01-100 µg/ml). PEI polymers are widely used as a transfection reagent in non-viral gene delivery. Used PEI polymers had a size of $12.02 \text{ nm} \pm 0.56$ when dispersed in HBSS in a concentration of 100 µg/ml. After addition of PEI, cells showed a time- and concentration-dependent decrease in oxygen consumption indicative for a cytotoxic effect of PEI. Concentrations up to 1 µg/ml caused no inhibition in cellular activity when compared to the buffer control. In contrast, cells treated with PEI in a concentration of 10 and 100 µg/ml exhibited a clear time- and concentration-dependent cytotoxic effect similar to that of the triton-X control (Figure 3.11).

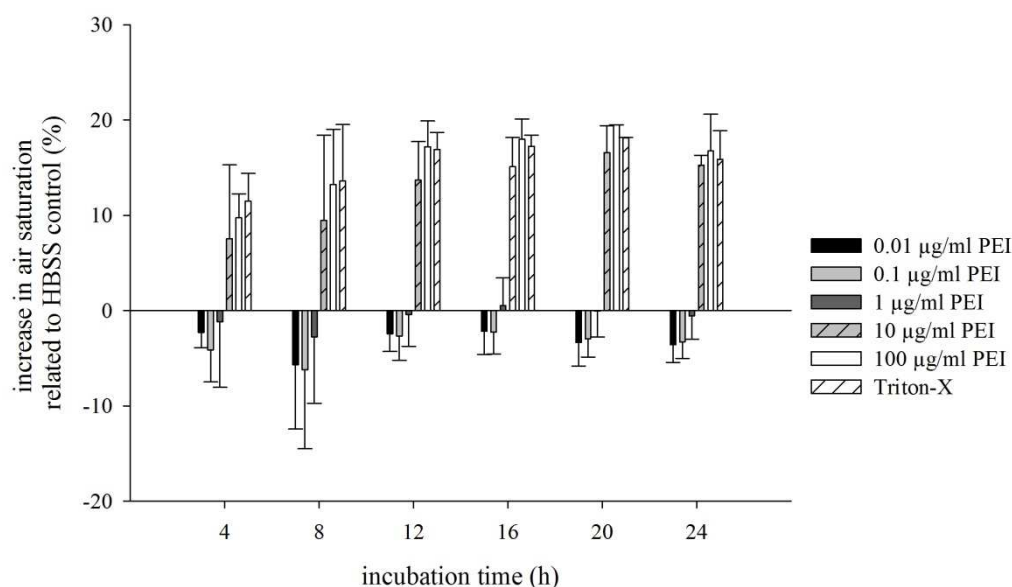


Figure 3.11: Cytotoxic potential of polyethylenimine (PEI) as a particulate model substance analysed via SDR. PEI in different concentrations (0.01-100 µg/ml) was added to Caco-2 cells cultivated for 96 hours. Measurements were performed every hour over 24 hours. Bars exhibit the additional consumption of O₂ related to the HBSS control after 4, 8, 12, 16, 20 and 24 hours. Data represent the mean \pm SD of three independent experiments.

For the cytotoxic evaluation of silica nanoparticles, various nanoparticles (N50-RITC, N50-P-RITC, N94-RITC and N94-P-RITC) were dispersed in HBSS in different concentrations (10, 100, 200 and 500 µg/ml) and were added to the cells. Triton-X in a concentration of 0.01% served as positive control for cytotoxicity. Measurements were performed every hour.

Already after 4 hours, a clear difference between the tested nanoparticles was visible. N50-RITC nanoparticles caused a clear increase in air saturation and consequently a reduced consumption of oxygen. Particularly, at higher concentrations (200-500 µg/ml) N50-RITC particles provoked a strong effect by adjusting to the air saturation values of the triton-X control indicative for cell death. After a 16-hour-incubation, N50-RITC particles in a concentration of 500 µg/ml caused a lower cellular oxygen consumption as the one documented for triton-X at this time point (Figure 3.12 A). N94-RITC particles as well as PEG-modified nanoparticles (N50-P-RITC and N94-P-RITC) showed no alteration in air saturation during the experiment when compared to the buffer control (HBSS) (Figure 3.12 B-D) and therefore did not generate cytotoxicity in Caco-2 cells. For N50-P-RITC and N94-P-RITC particles a minor cytotoxic effect could be detected after 24 hours.

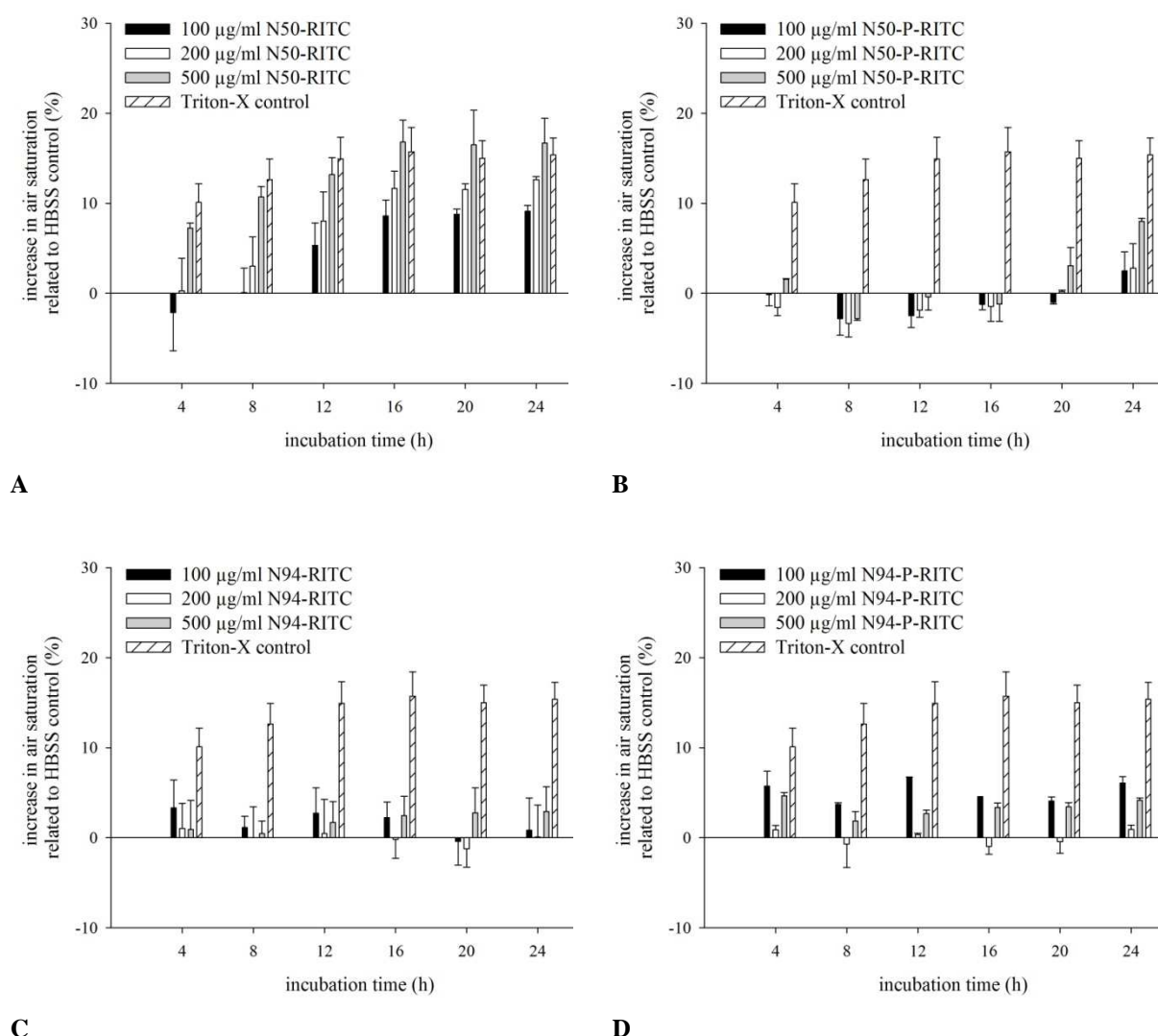


Figure 3.12: Determination of the cytotoxic potential of different RITC-labelled silica nanoparticles via SDR measurements. Nanoparticles in different concentrations (100-500 µg/ml) were added to Caco-2 cells. Measurements were performed every hour over 24 hours. **(A)** N50-RITC, unmodified nanoparticles, 50 nm, **(B)** N50-P-RITC, PEG-modified nanoparticles, 55 nm, **(C)** N94-RITC, unmodified nanoparticles, 94 nm, **(D)** N94-P-RITC, PEG-modified nanoparticles, 97 nm. Bars exhibit the additional consumption of O₂ related to the HBSS control after 4, 8, 12, 16, 20 and 24 hours. Data represent the mean \pm SD of three independent experiments.

To evidence the observed cytotoxicity, the LDH release after incubation with N50-RITC and N50-P-RITC particles in different concentrations (100-500 µg/ml) during the first 8 hours of the experiment were analysed simultaneously to the SDR measurements. A clear concentration- and time-dependent release of LDH could be detected for N50-RITC particles, whereas N50-P-RITC particles showed no increased LDH release compared to the HBSS control (Figure 3.13).

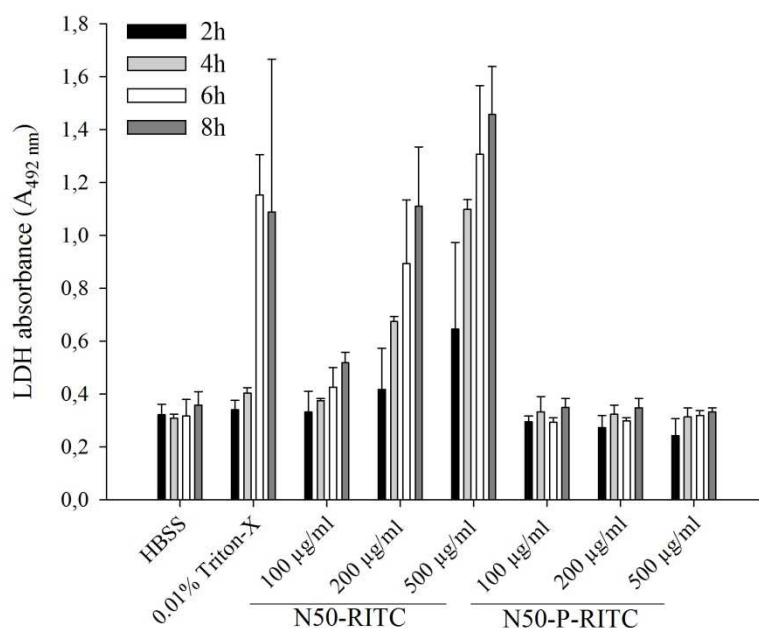


Figure 3.13: Determination of the cytotoxicity of silica nanoparticles via LDH assay. Caco-2 cells were incubated with N50-RITC and N50-P-RITC nanoparticles. Supernatants were collected and analyzed concerning LDH leakage after 2, 4, 6 and 8 hours. Data represent the mean \pm SD of three independent experiments.

In addition, an MTT assay was performed to evaluate the metabolic viability of the cells after incubation with nanoparticles. This assay was not able to detect the cytotoxic effects of N50-RITC nanoparticles which could be determined via LDH and SDR. Nanoparticles caused a decrease in metabolic viability over 24 hours but when compared to the HBSS control they all showed increased absorbance values indicative for an enhanced metabolic activity of the cells after nanoparticle incubation (data not shown).

Furthermore, to exclude a cytotoxic effect of the fluorescent dye RITC or other ingredients of the nanoparticle solution, Caco-2 cells were treated with free RITC and the supernatant of nanoparticle dispersions as well. No alteration in cellular viability could be demonstrated for these samples when compared to the buffer control. (data not shown).

3.4.3.3 PI-labelled nanoparticles caused a size-, time-, concentration-dependent and non-reversible cytotoxic effect in Caco-2 cells

As described before, Caco-2 cells were plated for 96 hours in OxoDish® plates. PI-labelled nanoparticles (N21-PI, N34-PI and N84-PI) were diluted in HBSS in different concentrations (20, 100, and 500 µg/ml) and were added to the cells. Again, triton-X in a concentration of 0.01% served as a positive control for cytotoxicity. Measurements were performed every hour over 24 hours. Caco-2 cells incubated with different sized nanoparticles in a concentration of 20 µg/ml exhibited no increase in air saturation when compared to the HBSS control. In contrast, nanoparticles in a concentration of 100 µg/ml and 500 µg/ml caused a clear size- and time-dependent cytotoxic effect. N84-PI nanoparticles in a concentration of 20 and 100 µg/ml had no influence on cellular viability at all. In a concentration of 500 µg/ml these particles already showed a very strong cytotoxic effect after an incubation of 8 hours (Figure 3.14 C). N34-PI nanoparticles in a concentration of 100 µg/ml demonstrated a clear effect after a 16-hour-incubation (Figure 3.14, B). Similar results could be also detected for N21-PI nanoparticles. They already caused cytotoxicity after a 8-hour-incubation (Figure 3.14, A) when applied in a concentration of 100 µg/ml. Higher concentrated (500 µg/ml) N34-PI and N21-PI nanoparticles exhibited a cytotoxic effect already after an incubation time of 4 hours.

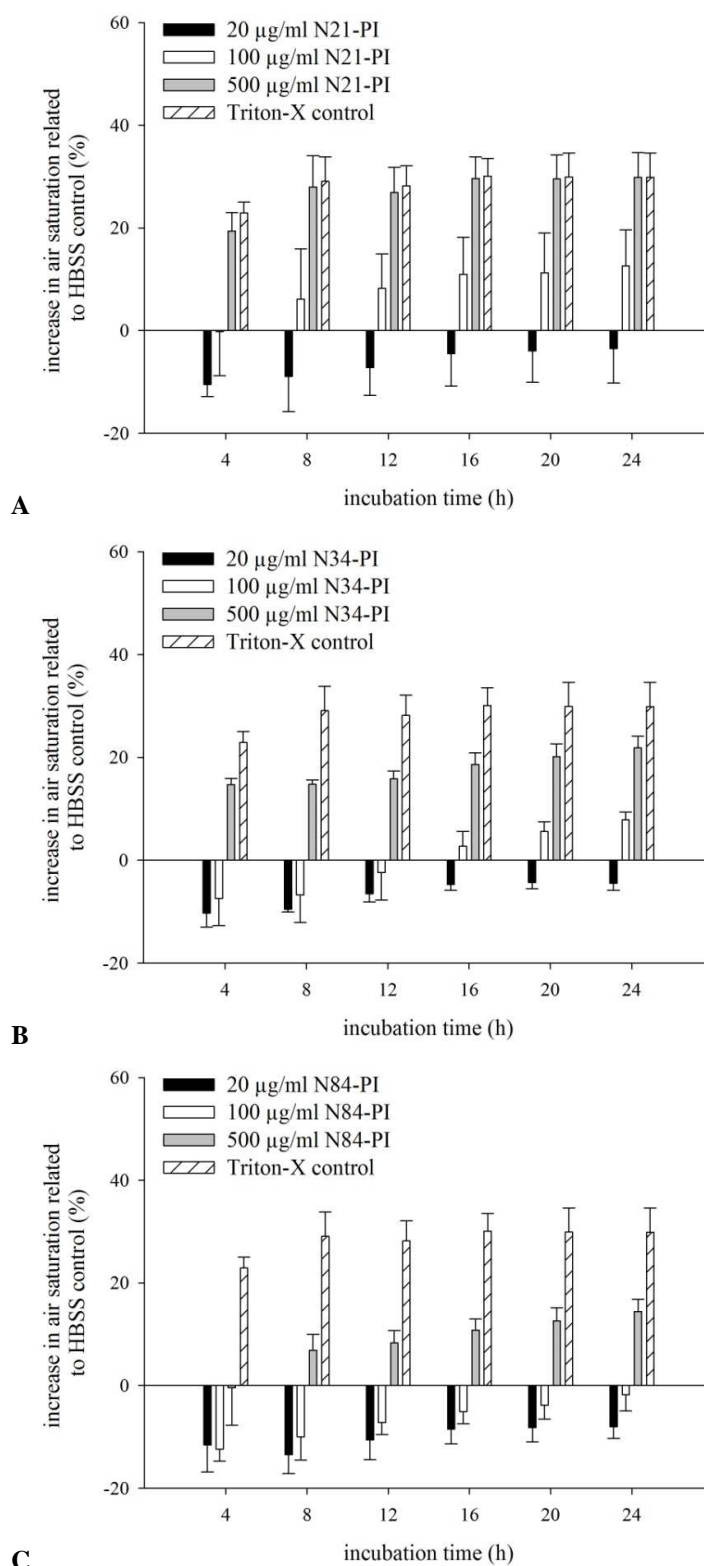


Figure 3.14: Determination of the cytotoxic potential of unmodified PI-labelled silica nanoparticles via SDR measurements. N21-PI, N34-PI and N84-PI nanoparticles in different concentrations (20, 100 and 500 µg/ml) were added to Caco-2 cells. Measurements were performed every hour over 24 hours. (A) N21-PI, (B) N34-PI, (C) N84-PI. Bars exhibit the additional consumption of O₂ related to the HBSS control after 4, 8, 12, 16, 20 and 24 hours. Data represent the mean ± SD of three independent experiments.

3.4.3.4 Nanoparticle-damaged Caco-2 cells do not regenerate

To investigate, if the observed cytotoxic effect of nanoparticles is reversible, Caco-2 cells were cultivated for 48 hours, subsequently cells were incubated with N34-PI or N84-PI nanoparticles for 4, 8 and 24 hours. As a control, cells were cultured in HBSS alone for 4, 8 and 24 hours. Figure 3.15 A shows exemplarily the SDR run of N34-PI treated cells with the corresponding HBSS controls, in comparison to cells cultured in DMEM (negative control) or in 0.01% triton-X (positive control). HBSS caused only a rather low decrease in cellular viability when compared to the DMEM control. In contrast, nanoparticle-treated cells exhibited a high increase in air saturation when compared to the DMEM control indicative for a decrease in cellular viability. After a 72-hour-incubation in DMEM, HBSS treated cells demonstrated still a consumption of oxygen indicative for metabolically active cells. In contrast, nanoparticle-incubated cells exhibited a size- and time-dependent decrease in oxygen consumption based on a cytotoxic effect of these nanoparticles. The nanoparticle induced cytotoxicity was not reversible within 72 hours (Figure 3.15 B).

As described before for RITC-labelled nanoparticles, a cytotoxic effect of the fluorescent dye PI or other ingredients of the nanoparticle solutions was excluded by treating cells with free PI or the supernatant of nanoparticle dispersions. No alteration in cellular viability could be demonstrated for these samples when compared to the buffer control. (data not shown).

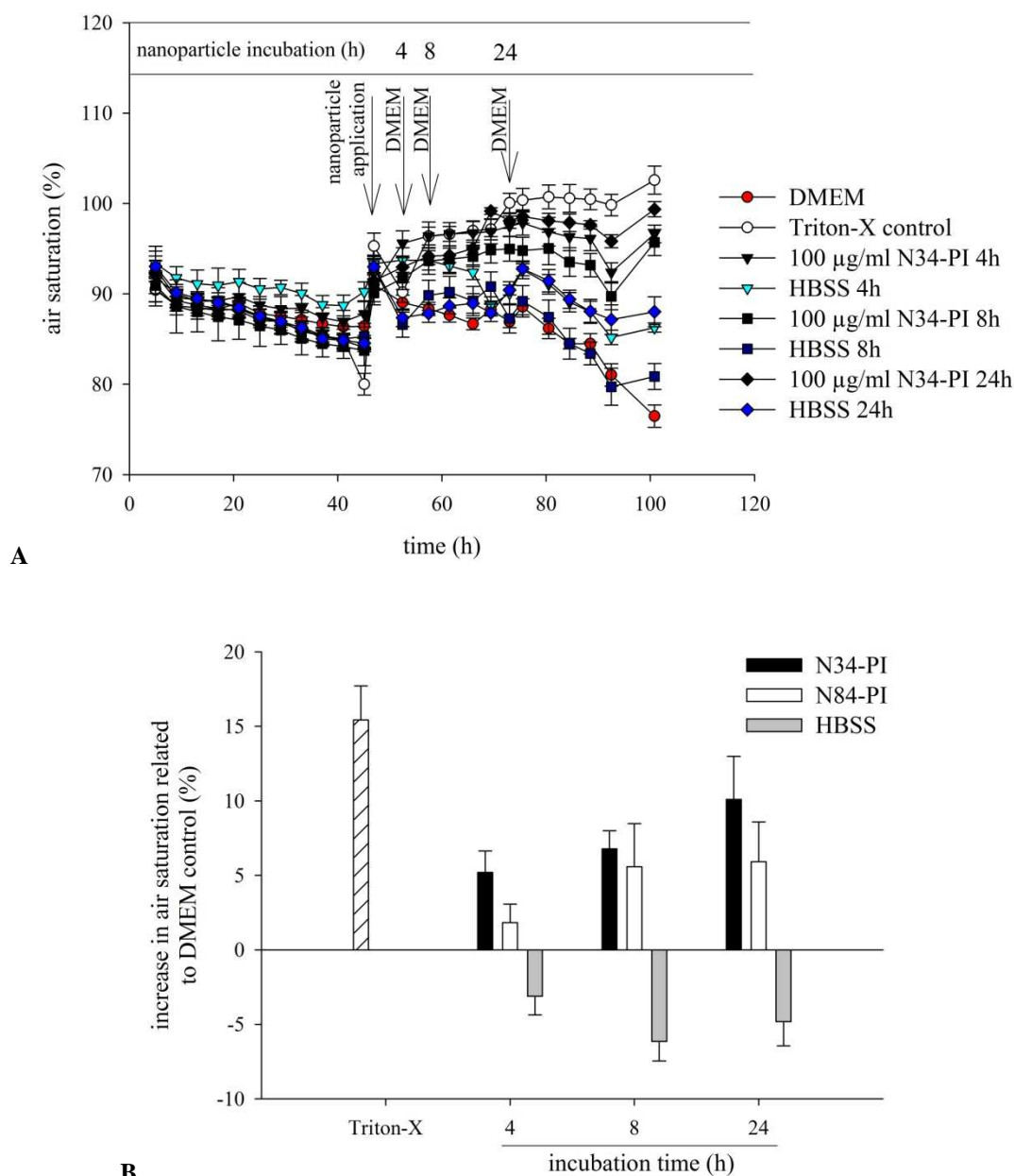


Figure 3.15: Reversibility of the nanoparticle induced cytotoxic effect. N34-PI and N84-PI nanoparticles in a concentration of 100 μ g/ml were added to Caco-2 cells and were incubated for 4, 8 and 24 hours. After this incubation time, cells were washed with HBSS and were cultivated in DMEM for further 72 hours under standard cell culture conditions. **(A)** SDR run of Caco-2 cells cultivated with N34-PI particles or HBSS for 4, 8 and 24 hours. Arrows mark the time point, when nanoparticle incubation was finished and Caco-2 cells were cultivated in DMEM again. Data represent the mean \pm SD of three wells. **(B)** Increase in air saturation related to the DMEM control after a 72-hour-incubation in DMEM. Triton-X in a concentration of 0.01% served as a positive control for cytotoxicity. Data represent the mean \pm SD of three independent experiments.

3.5 DISCUSSION

Silica nanoparticles have various advantages and characteristics which are promising tools in the medical and pharmaceutical field, but they are also known to cause cell damage such as oxidative stress or inhibition of cellular respiration (Eom & Choi, 2009; Park & Park, 2009; Tao et al., 2008; Wang et al., 2009). Recent publications reported the application of silica nanoparticles as drug and gene carrier (Bharali et al., 2005; Gemeinhart et al., 2005; Manzano et al., 2009; Simovic et al., 2010; Tan et al., 2010), which underline the importance to provide a safe method for the oxidative and cytotoxic evaluation of nanoparticles. Oxidative stress and cytotoxicity are two parameters which have to be analyzed, especially as these materials come into close contact with biological barriers, e.g., the gastrointestinal epithelium when administered via the oral route.

In case of oxidative stress, free radicals are the molecules of action. They seem to have a pathologic role in a variety of diseases such as atherosclerosis and cancer (Rice-Evans & Burdon, 1993; Trush & Kensler, 1991). Free radicals are produced permanently as natural metabolism products sustaining essential functions. By the time there is an imbalance of the generation and the decomposition of ROS, these molecules can impair cells. Typical sources of damaging ROS are e.g. ultraviolet rays as well as X- and ionising radiation. However, also pharmaceuticals such as diazepam or clofibrate (Bogdanska et al., 2007; Qu et al., 2001) and innovative drug delivery tools like nanoparticles can cause uncontrolled production of free radicals. Many different nanoparticles were already reported to induce oxidative stress in different cell lines. Cerium oxide nanoparticles caused an increase in ROS, which triggered the activation of cytosolic caspase-3 and a chromatin activation which led on the other hand to cytotoxicity via an apoptotic process (Park et al., 2008). Such an increase in ROS with a simultaneous decrease in glutathione could be also observed in human embryonic kidney cells after incubation with amorphous SiO₂ nanoparticles (Wang et al., 2009). In addition to the formation of ROS, silica nanoparticles have also been shown to induce heme-oxygenase-1, another antioxidative enzyme (Eom & Choi, 2009). A comparative study demonstrated that metallic nanoparticles caused oxidative stress eight times higher if compared to aqueous solutions of the same metals (Limbach et al., 2007). These findings suggest for an in-depth examination of these new materials with regard to the production of ROS.

For the detection of ROS *in vitro* various commercially available assays already exist using different markers for oxidative stress such as superoxide dismutase, glutathione or catalase. A well-established standard assay for the determination of ROS is the DCF-DA assay (Rosenkranz et al., 1992), a fluorescent based method which detects ROS generation by determining the conversion of DCF-DA into DCF. However, the assay exhibits several disadvantages as its long incubation time of at about 1 hour and particularly that it is an invasive and end-point assay. Furthermore, this assay shows various interactions with assay media or buffers. Grzelak et al. already demonstrated via DCF-DA assay a very high generation of ROS in many standard cell culture media such as DMEM or RPMI even without any addition of ROS-inducing substances (Grzelak et al., 2000; Grzelak et al., 2001). Similar results were obtained in a DCF-DA experiment with Caco-2 cells. In this study, it could be shown that pH indicators such as phenol red could cause interactions with the measurement principle. This common medium supplement resulted in a very high background fluorescence which interacted with the measuring wavelength of DCF. In contrast, experiments with DMEM without any addition of phenol red caused another difficulty. In these samples no difference in DCF-DA conversion between single H₂O₂ concentrations was visible. Because of its high complexity, cross reactions with various ingredients could not be excluded. Therefore, it was necessary to use special buffers coming along with an alteration in standard culture or experimental conditions. This again may result in stressed cells and consequently in an interference with experimental results. However, physiological buffers, such as HBSS, without any protein addition showed already in the negative control a very high conversion of DCF-DA into DCF causing a high background. The lack of proteins resulted in metabolically stressed cells. These experiments clarified the high limitation in the choice of buffers or media. Consequently, the DCF-DA assay is very sensitive to different cell culture buffers or media due to various interferences. Furthermore, new materials such as nanoparticles often show interactions with the measurement principles itself. This could already be demonstrated for standardized assays for the detection of cytotoxicity (Wahl et al., 2008; Worle-Knirsch et al., 2006). Therefore, it is recommended to evidence data of these techniques with at least two or more independent test systems (Worle-Knirsch et al., 2006). Opinions of different European institutions support this proposal (EFSA, 2009; SCCP, 2007).

These findings clarify the high demand for the establishment of alternatives to already available assays. Therefore, in the present study a non-invasive assay for the combined detection of ROS and cytotoxicity using the SDR was established. Thereby, the intestinal

adenocarcinoma cell line Caco-2 served as an *in vitro* model with regard to the development of oral nanoparticulate drug delivery systems. The innovative method is based on a fluorescent measuring principle detecting specifically solved molecular oxygen (O_2) in the samples (Beckers et al., 2009; Kensy et al., 2005). During the establishment for the detection of oxidative stress, H_2O_2 served as model substance for the generation of ROS *in vitro*. H_2O_2 can diffuse freely in and out of cells and tissue. Its ability to cross biological membranes allows targeting a wide range of intracellular and extracellular structures. *In vitro*, H_2O_2 oxidizes cellular ferrous iron into ferric iron, hydroxyl radical and hydroxyl anion via Fenton reaction by the following molecular equation: $Fe^{2+} + H_2O_2 \rightarrow Fe^{3+} + OH^\bullet + OH^-$. This reaction is a main source of oxidative stress in the cell based on the generation of hydroxyl radical (OH^\bullet). OH^\bullet can react with further cellular molecules, whereby the development of further ROS such as superoxide anion radical ($O_2^{\bullet-}$) or again H_2O_2 is possible. As the H_2O_2 induced increase in air saturation could be inhibited via addition of an SOD inhibitor (DDC), the strong rise of oxygen generation during SDR measurements after addition of H_2O_2 is related to the activation of the SOD. Therefore, $O_2^{\bullet-}$ seemed to be involved in the occurred cellular answer to H_2O_2 and its cellular consequences. The SOD is the first enzyme of the antioxidant defence mechanism and converts produced $O_2^{\bullet-}$ in the following reaction: $2O_2^{\bullet-} + 2H^+ + SOD \rightarrow H_2O_2 + O_2$ (Maier & Chan, 2002; Marklund, 1980). Thereupon, resulting H_2O_2 is degraded to molecular oxygen and water by the enzyme catalase: $2H_2O_2 \rightarrow 2H_2O + O_2$ (Sies, 1986). This reaction explains the increase in oxygen air saturation after H_2O_2 exposure. Different studies already described the association between H_2O_2 application and the increase in SOD activity (Bose Girigoswami et al., 2005; Drazkiewicz et al., 2003; Nagy et al., 1995). The reaction of the SOD is extremely fast, having a turnover of $2 \times 10^9 M^{-1} sec^{-1}$ (Malstrom et al., 1975). This fast reaction becomes apparent by the rapid increase in air saturation after the addition of H_2O_2 . However, further experiments would be necessary to proof the role of catalase in this reaction.

As no alteration in air saturation could be detected in a cell free milieu, a chemical interaction with medium ingredients or the oxygen sensor caused by H_2O_2 or its decomposition products could be excluded. The H_2O_2 -induced effect is completely absent due to the fact that antioxidative enzymes are not present and therefore not able to eliminate produced ROS. The cell concentration-dependent reaction to H_2O_2 is a further indication for a biological process. An increased amount of cells is associated with an increased O_2 detection after addition of H_2O_2 .

Besides oxidative stress, also cytotoxicity is an indispensable parameter which should be evaluated *in vitro*. Cytotoxicity can be a result of oxidative stress, as ROS can affect cell membranes and other molecules such as nucleic acids. For this reason cytotoxic effects are often accompanied with oxidative stress. Cellular response to silver (Ag) nanoparticles demonstrated a decrease in mitochondrial function with an increase in membrane leakage of LDH. Simultaneously, a significant depletion of the glutathione level and an increase of ROS levels could be detected. These findings hypothesized that cytotoxicity of Ag nanoparticles is likely mediated through oxidative stress (Hussain et al., 2005). In this context, the SDR allows the determination of cytotoxicity *in vitro* as well. The cytotoxic potential of a test substance or material can be determined by monitoring the cellular consumption of oxygen over time. Thereby, oxygen consumption is directly associated to the metabolic activity of cells. Consequently, the oxygen concentration in solution was decreased in the presence of viable cells due to the cellular consumption of oxygen. In contrast, stressed or dying cells caused an increase or a stagnation in O₂ concentration (Beckers et al., 2009). The cellular consumption of oxygen is a very sensitive and early state marker for detection of cytotoxicity. Events such as mitochondrial dysfunction, mitochondrial permeability transition and apoptosis come along with a decrease in cell respiration, which is directly related to cellular viability (Deshpande et al., 2004).

Triton-X permeabilizes cell membranes and served as a cytotoxic model reagent. Using different concentrations of triton-X (0.000001% to 1%) a clear concentration dependent increase in air saturation could be observed when compared to the medium control (DMEM) via SDR measurements. The SDR assay was able to detect small differences in the O₂ consumption of different triton-X concentrations in the standard cell culture medium. The SDR assay detected a cytotoxic potential for 0.01% triton-X in DMEM and HBSS. Thereby, the reduced cytotoxic effect in DMEM medium is based on the general improved growth conditions in a complex cell culture medium compared to a physiological buffer without further supplements such as proteins or amino acids. A comparative LDH assay showed no differences in LDH release between 0.000001% and 0.01% triton-X as well as the medium control. Just 0.1% and 1% triton-X caused a detectable LDH leakage. This experiment was performed in the standard cell culture medium containing phenol red which led to interactions with the LDH assay (very high background absorbance). In contrast, 0.01% triton-X diluted in HBSS showed a clear leakage of LDH compared to the HBSS control which demonstrated again the limitation in the choice of the media. Finally, the novel technique exhibited various

advantages over the standardized LDH assay. The SDR assay could be performed in physiological buffers as well as in highly complexed cell culture media. Furthermore, the sensitivity of the SDR assay allowed the determination of the concentration-dependent cytotoxicity of triton-X diluted in DMEM which was not possible via LDH. As a further control, Caco-2 cells were treated with PEI, which is a particulate substance that can mimic the cytotoxic effect of nanoparticles. Its already known cytotoxicity is based on its very strong absorption to the cell membrane. This results in a polymer layer on the cell surface which causes a perforation of cell membranes and a plasma membrane dysfunction leading to cell death via necrosis (Daum et al., 2009; Fischer et al., 1999).

The SDR assay allows an online sample analysis at different time points during the experiment. Standardized assays for the detection of cytotoxicity are all end-point and mostly invasive assays. Furthermore, the measurement principle of these assays often shows interaction with test materials, especially with nanomaterials. First of all, the MTT assay is known to cause a lot of interactions with nanoparticles due to their material properties (Laaksonen et al., 2007; Ulukaya et al., 2008; Worle-Knirsch et al., 2006). Single-walled carbon nanotubes appeared to interact with the formazan salt of MTT. This interference does not affect the enzymatic reaction but it stabilizes the chemical structure of the produced formazan salts and prevents them from being solubilized (Worle-Knirsch et al., 2006). Also porous silica microparticles exhibited interactions with the MTT assay, through which MTT was reduced in a spontaneous redox reaction. These findings demonstrate that there are various interactions of nanoparticles with assay reagents which do therefore not allow the use of standardized methods. In contrast to all these conventional assays the SDR showed no interference with fluorescently-labelled nanoparticles. Furthermore, the measurement principle of the SDR caused no interaction with media containing supplements such as phenol red and therefore analysis could be performed in buffer as well as in complex cell culture media.

Aim of the described evaluation was to apply this novel method for the combined determination of the oxidative and cytotoxic potential of silica nanoparticles. Therefore, silica nanoparticles with different sizes (21-94 nm) and with different surface modifications (unmodified and PEG-modified) were investigated with the SDR assay concerning their oxidative and cytotoxic capability. For the determination of the oxidative potential, these nanoparticles were analyzed via SDR and were compared in a DCF-DA assay. Particles in all

concentrations showed no increased air saturation independent of their surface modification. These results could be confirmed by the DCF-DA assay, where nanoparticles did not cause an increased conversion of DCF-DA into DCF, whereas H_2O_2 demonstrated a high rate of converted DCF after 3 hours. Thus, the tested silica nanoparticles did not generate ROS in Caco-2 cells. An increased generation of HO^\bullet was already described for crystalline silica nanoparticles. It was suggested, that Fenton reactions occurred on the particles surface which results in an increased ROS production. However, also amorphous silica nanoparticles were reported to cause oxidative stress in different cell systems such as human bronchial epithelial cells, macrophages and embryonic kidney cells (Eom & Choi, 2009; Park & Park, 2009; Wang et al., 2009). As amorphous silica nanoparticles used in this study caused no generation of ROS, it is suggested that the mentioned cell systems are more sensitive against oxidative stress than Caco-2 cells. Furthermore, the shape, size, composition and incubation time of nanoparticles play an essential role in these investigations.

Despite the missing oxidative effect, used silica particles showed strong differences in cytotoxicity. In contrast to particles with a size of 94 nm (N94-RITC) and PEG-modified nanoparticles (N50-P-RITC and N94-P-RITC), smaller particles with sizes between 21 and 84 nm (N50-RITC, N21-PI, N34-PI and N84-PI) exhibited a clear size-, concentration- and time-dependent cytotoxic reaction compared to the buffer control. These evidences suggested that N94-RITC particles and PEG-modified particles did not affect the cells in their viability. In contrast, all other particles showed a very strong reduction in the consumption of oxygen indicative for a decrease in cellular activity. This occurred cytotoxic effect could be also confirmed by an LDH assay, where N50-RITC or N50-P-RITC particles were added to the cells. Again, N50-RITC particles demonstrated a high LDH leakage over 8 hours comparable with the triton-X control. PEG-modified nanoparticles (N50-P-RITC) did not affect the cells and caused no increased LDH release when compared to the HBSS control. Comparison of the data with an MTT assay demonstrated that the evaluation of cytotoxicity via oxygen consumption is much more sensitive than the determination via these standard assays, because it was not possible to detect the cytotoxic potential of the used nanoparticles via MTT assay. Long-term toxicity studies demonstrated that the occurred cytotoxic effect of N34-PI and N84-PI nanoparticles was not reversible. Caco-2 cells which were incubated for 4, 8 or 24 hours exhibited still after an incubation in DMEM for further 72 hours a decreased oxygen consumption if compared to the HBSS controls. Apparently, nanoparticles caused invasive

cellular damages, so that cells could not regenerate in such a short recovery phase. Which cell structures were affected by nanoparticles, should be investigated in further experiments.

Hitherto, the molecular mechanism of nanoparticulate induced cytotoxicity is not fully understood and has to be investigated more detailed. It is assumed that cytotoxicity is caused by cellular injuries through a variety of mechanism such as membrane peroxidation, glutathione depletion, mitochondrial dysfunction and DNA damage (Tao et al., 2009). As it has been reported that nanoparticles were able to enter the cell nucleus as well, it is of particular importance, that also genotoxicity should become a stronger research field. Silver nanoparticles up-regulated DNA damage repair proteins and induced cell death. Furthermore, these genotoxic effects were again strong associated with the cellular uptake rate and intracellular localization of these particles (Ahamed et al., 2008). DNA damage was also caused by carbon nanotubes which were able to penetrate into the cell nucleus through nucleopores and caused a destruction of DNA strands (Pantarotto et al., 2004). Silica nanoparticles were described to enter the nucleus and thus influenced the gene expression of the cells as well (Chen & Mikecz von, 2005). Most likely, the size-, time-, concentration- and also surface modification-dependent cytotoxic effect, which could be observed in this study is based on the internalization of nanoparticles into the cell. It had been already suggested that acute cytotoxicity is primarily originated from the cellular internalization of nanoparticles rather than from physical damage of the cell membrane (Yang et al., 2009).

The observed cytotoxicity correlates with the results of conducted cell association and uptake studies (compare to chapter 4 and 5) showing that smaller particles had a very strong association with Caco-2 cells or even were taken up into the cells. N94-RITC particles as well as PEG-modified nanoparticles, which did not alter the cell growth behaviour, showed no association with Caco-2 cells. The absence of a cytotoxic effect of PEG-modified nanoparticles can be explained via the characteristics of PEG. A surface modification of nanoparticles with PEG caused a reduction in the adhesion of opsonin proteins in the blood serum *in vivo*, which resulted in a higher biologic resistance and stability of such modified nanoparticles (Peracchia et al., 1999; Peracchia et al., 1999). *In vitro*, a similar mechanism could play a role in the decreased cellular association of PEG-modified nanoparticles. Proteins, which are involved in the docking of particles to the outer cell surface, could not adhere to particles modified with PEG. As a result, nanoparticles, which are not able to come into close contact with cells, do not influence cellular viability.

3.6 CONCLUSION

The SDR represents a sensitive, rapid, convenient and first of all a non-invasive method for the simultaneous detection of ROS generation and cytotoxicity in cell culture systems. Furthermore, it allows long-term measurements and online documentation of the cell behaviour. Another advantage of this method is that no additional reagents are required. This is very important when evaluating the oxidative or cytotoxic effect of nanoparticles, because they often show interactions with these assay reagents. Furthermore, its very short assay duration permits the evaluation of a great number of samples in a reasonable time and therefore can be used in high throughput screenings. In conclusion, the SDR represents a potential alternative to well-known standard assays for the detection of oxidative stress and cytotoxicity. So far, no non-invasive assay for the long-term evaluation of oxidative stress or cytotoxicity exists, which make the SDR to a highly innovative and promising method in this research field.

Used silica nanoparticles caused no generation of ROS in Caco-2 cells but exhibited a size-, time-, concentration- and surface modification-dependent cytotoxic effect. These findings were closely associated with conducted cell association and uptake studies (compare to chapter 4 and 5). Nanoparticles which were associated with cells or were even taken up into cells caused cytotoxicity as well. Therefore, it was supposed, that the cellular internalization of nanoparticles influences the cell viability.

Cellular binding, association and transport of rhodamine B-isothiocyanate-labelled silica nanoparticles

Parts of this chapter have been submitted for publication as a journal article:

A. Neumeyer, M. Bukowski, M. Veith, C.-M. Lehr & N. Daum. PI-labelling of nanoparticles as novel tool for the quantification of cellular binding and uptake. Submitted to Nanomedicine: Nanotechnology, Biology and Medicine

Silica nanoparticles are promising tools in the field of oral drug delivery. The main obstacle of this application route is the overcoming of the intestinal barrier and the insistance against cells of the immune system. In the present study rhodamine B-isothiocyanate (RITC)-labelled silica nanoparticles with different sizes (25-94 nm) and surface modifications (+/- poly ethylene glycol, PEG) were investigated concerning their cellular association and uptake properties in Caco-2 cells. In flow cytometry studies a clear size-and time-dependent cell association could be detected for unmodified RITC-labelled nanoparticles with a size of 50 and 77 nm, whereas large particles (94 nm) and PEG-modified nanoparticles showed no interaction with Caco-2 cells. These findings were also confirmed via confocal microscopy. Different cell preparation protocols gave further information about the cellular localization of these particles. Conducted transport experiments correlated with the association studies. Small and unmodified nanoparticles showed the highest transport across Caoc-2 monolayers, whereas PEG-modified nanoparticles were not or rather low transported.

4.1 INTRODUCTION

Oral delivery is the most attractive route for drug application due to the high patient compliance. However, oral bioavailability of new macromolecular drug candidates such as peptides or oligonucleotides is very low because administered drugs have to overcome several biological obstacles. Besides degradation by pancreatic and gastric enzymes, primarily they have to resist the high acidity of the stomach. Furthermore, the intestinal epithelial barrier exhibits a metabolic as well as a physical barrier and thus prevents the uptake of microorganisms and other particles (Hamman et al., 2005; Mustata & Dinh, 2006; Soltero & Ekwuribe, 2005). The intestinal epithelium consists of a cell monolayer mostly composed of enterocytes which build a tight interface. Molecules which are absorbed in the intestine can be delivered to the hepatic portal vein and finally enter the systemic circulation (Soltero & Ekwuribe, 2005). In this study, the enterocyte-like Caco-2 cell line served as an *in vitro* model of the small intestine. These cells form a polarized monolayer with an apical brush border morphologically comparable to that of the human colon (Hidalgo et al., 1989; Hilgers et al., 1990). In addition to the overcoming of biological barriers, the opsonization and clearance by macrophages is another major obstacle in drug delivery which reduces oral bioavailability remarkably (Gref et al., 2003; Gref et al., 1994; Owens & Peppas, 2006).

An overcoming or circumvention of these barriers would lead to an enhancement in the oral bioavailability of new drug candidates such as peptides, proteins, plasmids, antibodies and nucleic acids. One delivery strategy could be based on the encapsulation into or adsorption of drugs and molecules to nanoparticles. Nanoparticle surface modification with poly ethylene glycol (PEG) extend the residence time of nanoparticles in the blood. The effect of PEG is based on the defilade of nanoparticles over surface chemistry, hence avoiding the phagocytic system (Owens & Peppas, 2006). PEG conjugation can reduce reticuloendothelial clearance, the uptake by macrophages, the recognition by the immune system and the degradation by proteolytic enzymes (Roberts et al., 2002). Furthermore, PEG shows stabilizing properties on the nanoparticle surface due to a steric barrier formed by the PEG chains (Behrens et al., 2002; Tobio et al., 2000).

Hitherto, various studies demonstrate an uptake of silica nanoparticles in cells or nuclei (Chen & Mikecz von, 2005; Peng et al., 2006; Vallhov et al., 2007) using confocal microscopy (CLSM) as a qualitative visualization technique. However, there is a lack of studies

quantifying the amount of particles associated with cells. The quantification of nanoparticulate uptake is very important, especially when different materials or studies should be compared.

4.2 AIM OF THE STUDY

The aim of this study was to evaluate the cellular association of rhodamine B-isothiocyanate (RITC)-labelled silica nanoparticles with different sizes and surface modifications in a quantitative way using flow cytometry. As flow cytometry measurements can not distinguish between adsorbed and internalized nanoparticles, different buffers were tested to remove particles from the outer cell membranes.

Furthermore, the transport properties of RITC-labelled silica nanoparticles across Caco-2 monolayers were investigated.

4.3 MATERIALS AND METHODS

4.3.1 Materials

Dulbecco's modified eagle medium (DMEM) with high glucose (4.5 g/l) and L-glutamine was obtained from Gibco (Karlsruhe, Germany), fetal bovine serum was purchased from PAN-Biotech (Aidenbach, Germany), non-essential amino acids were obtained from PAA (Cölbe, Germany). Composition of Hank's balanced salt solution (HBSS) was as follows: 136.9 mM NaCl, 5.4 mM KCl, 4.26 mM NaHCO₃, 0.34 mM Na₂HPO₄*7H₂O, 0.35 mM KH₂PO₄, 5.5 mM glucose, 10 mM HEPES, 1.26 mM CaCl₂, 0.5 mM MgCl₂*6H₂O, and 0.4 mM MgSO₄*7H₂O. HBSS was adjusted to pH 7.4 by means of NaOH. Phosphate buffered saline (PBS) was as follows: 129 mM NaCl, 2.5 mM KCl, 7 mM Na₂HPO₄*7H₂O and 1.3 mM KH₂PO₄. PBS was adjusted to pH 7.4 by means of NaOH, as well. The pH 5 buffer was as follows: 28 mM C₂H₃NaO₂, 117 mM NaCl and 2 mM EGTA. The pH 5 buffer was adjusted to pH 5 by means of HCl. Citric acid, tween 20 and bovine serum albumin were obtained from Sigma (Munich, Germany). FITC-labelled wheat germ agglutinin (WGA) was

purchased from Vector Laboratories (Burlingame, CA). Culture slides were obtained from BD Falcon (Franklin Lakes, NJ).

4.3.2 Caco-2 cell culture

The human colon adenocarcinoma cell line, Caco-2, clone C2Bbe1, was purchased from American Tissue Culture Collection (ATCC, Manassas, VA) and used at passages 60-80. Cells were cultured in Dulbecco's modified eagle medium (DMEM) with high glucose (4.5 g/l) and L-glutamine, supplemented with 10% fetal calf serum (FCS) and 1% non-essential amino acids and were maintained under standard culture conditions at a temperature of 37°C and in a humidified atmosphere of 5% CO₂. The culture medium was changed three times a week. For flow cytometry studies, Caco-2 cells were cultured in 6-well plates at a seeding density of 5×10^5 cells per well in 2 ml culture medium and were allowed to attach and proliferate for 48 hours. For confocal laser scanning microscopy (CLSM) experiments, Caco-2 cells were plated on 4 chamber glass culture slides at a seeding density of 1×10^5 cell per well in 1 ml medium and allowed to attach and proliferate for 8 to 10 days until reaching a confluence of 60-70%.

4.3.3 Visualization of cellular association by confocal laser scanning microscopy (CLSM)

Caco-2 cells (1×10^5 per well) were cultured on 4 chamber glass culture slides for 8 to 10 days under standard cell culture conditions. Afterwards, adherent cells were incubated with RITC-labelled nanoparticles (N50-RITC, N50-P-RITC, N77-RITC, N77-P-RITC, N94-RITC and N94-P-RITC) for 4 hours under standard cell culture conditions. After incubation with these nanoparticles, cell membranes were stained with FITC-labelled wheat germ agglutinin (WGA) and cells were fixed with 4% formalin in PBS. If required, nuclei were stained with 4',6-diamidino-2-phenylindole (DAPI). After the staining procedure fixed cells were imaged via CLSM using LSM510 (Zeiss, Jena, Germany). The used objective was a water immersion objective 63x. Measurements were performed with Zeiss LSM510 Software.

4.3.4 Quantification of cellular or nuclear association by flow cytometry (FACS)

Quantification of the cellular or nuclear association of RITC-labelled nanoparticles was investigated via flow cytometry using a FACSCalibur (Beckon Dickinson, Heidelberg, Germany). Data were analysed with the BD CellQuest Pro software and FlowJo flow cytometry analysis software. Control cells or nuclei which were not incubated with nanoparticles emitted always a weak background fluorescence (Figure 4.1 A, grey peak). In contrast, cells which were associated with fluorescently-labelled nanoparticles showed a shift to higher fluorescence intensities (Figure 4.1 A, black line). Emitted light resulting from RITC-labelled nanoparticles was detected by the FL2 detector. The measurement of the green fluorescence (e.g. FITC wavelength) served as a negative control because used cells should exhibit no alteration in the emission of this wavelength. To calculate the background fluorescence of unlabelled cells, cells without any addition of nanoparticles (HBSS treated cells) were carried along as a buffer control in every measurement. Quantitative analysis was performed by means of quadrant statistics placing a quadrant marker which divides a 2D plot into four quadrants. Thus, the percentage of cells in each quadrant could be calculated. The unlabelled cell population was placed in the lower left quadrant of the dot plot and exhibited cells without associated nanoparticles. In contrast, nanoparticle associated and therefore fluorescently-labelled cells were placed in the lower right quadrant (Figure 4.1 B-D).

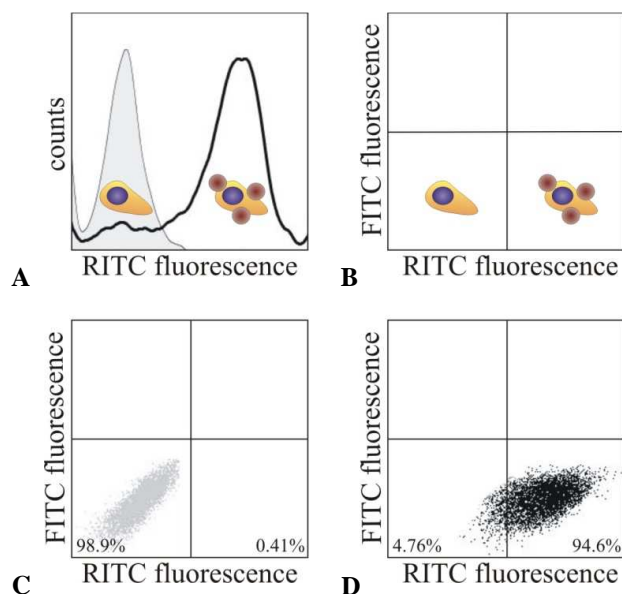


Figure 4.1: Analysis of the quantification of the cellular association of nanoparticles. (A) Histogram of Caco-2 cells incubated in HBSS (grey peak) and associated with RITC-labelled nanoparticles (black line). (B) Division of a 2D dot plot in quadrants. Unlabelled cells were placed in the lower left quadrant. Cells which were associated with RITC-labelled nanoparticles were located in the lower right quadrant. (C) Dot plot inclusive quadrant statistics of unlabelled Caco-2 cells and (D) cells associated with RITC-labelled nanoparticles.

4.3.5 Cell preparation protocols

Caco-2 cells in a concentration of 5×10^5 per well were plated in 6-well plates and cultured for 48 hours under standard cell culture conditions. Afterwards, adherent cells were incubated for different times (1, 2, 4 or 8 hours) under standard cell culture conditions with unmodified (N50-RITC, N77-RITC, N94-RITC) or PEG-modified silica nanoparticles (N50-P-RITC, N77-P-RITC and N94-P-RITC). For the following flow cytometry analysis, cells were prepared in three different ways: (i) whole cell preparation, (ii) nucleus preparation and (iii) nucleus isolation. For whole cell and nuclei preparation analysis 10 000 cells or nuclei were counted, for nuclei isolation analysis 5 000 nuclei were counted. Size was determined via the forward scatter (FSC) and granularity was determined via the sideward scatter (SSC).

(i) Whole cell preparation

Caco-2 cells were harvested with trypsin and washed three times with PBS. Whole cells exhibited a very low granularity due to an intact cell membrane (Figure 4.2 A).

(ii) Nucleus preparation

Cells were harvested with trypsin as well, washed with PBS and fixed in 70% ethanol for 24 hours. After this procedure fixed cells were incubated with a triton-X containing permeability buffer (PBS + 0.5% triton-X) and washed again with PBS supplemented with 1% BSA. Prepared nuclei were still associated with cytoplasm, various cell organelles and parts of the permeabilized cell membrane which resulted in a high granularity (Figure 4.2 B).

(iii) Nucleus isolation

Adherent cells were incubated with a citric acid/tween20 buffer (H_2O + 2.1% citric acid and 0.5% tween20). Nuclei were collected and were fixed in 70% ethanol for 24 hours. After this fixation nuclei were washed several times in PBS containing 1% tween20 and were collected finally in PBS. A dot plot of these isolated nuclei showed small structures with a very low granularity (Figure 4.2 C).

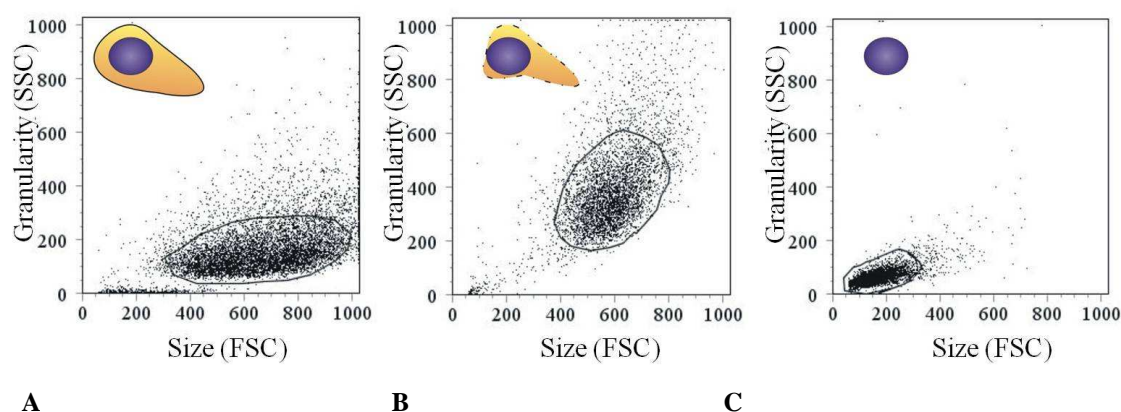


Figure 4.2: Cell or nucleus preparation and nucleus isolation. **(A)** Analysis of whole Caco-2 cells. Cells were trypsinized and washed three times with PBS. **(B)** Analysis of prepared cell nuclei. Cells were trypsinized, fixed in ethanol for 24 hours and permeabilized with a triton-X containing buffer. **(C)** Analysis of isolated nuclei. Adherent cells were incubated in a citric acid/tween20 buffer, nuclei were collected, fixed in ethanol for 24 hours and washed several times with PBS containing tween 20. Dot plots are the result of 10 000 measured cells or prepared nuclei or 5 000 isolated nuclei, respectively. Analysed cell populations are marked with a gate.

4.3.6 Cell washing procedures

Caco-2 cells in a concentration of 5×10^5 per well were plated in 6-well plates and were cultured for 48 hours as described before. Afterwards, adherent cells were incubated for 1 minute with N25-RITC nanoparticles. This short incubation time excluded a real uptake into the cell. Afterwards cells were washed with different buffers for several times (Table 4.1). Whole cells were analysed via flow cytometry as described in chapter 4.3.4.

Table 4.1: Washing buffers to remove nanoparticles from the outer cell surface.

Buffer	Ingredients	Concentrations
pH 5 buffer	Sodium acetate	28 mM
	Sodium chloride	117 mM
	EGTA	2 mM
Trypsin 50	Trypsin	50%
	PBS	
Trypsin 10	Trypsin	10%
	PBS	
Triton-X 0.0001	Triton-X	0.0001%
	PBS	
Triton-X 0.001	Triton-X	0.001%
	PBS	
Pronase 0.5	Pronase	0.5 mg/ml
	PBS	
Pronase 1	Pronase	1 mg/ml
	PBS	

4.3.7 Transport studies

Caco-2 cells in a concentration of 6×10^4 per well were plated in 12-well Transwell[®] plates using polycarbonate membranes with a pore size of 0.4 μm . The assembling of such a Transwell system is presented in figure 4.3. Cells were cultured on these membranes for 21 - 28 days under standard cell culture conditions. During this cultivation, the development of the transepithelial electrical resistance (TEER) was determined at regular intervals to ensure membrane integrity of the monolayers. The TEER was measured via chopstick electrodes connected to an epithelial voltohmmeter (EVOM, World Precision Instruments, Sarasota, FL). The long-term development of the TEER of a Caco-2 cell monolayer was determined with the CellZscope[®] (nanoAnalytics, Münster, Germany) as well. The CellZscope[®] is an instrument measuring the transepithelial impedance of cell layers under physiological conditions. It is computer-controlled and allows automated and a long-term monitoring of cell cultures.

Before starting the experiment, Caco-2 cell monolayers were pre-incubated with the transport buffer (HBSS) for 30 minutes. Transport of nanoparticles was investigated in absorptive direction (apical to basolateral compartment). During the experiments, Transwell® plates were agitated using an orbital shaker at 150 rpm. Samples were taken after 4, 8 and 24 hours from the receiver compartment. After each sample collection, an equal volume of fresh transport buffer (pre-warmed to 37°C) was added to the receiver compartment. TEER was measured after pre-incubation and at the end of the experiment.

Transport of RITC-labelled nanoparticles were quantified via a fluorescence plate reader (Infinite M200, Tecan, Crailsheim, Germany) using an excitation wavelength of 560 nm and an emission wavelength of 600 nm. Fluorescence of RITC was linear in a range between 0.05 and 100 µg/ml ($R^2=0.9992$). As a result, the amount of substance in the acceptor compartment as well as the apparent permeability (P_{app}) were calculated. The apparent permeability describes the permeability of a cell monolayer for a substance and the estimated membrane permeability (cm/sec). It was calculated according to: $P_{app} = (\Delta Q / \Delta t) * (1/A) * (1/c_0)$, where $\Delta Q / \Delta t$ is the permeability rate (µg/min), A (cm²) is the surface area of the monolayer and c_0 (µg/ml) is the nanoparticle concentration in the donor compartment at time (t)=0.

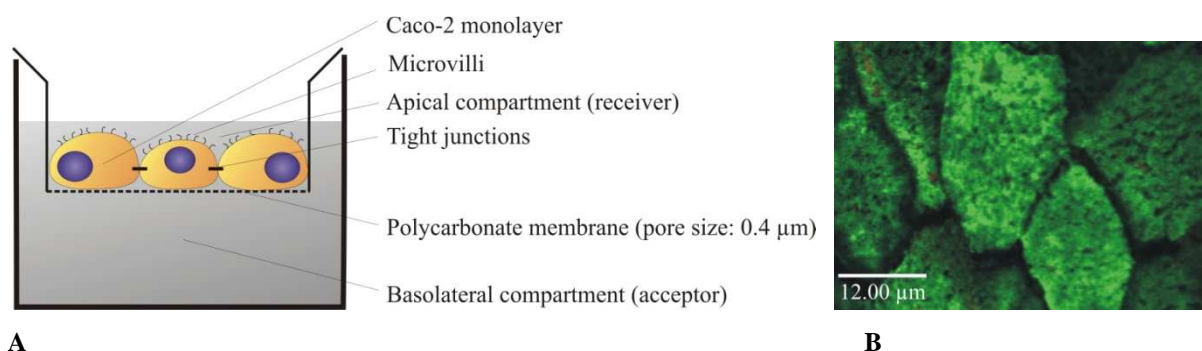


Figure 4.3: Assembling of a Transwell® system. **(A)** Caco-2 cells were cultivated on the polycarbonate membrane of an insert. Thus, the monolayer separates the chamber into an upper (apical) and a lower (basolateral) compartment. **(B)** Caco-2 monolayer grown on a polycarbonate membrane. Cells were stained with FITC-labelled wheat germ agglutinin. Bar=12.00 µm.

4.4 RESULTS

4.4.1 Size-, time- and surface modification-dependent association of RITC-labelled silica nanoparticles

Unmodified RITC-labelled silica nanoparticles (N50-RITC, N77-RITC, N94-RITC) with different sizes (50, 77 and 94 nm) were dispersed in HBSS to a concentration of 100 µg/ml and were incubated with Caco-2 cells for 4 hours under standard cell culture conditions. Flow cytometry (FACS) analysis of whole cells presented a clear cell association for N50-RITC ($85.9\% \pm 6.05$) and N77-RITC ($84.9\% \pm 4.07$) particles, whereas N94-RITC particles exhibited no or a rather low cell association of $0.4\% \pm 0.42$ (Figure 4.4 A, black bars). Prepared nuclei which were still associated with cell fragments showed a decreased cellular particle association with a size-dependency: N50-RITC particles demonstrated a cell association of $84.9\% \pm 1.90$, whereas N77-RITC particles exhibited only a cell association of $76.1\% \pm 4.77$ (Figure 4.4 A, white bars). Isolated nuclei demonstrated a highly significant reduction ($p \leq 0.001$) in particle association when compared to prepared cell nuclei. $30.7\% \pm 5.97$ of N50-RITC particles and $16.9\% \pm 7.53$ of N77-RITC particles were associated with nuclei of Caco-2 cells (Figure 4.4 A, grey bars). The same nanoparticles but with an additional PEG modification (N50-P-RITC, N77-P-RITC and N94-P-RITC) showed no association with cells or nuclei at all (Figure 4.4 B).

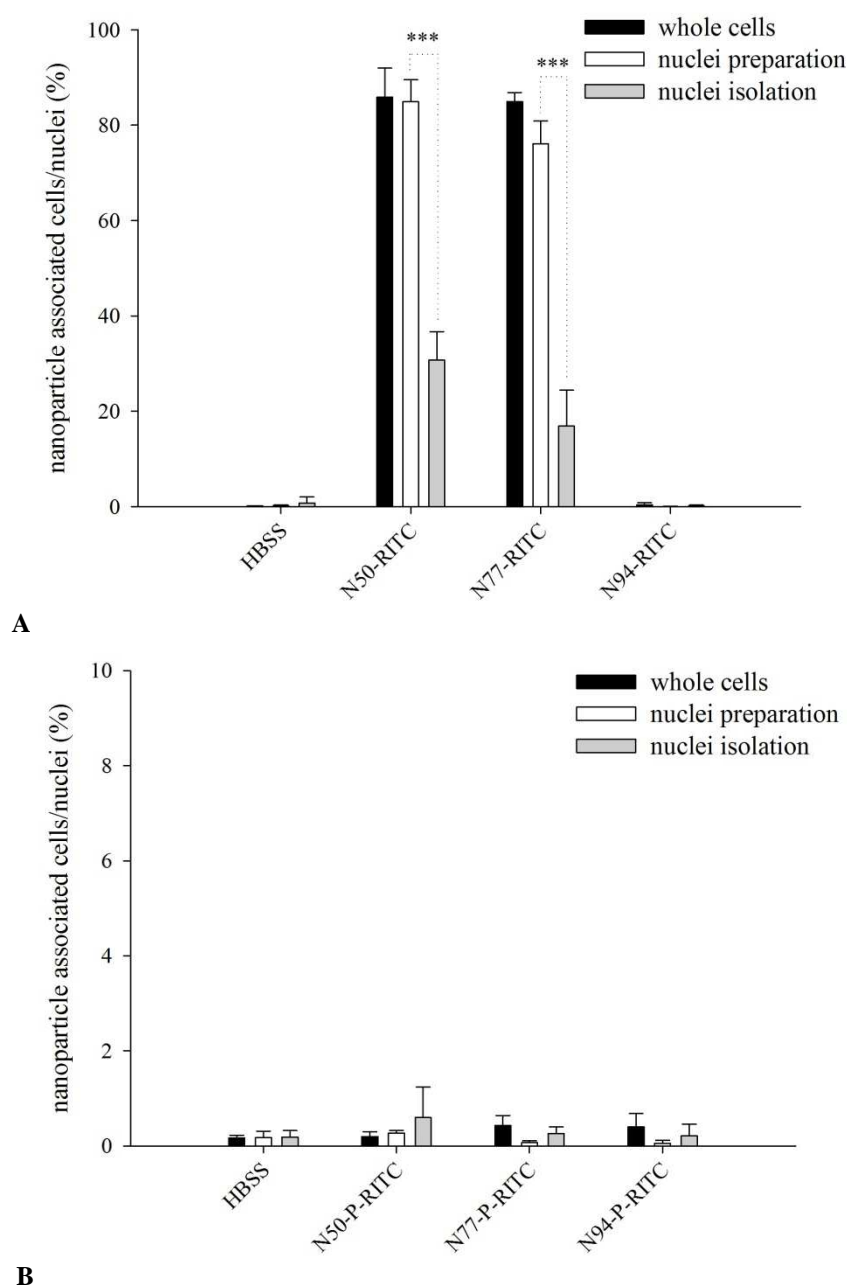


Figure 4.4: Size- and surface modification-dependent association of RITC-labelled silica nanoparticles. Different nanoparticles were added to Caco-2 cells in a concentration of 100 $\mu\text{g/ml}$ and were incubated for 4 hours under standard cell culture conditions. HBSS served as a negative control. Whole cells as well as prepared and isolated nuclei were analyzed via flow cytometry. **(A)** Size-dependent association of unmodified nanoparticles (N50-RITC, N77-RITC and N94-RITC). **(B)** Association of PEG-modified nanoparticles (N50-P-RITC, N77-P-RITC and N94-P-RITC). Data represent the mean \pm SD of three independent experiments. The asterisks depict significant differences between prepared and isolated nuclei ($p \leq 0.001$ ***).

The size- and surface-dependent association of RITC-labelled nanoparticles with Caco-2 cells was confirmed via CLSM. It could be demonstrated that N50-RITC and N77-RITC nanoparticles were adsorbed to the cell membranes of Caco-2 cells after a 4-hour-incubation

(Figure 4.5 A-B, arrows), whereas all other particles were not detectable (Figure 4.5 C-F). A series of images at different points along the z-axis (Z-stack) exhibited no or a rather low uptake of N50-RITC and N77-RITC particles into the cells (Figure 4.6).

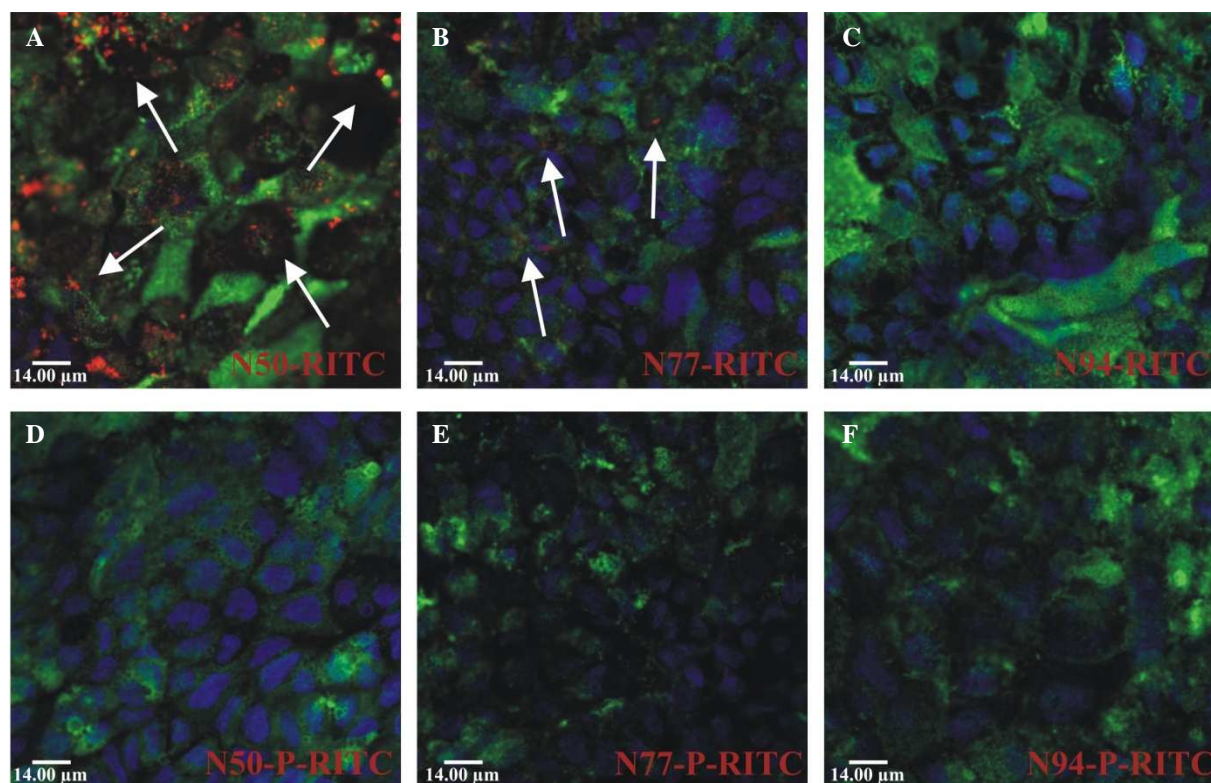


Figure 4.5: Size- and surface modification-dependent association of RITC-labelled silica nanoparticles with Caco-2 cells. Cells were plated on glass culture slides. Different RITC-labelled nanoparticles (red) were added to the cells and were incubated in a concentration of 100 µg/ml for 4 hours under standard cell culture conditions. Membranes were stained with FITC-labelled WGA (green). After fixation with 4% formalin, nuclei were stained with DAPI (blue). Analysis was performed via CLSM. **(A)** Unmodified nanoparticles N50-RITC, 50 nm. **(B)** Unmodified nanoparticles N77-RITC, 77 nm. **(C)** Unmodified nanoparticles N94-RITC, 94 nm. **(D)** PEG-modified nanoparticles N50-P-RITC, 55 nm. **(E)** PEG-modified nanoparticles N77-P-RITC, 87 nm. **(F)** PEG-modified nanoparticles N94-P-RITC, 97 nm. Bars=14.00 µm.

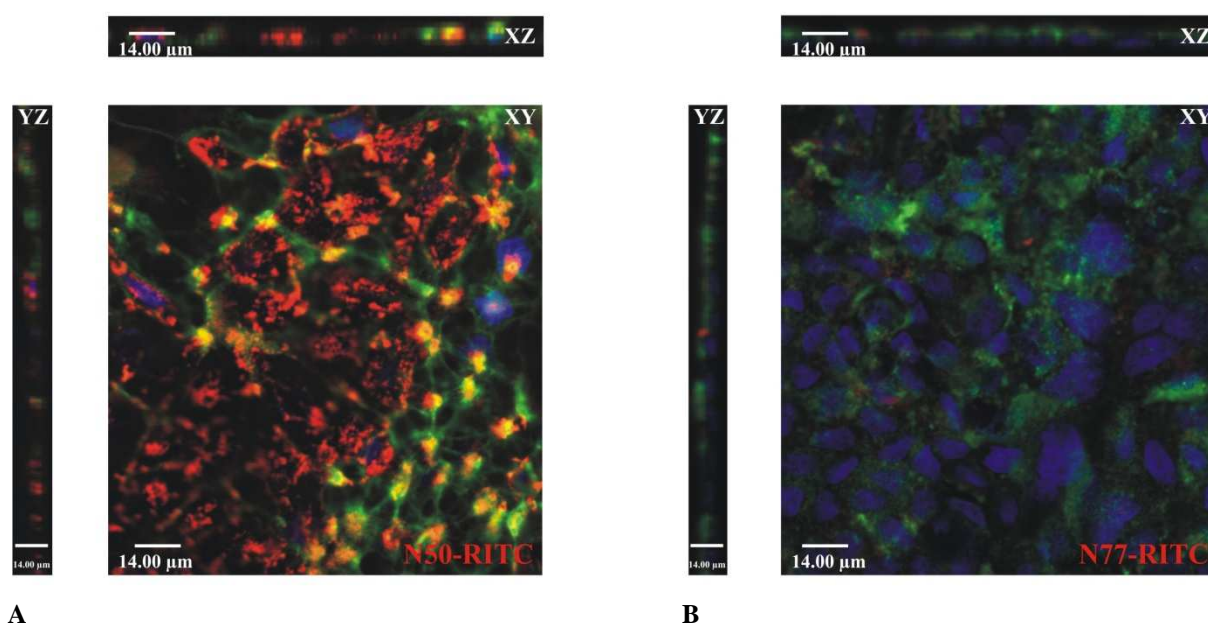


Figure 4.6: Size-dependent association of RITC-labelled silica nanoparticles with Caco-2 cells. Cells were cultured on glass culture slides. Nanoparticles (red) were added to the cells and were incubated in a concentration of 100 $\mu\text{g/ml}$ for 4 hours under standard cell culture conditions. Membranes were stained with FITC-labelled WGA (green). After fixation with 4% formalin, nuclei were stained with DAPI (blue). Analysis was performed via CLSM. **(A)** Unmodified nanoparticles N50-RITC, 50 nm. **(B)** Unmodified nanoparticles N77-RITC, 77 nm. Besides an XY image, XZ- and YZ-cross sections through an image stack were performed as well. Bars=14.00 μm .

Furthermore, N50-RITC and N77-RITC particles demonstrated a time-dependent cell association over 8 hours. Cellular association of N50-RITC and N77-RITC particles differed mainly in the early stage of the experiment. After a 1-hour-incubation $78.4\% \pm 0.62$ of the cells were associated with N50-RITC particles, whereas only $45.4\% \pm 6.81$ of the cells were in contact with N77-RITC particles (Figure 4.7, black bars). After a 4-hour-incubation, the association rate of these two particles differed about 3.8% (Figure 4.7, white bars). After 4 hours the cellular association reached a plateau. Therefore, a significant difference in the cellular association rate of nanoparticles was only observed after an incubation of 1 hour and after a 4-hour-incubation.

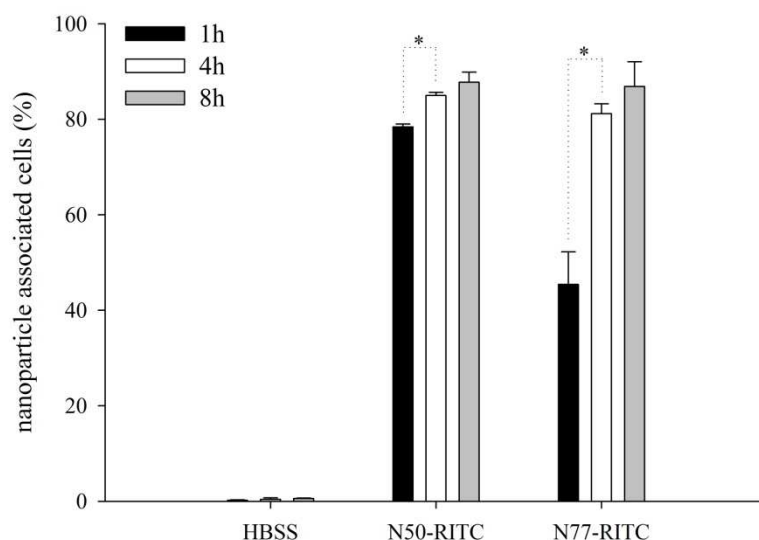


Figure 4.7: Time-dependent association of RITC-labelled silica nanoparticles with Caco-2 cells. Different nanoparticles (N50-RITC and N77-RITC) were added to Caco-2 cells in a concentration of 100 $\mu\text{g/ml}$ and were incubated for 1, 4 or 8 hours. Whole cells were analyzed via flow cytometry. Data represent the mean \pm SD of three independent experiments. The asterisks depict significant differences between cells incubated with nanoparticles for 1 hour and cells incubated with nanoparticles for 4 hours ($p \leq 0.05$ *).

4.4.2 Removal of nanoparticles adsorbed to the outer cell membrane

FACS measurements do not allow a differentiation between nanoparticles adsorbed to the outer cell surface and nanoparticles internalized into a cell. Thus, a measured fluorescence signal of a cell comprises nanoparticles which entered the cell as well as nanoparticles, which are only adsorbed to the outer cell membrane (Figure 4.8). Therefore, in this study, different buffers were used to remove particles from the outer cell membrane to consequently measure only cellular internalized nanoparticles.

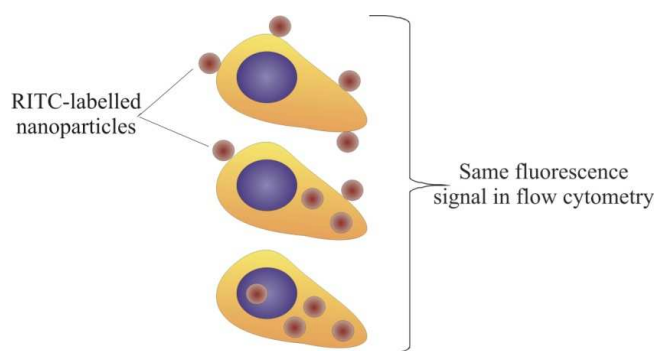


Figure 4.8: Flow cytometry fluorescence signals of Caco-2 cells incubated with RITC-labelled nanoparticles. The generated signal is independent of the cellular localization of nanoparticles.

Caco-2 cells showed already after a 1-minute-incubation with RITC-labelled nanoparticles a very high fluorescence signal. As this short incubation time excludes an uptake of the particles into the cell, the signal resulted from nanoparticles adsorbed to the outer cell membrane. Cells with adsorbed nanoparticles were washed with different buffers for several times. Afterwards, cells were analysed via flow cytometry. Figure 4.9 summarizes the removal potential of the different buffers.

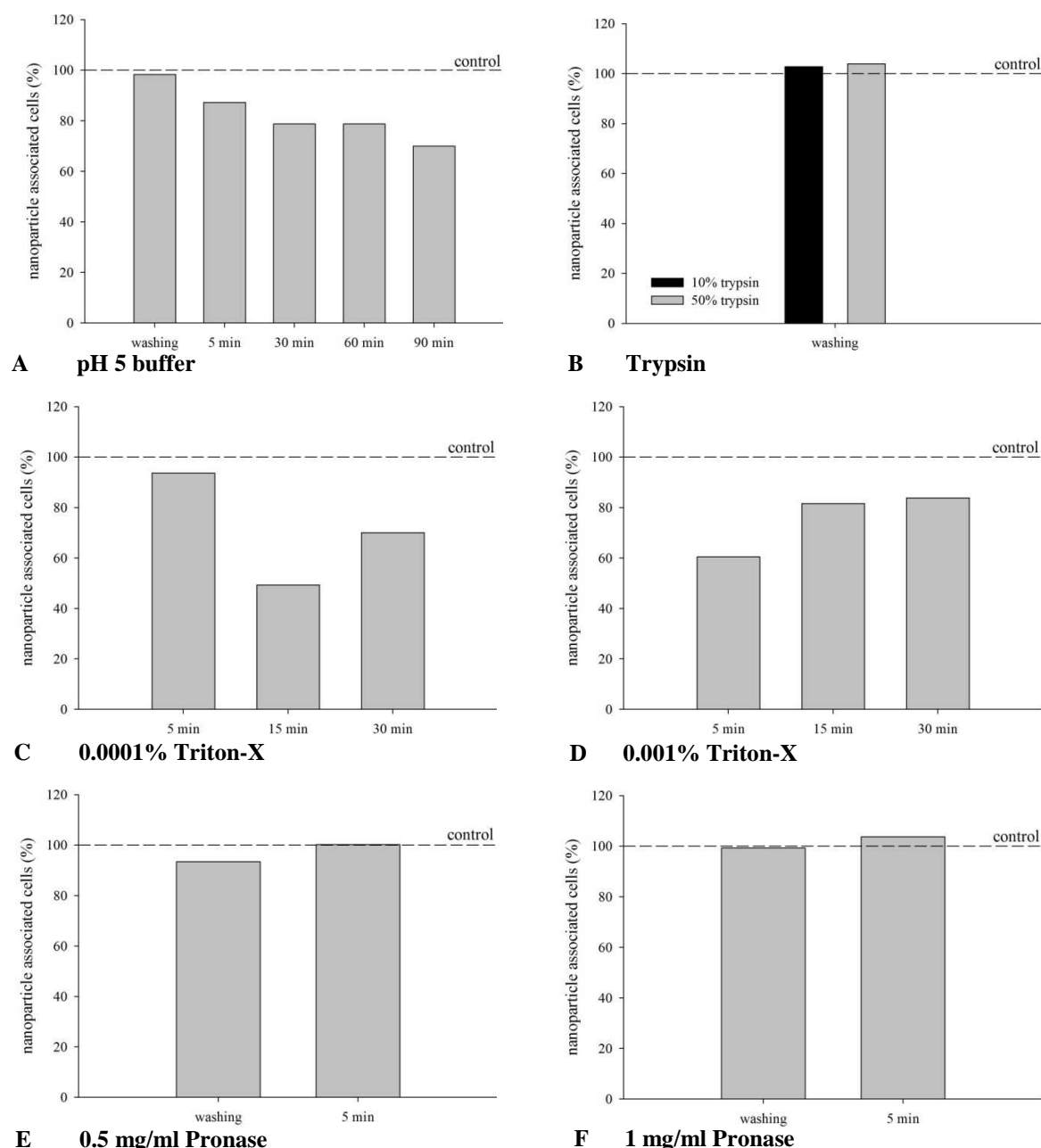


Figure 4.9: Washing experiments for the removal of nanoparticles from the outer cell membrane. Caco-2 cells were incubated for 1 minute with unmodified RITC-labelled nanoparticles (N25-RITC). Subsequently, cells were washed three times or were incubated for several times with different buffers. Unwashed cells served as control (dashed line). (A) pH 5 buffer. (B) trypsin. (C) 0.0001% triton-X. (D) 0.001% triton-X. (E) 0.5 mg/ml pronase. (F) 1 mg/ml pronase.

Trypsin and pronase buffers could not remove any particles from the cells. Triton-X could eliminate some particles but resulted in massive cell damage due to its permeabilization characteristics. The pH 5 buffer caused an incubation time-dependent removal of nanoparticles from the outer cell surface. However, after 90 minutes the amount of nanoparticle associated cells was reduced to only 70%. A longer incubation with the pH 5 buffer to delete more particles was not possible because of its unphysiological pH causing deleterious effects on cells.

4.4.3 Transport properties of RITC-labelled silica nanoparticles

As HBSS was used as transport buffer during transport studies, the barrier function of Caco-2 cells in HBSS had to be documented. Therefore, long-term measurements with the CellZscope[®] instrument were performed. The TEER of a Caco-2 monolayer incubated in HBSS was sustained for 40 hours. Afterwards the TEER declined rapidly (data not shown). This experiment demonstrated that Caco-2 monolayers built a tight barrier in HBSS up to an incubation time of 40 hours, which allows an examination of the nanoparticulate transport during this period.

The passage of different RITC-labelled nanoparticles (N25-RITC, N37-RITC, N62-RITC, N50-RITC, N50-P-RITC, N94-RITC and N94-P-RITC) across a Caco-2 cell monolayer was investigated using Transwell[®] plates with a polycarbonate membrane with pore sizes of 0.4 μm . Samples were collected from the acceptor compartment after 4, 8 and 24 hours. In a first experiment, the transport behaviour of unmodified RITC-labelled nanoparticles with different sizes (N25-RITC, N37-RITC and N62-RITC) without influence of cells was investigated over 8 hours. The transport across the blank filter was time- and size-dependent. After 8 hours, $6.26\% \pm 0.31$ of N25-RITC particles arrived in the acceptor, the amount of N37-RITC particles in the acceptor was $1.69\% \pm 0.21$. In contrast, N62-RITC showed no or a rather low transport rate of $0.66\% \pm 1.36$. Furthermore, it could be demonstrated, that the passage across the filter started not before a 1-hour-incubation (Figure 4.10 A).

With the influence of Caco-2 cells, the transport rate of the used nanoparticles was reduced due to the additional cellular barrier. Compared to the cell-free experiment after 8 hours, N25-RITC particles showed a decrease in transport of 94.49% (actual transport rate $0.34\% \pm 0.59$),

N37-RITC of 97.63% (actual transport rate $0.59\% \pm 0.04$) and the transport of N62-RITC particles was reduced of 94.39% (actual transport rate $0.03\% \pm 0.06$), whereby all transport rates were below the detection limit of 0.5%. After 24 hours, the transport experiment demonstrated a clear size-dependent transport rate: The amount of N25-RITC nanoparticles in the acceptor was $7.29\% \pm 1.75$ of the initial particle concentration. The transport rate of N37-RITC particles was $0.94\% \pm 0.08$ and the one of N62-RITC nanoparticles was $0.04\% \pm 0.06$ which was below the detection limit (Figure 4.10 B). TEER values were stable during the whole experiment (data not shown).

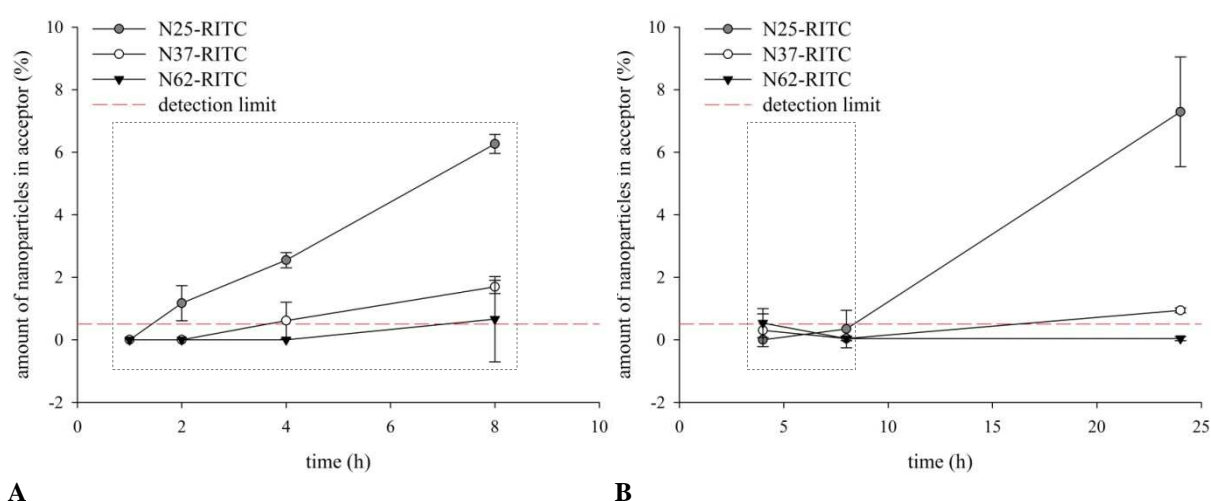


Figure 4.10: Transport of RITC-labelled silica nanoparticles across a (A) polycarbonate membrane with pore sizes of $0.4\ \mu\text{m}$ over 8 hours and (B) an additional Caco-2 cell monolayer over 24 hours. Caco-2 cells were cultured for 21 days under standard cell culture conditions. Red dashed lines indicate the detection limit of the used nanoparticles. Data represent the mean \pm SD of three wells.

Another transport experiment with unmodified RITC-labelled nanoparticles (N50-RITC and N94-RITC) and PEG-modified nanoparticles (N50-P-RITC and N94-P-RITC) showed again a size-dependent transport as well as a surface-modification-dependent effect. N50-RITC particles showed after 24 hours a transport rate of $1.66\% \pm 0.19$ and N94-RITC nanoparticles exhibited a transport of $1.11\% \pm 0.13$. In contrast, PEG-modified nanoparticles demonstrated no or a very low transport across the Caco-2 cell monolayer. After 24 hours, $0.48\% \pm 0.09$ of N50-P-RITC and $0.61\% \pm 0.06$ of N94-P-RITC particles were transported across the cells (Figure 4.11). These transport profiles were reflected in the P_{app} values as well (Table 4.2). TEER values were stable during the whole experiment (data not shown).

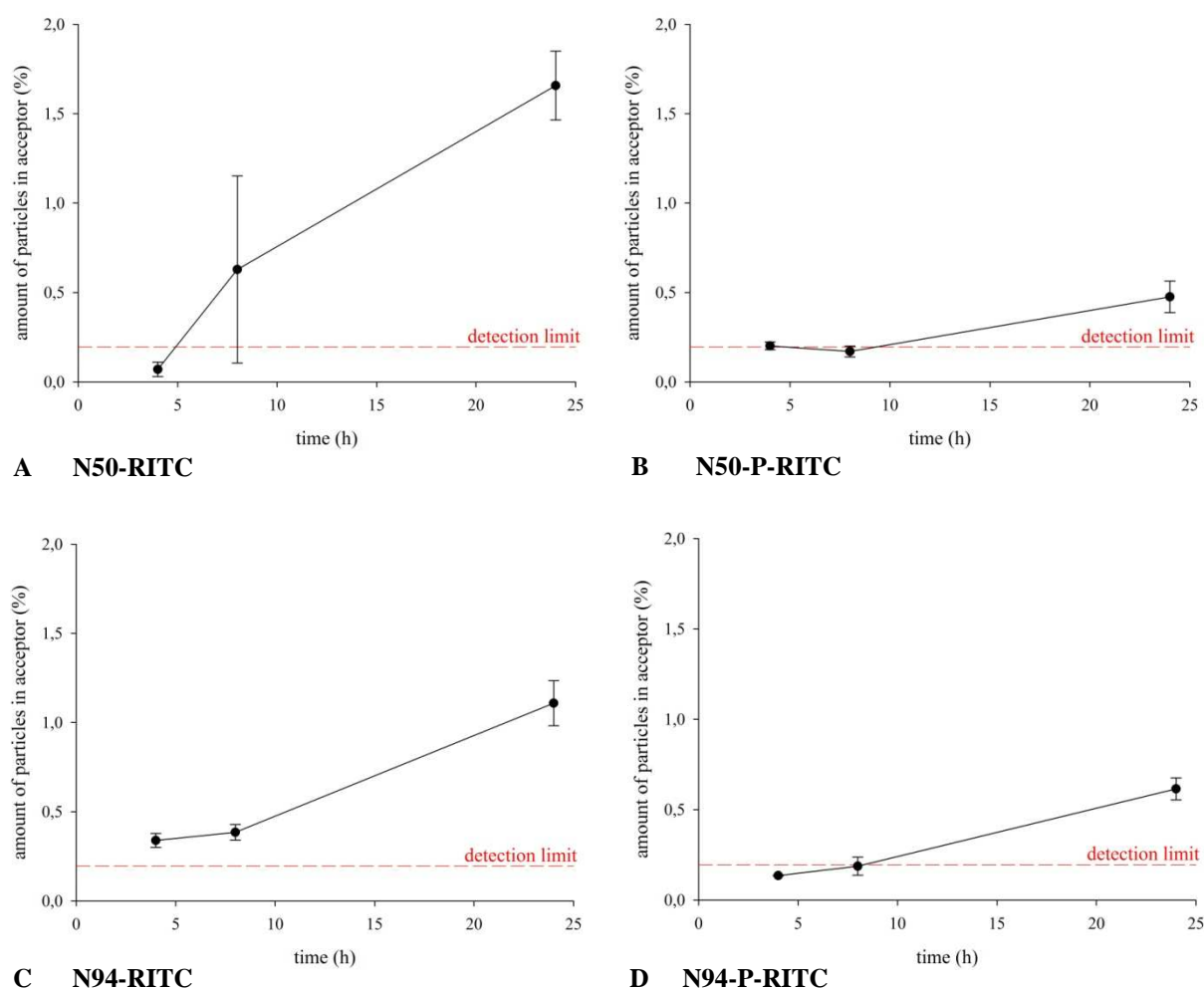


Figure 4.11: Transport of unmodified and PEG-modified RITC-labelled silica nanoparticles across a Caco-2 cell monolayer cultured for 21 days on polycarbonate membranes with pore sizes of 0.4 μm . (A) Unmodified nanoparticles N50-RITC, 50 nm. (B) PEG-modified nanoparticles N50-P-RITC, 55 nm. (C) Unmodified nanoparticles N94-RITC, 94 nm. (D) PEG-modified nanoparticles N94-P-RITC, 97 nm. Red dashed lines indicate the detection limit of the used nanoparticles. Data represent the mean \pm SD of two wells.

Table 4.2: P_{app} values of unmodified and PEG-modified RITC-labelled silica nanoparticles across a Caco-2 cell monolayer.

Nanoparticle	P_{app} (cm/sec)
N50-RITC	4.26×10^{-8}
N50-P-RITC	2.12×10^{-8}
N94-RITC	3.94×10^{-8}
N94-P-RITC	2.06×10^{-8}

4.5 DISCUSSION

Nanoparticles exhibit a broad promising spectrum of potential applications in the pharmaceutical and medical field. Typical challenges of drug delivery such as solubility, diffusivity, blood circulation half-life and drug release characteristics could be influenced with materials in the nanoscale range. Hitherto, a number of nanoparticulate therapeutics and diagnostic agents have been developed, e.g. for the treatment of cancer or diabetes (Brannon-Peppas & Blanchette, 2004; Hirsch et al., 2003; Lin et al., 2007). The advantages of these “nanodrugs” are their higher bioavailability and their lower therapeutic toxicity resulting in a reduction of side effects. Furthermore, nanoparticulate delivery systems allow a targeted delivery and a controlled release. Because of the improvements of all these parameters, it is possible to administer these drugs also via more convenient routes, e.g., the oral route. However, for the application in this field, the cellular binding, association, the uptake properties and the localization of nanoparticles within the cell have to be investigated in detail. Especially, the quantification of cellular uptake is a sparsely explored topic but is very important for the comparison of different studies. However, most publications dealing with particle uptake utilize microscopic methods such as confocal laser scanning microscopy (CLSM) or transmission electron microscopy (TEM) (Behrens et al., 2002; Beisner et al., 2009; Chen & Mikecz von, 2005; Taetz et al., 2009). Hitherto, there are a few studies using flow cytometry (FACS) as quantitative method (Gabor et al., 2008; Taetz et al., 2009). A study of Gabor et al. managed this challenge by analysing the changes in granularity via analysing the sideward scatter signal in flow cytometry measurements. As a result, the mean granularity of Caco-2 cells was increased due to the cellular association of nanoparticles (Gabor et al., 2008). However, this measurement parameter was not applicable for the silica nanoparticles used in the present study. These particles did not cause any alteration in the sideward scatter signal (data not shown), although they showed a clear increase in the FL2 fluorescence signal.

RITC-labelled silica nanoparticles exhibited a size- and time-dependent cellular and nuclear association to Caco-2 cells. Such a size dependency could be already observed for fluorescently-labelled silica nanoparticles sized between 40 nm and 5 μ m in Hep-2 cells or nuclei which could be determined via CLSM (Chen & Mikecz von, 2005). Small unmodified nanoparticles (N50-RITC and N77-RITC) seemed to be in a strong association with cell

membranes, whereas larger and PEG-modified nanoparticles did not show these cellular interactions. These results represent one important characteristic of PEG. *In vivo*, PEGylation of nanoparticles results in a blocking of the adhesion of opsonin proteins present in the blood serum (Peracchia et al., 1999; Peracchia et al., 1999). A similar mechanism could play a role in the decreased cellular association of PEG-modified nanoparticles *in vitro*. Obviously proteins, which are involved in the docking of particles to the cell membrane, could not adhere to particles due to PEGylation of the particle surface. In this context, similar results could be observed in recent publications. PEG-modified poly lactic acid nanoparticles exhibited no interaction with Caco-2 cells in contrast to unmodified hydrophobic polystyrene nanoparticles which showed a very strong cellular association (Behrens et al., 2002). The coating of polystyrene nanoparticles with a poloxamer, leading to an increased hydrophilicity, caused a reduction in intestinal uptake as well (Hillery & Florence, 1996). These findings confirm the hypothesis which suggested that the association between nanoparticles and cell membranes are based on hydrophobic interactions (Lehr et al., 1991). Thus, surface modifications with hydrophilic molecules avoid the cellular association and consequently the uptake into the cells. This reaction is useful avoiding the elimination by macrophages but could be an obstruction when the uptake into other cell types is requested e.g. in the treatment of tumour cells. Therefore, nanoparticles need further highly specific surface modifications to target their cell-specific transport.

Results of these cell association studies correlate with performed cytotoxicity studies. N50-RITC particles caused a clear decrease in cellular viability over time. In contrast, nanoparticles which showed no association with Caco-2 cells (N50-P-RITC, N94-RITC and N94-P-RITC) exhibited no cytotoxic potential. The generation of a cytotoxic effect necessitates a close contact between nanoparticles and the biological system. Thereby, mainly size, time and surface modification but also the particle concentration influenced the extent of the cytotoxic effect (compare to chapter 3) (Gu et al., 2009; Napierska et al., 2009; Pan et al., 2007; Win & Feng, 2005).

Most research groups, which investigate cellular uptake of nanoparticles, present their data in a qualitative way such as CLSM. The advantage of this method is the possibility to visualize particle uptake using Z-stack tools. Thus, adsorbed particles can be distinguished from internalized particles. This distinction is not possible with flow cytometry measurements

using conventional fluorescence dyes such as RITC or FITC. However, for a better comparison between different studies it is of great interest to quantify nanoparticulate uptake as well. Besides the ability to quantify cellular interactions of nanoparticles, flow cytometry measurements show another advantage over confocal microscopy analysis regarding the detection limit. CLSM images of Caco-2 cells incubated with N50-RITC particles in a concentration of 100 $\mu\text{g/ml}$, resulted in a low number of detectable nanoparticles. N50-RITC particles in a concentration of 50 $\mu\text{g/ml}$ could not be visualized anymore via CLSM. In contrast, flow cytometry studies showed no alteration in the emitted fluorescence (indication for cellular association), when incubating cells with N50-RITC particles in various concentrations (20-100 $\mu\text{g/ml}$). N50-RITC particles in a concentration of 10 $\mu\text{g/ml}$ still exhibited a clearly detectable fluorescence signal in flow cytometry studies. As a result, flow cytometry measurements allow a more sensitive determination of the nanoparticulate association as CLSM.

As mentioned before, most fluorescently-labelled nanoparticles, such as RITC-labelled nanoparticles, have the disadvantage that it is not possible to distinguish between internalized and adsorbed particles in a quantitative way (e.g. via flow cytometry). Whole cells which exhibit a fluorescence signal via flow cytometry can be associated with nanoparticles in two different ways: Either particles are adsorbed to the outer cell surface or are taken up into the cells. RITC-labelled nanoparticles showed already after a very short incubation time of 1 minute a high fluorescence signal due to particles associated with the outer cell membrane. Thereby, the short incubation time excluded an uptake into the cell which could also be confirmed via CLSM. Hitherto, there are a few publications dealing with this question. In recent studies, the resulting fluorescence of adsorbed FITC-labelled nanoparticles was quenched with trypan blue which has been demonstrated to quench the fluorescence of FITC-labelled compounds (Huang et al., 2004; Ma & Lim, 2003; Sahlin et al., 1983). However, this method requires an addition of a supplemental reagent which can again result in interactions with nanoparticles. Due to their chemical properties nanoparticles often show strong interactions with a lot of standardized chemicals. Therefore, it is suggested to avoid the application of additional reagents (Wahl et al., 2008; Worle-Knirsch et al., 2006). Furthermore, these methods give no information about the localization of the particles within the cell. The performed washing experiments for the removal of nanoparticles from the outer cell membrane failed. Contents of the used buffers were very aggressive and caused fatal cell

damages which resulted in the loss of the barrier function. However, a promising approach allowing a distinction between internalized and adsorbed nanoparticles will be discussed in chapter 5.

Transport experiments correlated with conducted cell association studies since the transport rate of silica nanoparticles was related to their cellular association. The transport rate is as well size- and time-dependent, whereupon the transport of PEG-modified nanoparticles was very low. These results were conceivable, as particles showing no or a very low association to the outer cell membrane, could not be internalized and consequently could not be transported across a cell monolayer. The transport speed of nanoparticles was very low. Compared to the compound [^{14}C]mannitol, which is a drug belonging to class 4 (drugs with low solubility and low permeability) of the Biopharmaceutic Classification System (BCS), a guidance for predicting the intestinal drug absorption, the used nanoparticles were transported even slower. Mannitol demonstrated a P_{app} of 1.77×10^{-7} cm/sec (Hidalgo et al., 1989), silica nanoparticles were in the range of 2.06×10^{-8} to 4.26×10^{-8} cm/sec.

Various studies suggested that the uptake and the following transport across the intestinal epithelial barrier may not occur in enterocytes but in the intestinal M cells. M cells are parts of the follicle associated epithelium which covers the Peyer's patches. They consist of a small amount of microvilli which can result in a reduced clearance of adsorbed particles. Furthermore, M cells are able to internalize antigens, macromolecules such as bacteria or viruses and also nanoparticles from the apical side in an endocytotic process (Clark et al., 2001; Frey & Neutra, 1997). Therefore, M cells present the potential portal for oral delivery of nanoparticles and should be investigated in detail and should be attracted more notice in further studies (des Rieux et al., 2005; Kraehenbuhl & Neutra, 2000). Des Rieux et al. dealt with this topic and developed an *in vitro* model for the human intestinal follicle associated epithelium which could be a promising starting point for research in this area (des Rieux et al., 2005).

4.6 CONCLUSION

The identification of potential drug candidates and the treatment of diseases like cancer by new methods such as antisense therapy assign new tasks for the pharmaceutical nanotechnology. Thereby, cellular binding, association, uptake, transport and localization of nanoparticles are important parameters in the field of nanoparticulate drug or gene delivery. For a better comparison of different materials and applications it is of great interest to quantify the uptake and the localization of these nanoparticulate carriers. The size of the particles as well as their surface modifications had an essential function in the association and transport of these novel materials. However, the differentiation between adsorbed and internalized nanoparticles is still a problem. Therefore, the next step in this research field was the finding of new approaches for a clear distinction between nanoparticles associated with the outer cell surface and particles, which are taken up into the cell. As the removal of nanoparticles by the means of different washing buffers failed, the answer to this problem was found in the labelling of the particles in principle (see chapter 5).

5

Cellular uptake and localization of propidium iodide-labelled silica nanoparticles.

Parts of this chapter have been submitted or are in preparation for publication as journal articles:

1. A. Neumeyer, M. Bukowski, M. Veith, C.-M. Lehr & N. Daum. PI-labelling of nanoparticles as novel tool for the quantification of cellular binding and uptake. Submitted to *Nanomedicine: Nanotechnology, Biology and Medicine*

2. A. Neumeyer, M. Bukowski, M. Veith, C.-M. Lehr & N. Daum. Identification of the endocytotic mechanisms involved in the cellular uptake of silica nanoparticles. In preparation.

For a closer investigation of the cellular uptake and localization of nanoparticles within Caco-2 cells, particles with adsorbed propidium iodide (PI) were prepared. These particles only give a fluorescence signal when associated with DNA or RNA. Consequently, particles adsorbed to the outer cell surface are not detected, whereas internalized particles exhibit a clear fluorescence signal. Flow cytometry measurements demonstrated that PI-labelled nanoparticles with a size of 21 nm showed a clear time-dependent uptake into the cell. Further experiments exhibited that a PI signal could be detected in the cytoplasm and less in the nucleus, what could be confirmed via confocal microscopy. Furthermore, this approach allowed the identification of cellular endocytosis mechanisms involved in the uptake of nanoparticles in a quantitative way. In addition, the carrier function of silica nanoparticles could be demonstrated by comparing the cellular uptake of free PI and nanoparticle-bound PI. Free PI was not able to enter Caco-2 cells, whereas PI bound to nanoparticles showed a clear internalization. In summary, the PI-labelling of nanoparticles in combination with flow

cytometry measurements are an innovative and promising tool for the quantification of nanoparticulate uptake.

5.1 INTRODUCTION

Nanoparticles provide innovative characteristics as drug carrier. Nanoparticle-encapsulated or -adsorbed drug molecules show a remarkably increased bioavailability by improving the overcoming of several biological barriers. In this context, silica nanoparticles show various advantages. They are non-toxic, can be easily surface modified, are insensitive to microorganisms and show high pH stability. Recent studies already demonstrated an uptake of silica nanoparticles in cells and nuclei using confocal microscopy (Chen & Mikecz von, 2005; Peng et al., 2006; Vallhov et al., 2007). However, there is a lack of studies which determine the nanoparticulate uptake in a quantitative way. The quantification in this field of application is essential, especially, when different materials or studies should be compared.

Most fluorescent labellings (such as Rhodamine B-isothiocyanate, RITC) (compare to chapter 4) lack the possibility to distinguish between particles internalized into the cell and particles adsorbed to the outer cell surface via quantitative analysis (e.g. flow cytometry). To allow a distinction between internalized and adsorbed particles as well as to obtain information about the cellular localization, propidium iodide (PI)-labelled nanoparticles were prepared. These nanoparticles only emit fluorescence when associated with DNA or RNA. Consequently, ingested nanoparticles generate a signal, whereas particles adsorbed to the outer cell membranes are not detected.

By means of this novel staining, it is possible to explore the uptake of nanoparticles in more detail, receive information about the cellular localization and clarify in a quantitative way the cellular endocytosis mechanisms which are involved in the nanoparticulate internalization. For an efficient optimization of nanoparticulate carriers it is very important to profile their cellular uptake, because this determines their intracellular transport and fate. For the uptake of nanocarriers two main internalization pathways are described: either the phagocytosis or endocytosis pathways such as clathrin- and caveolae-mediated endocytosis. Thereby,

phagocytosis occurs primarily in specialized cells like macrophages, monocytes, neutrophils or dendritic cells. But also epithelial and endothelial cells have been described to show some phagocytic activity. In contrast to phagocytosis, endocytic pathways occur in all cells and can be divided into three groups: clathrin-mediated endocytosis, caveolae-mediated endocytosis, and other clathrin- and caveolae-independent pathways (Conner & Schmid, 2003; Hillaireau & Couvreur, 2009; Rabinovitch, 1995). With means of endocytosis inhibitors, the mechanisms involved in the uptake of nanoparticles could be identified. Cytochalasin D is a cell permeable and potent inhibitor of actin polymerization of the class of mycotoxins (May et al., 1998). As phagocytosis is an actin-based mechanism, cytochalasin D can inhibit the uptake of particles via this pathway (Lamaze & Schmid, 1995; Parton et al., 1994). The clathrin-dependent endocytosis can be prevented via cellular incubation with chlorpromazine. Chlorpromazine is a lipophilic phenothiazine derivative which easily binds with membranes and proteins. As a result it inhibits the clathrin-coated pit formation by reversible translocation of clathrin and its adapter proteins from the outer cell membrane to intracellular vesicles (Diaz-Moscoso et al., 2010; Wang et al., 1993). The caveolae-dependent pathway is obstructed via nystatin, a polyene antifungal drug which sequesters cholesterol and thus, causes a depletion of cholesterol. As cholesterol is needed for the maintaining of caveolae development, the mentioned pathway is inhibited (Lamaze & Schmid, 1995; Rothberg et al., 1990). Monensin, a polyether ionophore antibiotic inhibits caveolae- and clathrin-independent mechanisms by preventing the transition of mid and late endosomes to lysosomes and avoiding an endosome acidification (Basu et al., 1981; Mollenhauer et al., 1990). Figure 5.1 gives an overview of all mentioned endocytosis pathways.

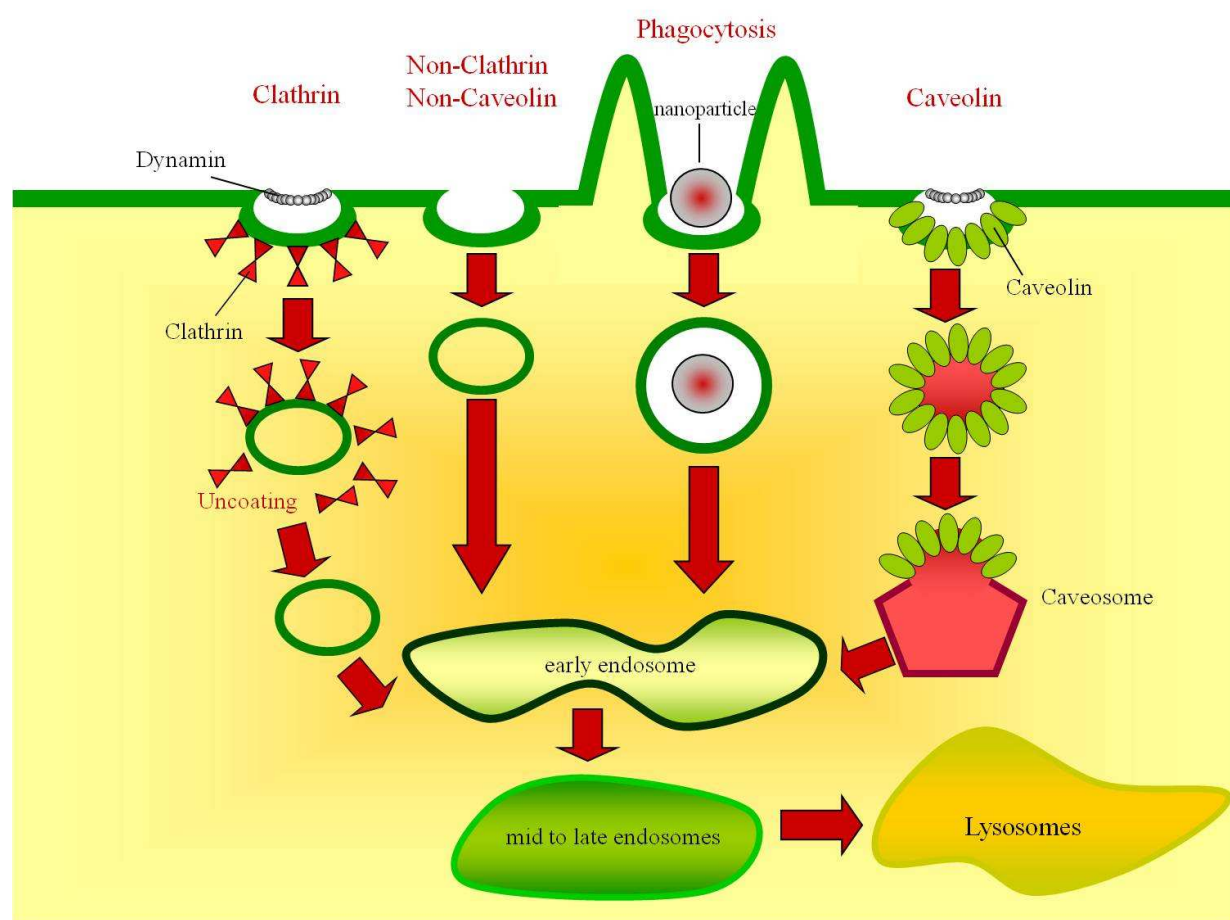


Figure 5.1: Summary of endocytotic pathways. Large particles can be taken up by phagocytosis, which is a process dependent on actin-mediated remodelling of the cell membrane. Particles can be endocytosed by different mechanisms that are independent of the coating protein clathrin and dynamin as well (non-clathrin/non-caveolin endocytosis). Most internalized molecules are delivered to the early endosome via clathrin- or caveolin-coated vesicles that are derived from the cell membrane (clathrin- or caveolin-dependent endocytosis).

5.2 AIM OF THE STUDY

The aim of this study was to allow the differentiation between particles adsorbed to the outer cell membrane and particles taken up into the cell or the nucleus. Afterwards, the uptake properties and the involved uptake mechanisms of PI-labelled silica nanoparticles with different sizes and surface modifications should be evaluated in a quantitative way using flow cytometry.

5.3 MATERIALS AND METHODS

5.3.1 Materials

Dulbecco's modified eagle medium (DMEM) with high glucose (4.5 g/l) and L-glutamine was obtained from Gibco (Karlsruhe, Germany), fetal bovine serum was purchased from PAN-Biotech (Aidenbach, Germany), non-essential amino acids were obtained from PAA (Cölbe, Germany). Composition of Hank's balanced salt solution (HBSS) was as follows: 136.9 mM NaCl, 5.4 mM KCl, 4.26 mM NaHCO₃, 0.34 mM Na₂HPO₄*7H₂O, 0.35 mM KH₂PO₄, 5.5 mM glucose, 10 mM HEPES, 1.26 mM CaCl₂, 0.5 mM MgCl₂*6H₂O, and 0.4 mM MgSO₄*7H₂O. HBSS was adjusted to pH 7.4 by means of NaOH. Phosphate buffered saline (PBS) was as follows: 129 mM NaCl, 2.5 mM KCl, 7 mM Na₂HPO₄*7H₂O and 1.3 mM KH₂PO₄. PBS was adjusted to pH 7.4 by means of NaOH, as well. Citric acid, tween 20, thiazolyl blue tetrazolium bromide, bovine serum albumin and propidium iodide (PI) were obtained from Sigma (Munich, Germany). RNase A was obtained from Qiagen (Hilden, Germany) and FITC-labelled wheat germ agglutinin (WGA) was purchased from Vector Laboratories (Burlingame, CA). Culture slides were obtained from BD Falcon (Franklin Lakes, NJ). Centrisart[®] centrifugation vials were purchased from Sartorius (Goettingen, Germany).

5.3.2 Caco-2 cell culture

The human colon adenocarcinoma cell line, Caco-2, clone C2Bbe1, was purchased from American Tissue Culture Collection (ATCC, Manassas, VA) and used at passages 60-80. Cells were cultured in Dulbecco's modified eagle medium (DMEM) with high glucose (4.5 g/l) and L-glutamine, supplemented with 10% fetal calf serum (FCS) and 1% non-essential amino acids and were maintained under standard culture conditions at a temperature of 37°C and in a humidified atmosphere of 5% CO₂. The culture medium was changed three times a week.

5.3.3 Stability of the binding between PI and silica nanoparticles

The stability of the binding between the fluorescence dye PI and the silica nanoparticles were analysed dispersing PI-labelled silica nanoparticles in a concentration of 100 µg/ml in HBSS

with different pH values (5.0, 5.5, 6.0, 6.5, 7.0 and 7.4). Nanoparticle dispersions were incubated for 4 hours under standard cell culture conditions. Afterwards, they were centrifuged using Centriscart[®] centrifugation vials with a molecular weight cut off of 5 000 Dalton. Supernatants of the different dispersions were analysed via fluorescence measurements with an emission filter of 617 nm and an excitation filter of 536 nm.

5.3.4 Determination of the cellular uptake of PI-labelled nanoparticles via flow cytometry

Quantification of the cellular or nuclear uptake of PI-labelled nanoparticles was determined via flow cytometry as described before in chapter 4 (compare 4.3.4) with the introduced cell preparation protocols (compare 4.3.5). Emitted light resulting from internalized PI-labelled nanoparticles was detected by the FL3 detector. For a distinction between active and passive uptake mechanisms, uptake experiments were performed at a temperature of 4°C as well.

5.3.5 PI-labelled nanoparticles as carriers for PI

One characteristic of PI is that it is excluded from viable cells and is not capable to cross intact cell membranes. Therefore, it could be used as a model substance for drugs with a low bioavailability and it could be tested if silica nanoparticles could improve the transport of a membrane impermeable compound like PI. For this purpose, Caco-2 cells were incubated with nanoparticle-bound PI as well as with free PI in solution. The concentration of the used unbound PI was equivalent to the amount of PI associated with N21-PI nanoparticles in respective concentrations (Table 5.1).

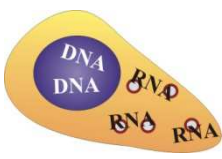
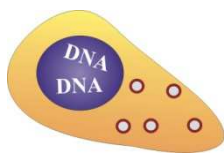
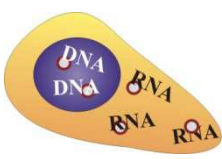
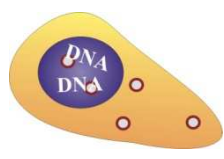
Table 5.1: Concentrations of PI-labelled nanoparticles (N21-PI) (µg/ml) and the corresponding concentrations of free PI (ng/ml).

N21-PI concentration (µg/ml)	Free PI concentration (ng/ml)
1	0.00727
10	0.0727
50	0.364
100	0.727
200	1.45
500	3.64

5.3.6 Determination of the cellular localization of PI-labelled silica nanoparticles via RNase

The binding characteristics of PI allow a distinction between nanoparticles localized in the nucleus and nanoparticles localized in the cytoplasm. For this purpose, cells were pre-incubated with RNase A to enzymatically degrade the ribose backbone of the RNA and thereby eliminating RNA molecules. In contrast, DNA molecules were not influenced by this RNase treatment. As a result PI-labelled nanoparticles were not able to bind to RNA anymore but had the continuing ability to intercalate into DNA. DNA is predominantly located in the nuclei, whereas RNA is found in the form of mRNA and tRNA and furthermore in small quantities as pre-mRNA and snRNA in the cytoplasm (Barciszewski & Clark, 1999). Thus, a fluorescence signal (e.g. via flow cytometry) generated after pre-incubation with RNase was due to an association of PI-labelled nanoparticles with DNA indicative for an uptake into the nucleus (Table 5.2).

Table 5.2: Dependency between PI fluorescence and localization of PI-labelled silica nanoparticles (with/without RNase pre-incubation).

	without RNase	with RNase
cellular localization	 <p>fluorescence signal</p>	 <p>no signal</p>
nuclear localization	 <p>fluorescence signal</p>	 <p>fluorescence signal</p>

5.3.7 Determination of the cellular uptake mechanisms of silica nanoparticles

For the clarification of the endocytosis mechanisms involved in the cellular uptake of silica nanoparticles, different endocytosis inhibitors (cytochalasin D, chlorpromazine, nystatin and monensin) were used. Stock solutions of these inhibitors were diluted to a final concentration of 5 mg/ml in DMSO (cytochalasin D and chlorpromazine), water (nystatin) or ethanol

(monensin). Table 5.3 summarizes the used endocytosis inhibitors and the corresponding inhibited pathways. To investigate the involved uptake mechanisms, Caco-2 cells were pre-incubated with the mentioned endocytosis inhibitors in different concentrations (Table 5.3) for 2 hours. Subsequently, PI-labelled nanoparticles with different sizes (21-84 nm) were added to the cells. Afterwards, cells were prepared as described before (compare 4.3.5) and were analysed via flow cytometry.

Table 5.3: Endocytosis inhibitors and their corresponding inhibited endocytosis pathways.

Endocytosis inhibitors	Inhibited endocytosis pathway	Used concentrations
Cytochalasin D	Phagocytosis	1, 5 and 10 $\mu\text{g/ml}$
Chlorpromazine	Clathrin-dependent pathway	5, 10 and 20 $\mu\text{g/ml}$
Nystatin	Caveolae-dependent pathway	1, 10 and 20 $\mu\text{g/ml}$
Monensin	Caveolae- and clathrin-independent pathways	5, 15 and 30 $\mu\text{g/ml}$

5.4 RESULTS

5.4.1 PI-labelling allows a clear distinction between adsorbed and internalized silica nanoparticles

As mentioned before, most fluorescently-labelled nanoparticles, such as RITC-labelled nanoparticles, have the disadvantage that it is not possible to distinguish between internalized and adsorbed particles in a quantitative way (e.g. via flow cytometry). Whole cells which exhibited a fluorescence signal via flow cytometry can be associated with nanoparticles in two different ways: either particles are adsorbed to the outer cell surface or cells contain of internalized particles. The main advantage of PI is that its basic fluorescence is increased by 20 to 30 fold if it is integrated between bases of DNA or RNA strands. As a result, nanoparticles which are located at the outer cell surface and which are not in any contact with DNA or RNA generate no fluorescence signal. In contrast, nanoparticles which have entered the cells and have the possibility to intercalate between DNA or RNA bases emit a fluorescence signal. To proof this concept, PI-labelled nanoparticles as well as RITC-labelled

nanoparticles with similar sizes (21 and 25 nm) were incubated with Caco-2 cells for 1 minute. This short incubation time excluded an uptake of nanoparticles into the cells which could also be confirmed by CLSM (data not shown). RITC-labelled nanoparticles showed already after this short 1-minute-incubation a high fluorescence signal (Figure 5.2 A) due to particles associated with the outer cell membrane. In contrast, PI-labelled nanoparticles incubated for 1 minute showed no signal at all due to their localization at the outer cell surface, where DNA or RNA was absent (Figure 5.2 B).

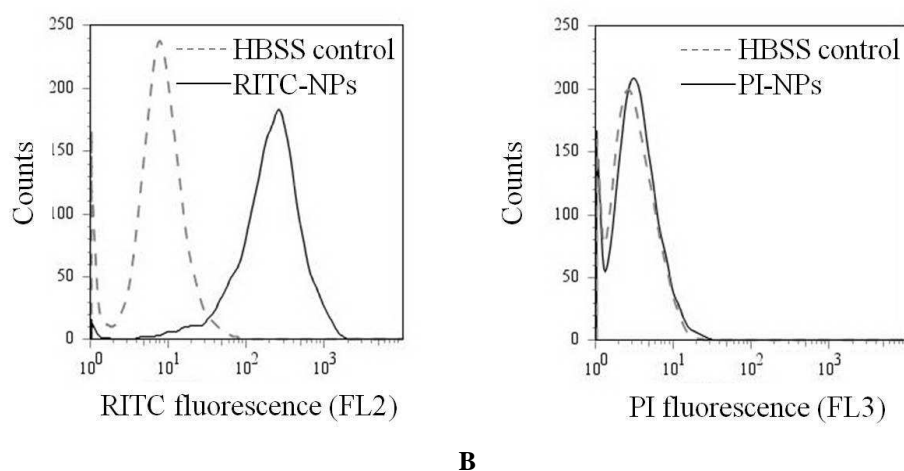


Figure 5.2: Fluorescence signal of RITC- and PI-labelled silica nanoparticles. Nanoparticles were added to Caco-2 cells for 1 minute. Afterwards, cells were washed three times with PBS and were analyzed via flow cytometry. Histograms are the result of 10 000 analysed cells. HBSS treated cells served as a negative control (dashed line). **(A)** RITC-labelled nanoparticles (RITC-NPs) were detected with FL2 and **(B)** PI-labelled nanoparticles (PI-NPs) were detected with FL3.

As the cellular uptake of nanoparticles is strongly associated with an alteration in pH, a further experiment investigated the stability of the binding between PI molecules and silica nanoparticles at different pH values. The binding between the fluorescence dye PI and the nanoparticles was stable for 4 hours in all pH values reaching from 5.0 to 7.4. After a 4-hour-incubation at 37°C, 0.35% to 1.20% of the PI dye was released from the particles. Due to these results, it could be suggested, that the detected fluorescence signals were based on nanoparticle-bound PI rather than free PI, released from nanoparticles (Figure 5.3).

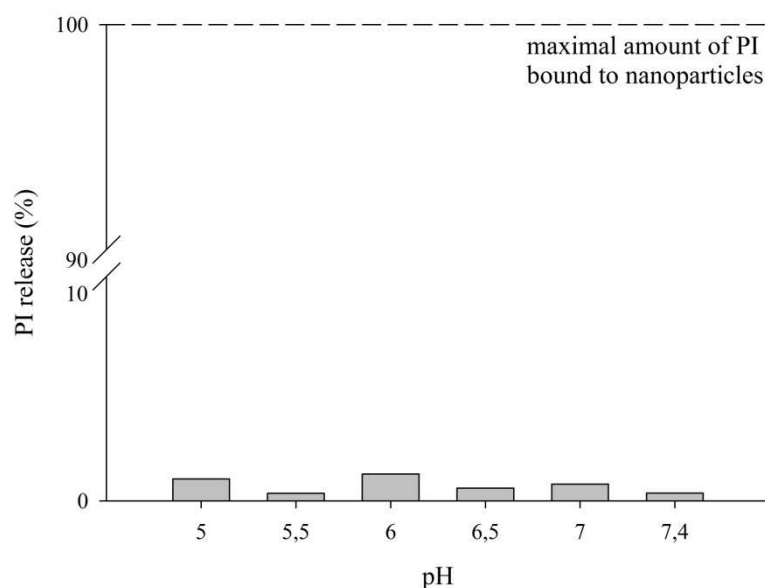


Figure 5.3: PI release from PI-labelled silica nanoparticles. PI-labelled nanoparticles were incubated for 4 hours in HBSS with different pH values (5.0-7.4). Afterwards, particle dispersions were centrifuged in Centrisart® centrifugation vials. Supernatants were analysed using an emission filter of 617 nm and an excitation filter of 536 nm. The dashed line indicates the maximal amount of PI bound to the used silica nanoparticles.

5.4.2 Silica nanoparticles serve as drug carriers for free PI

A further advantage of PI is that it is excluded from viable cells and is not capable to cross intact cell membranes. Therefore, it was tested if silica nanoparticles could improve the transport of a membrane impermeable compound like PI. For this purpose Caco-2 cells were incubated with nanoparticle-bound PI as well as with free PI in solution. The concentration of the used unbound PI was equivalent to the amount of PI associated with N21-PI nanoparticles in respective concentrations (Table 5.1). Flow cytometry analysis demonstrated that free PI (0.727 ng/ml) is excluded from viable cells over time when compared to N21-PI particles in a concentration of 100 µg/ml (100 µg/ml N21-PI particles contain 0.727 ng/ml adsorbed PI) (Figure 5.4, grey bars). In contrast, N21-PI particles showed a time-dependent uptake over 4 hours. After an incubation of 1 hour no or a rather low cellular uptake ($0.33\% \pm 0.14$) could be detected. After a 2-hour-incubation $2.85\% \pm 0.57$ of the cells contained ingested particles $12.7\% \pm 3.75$ of the cells were positive for a PI staining after a 4-hour-incubation (Figure 5.4, black bars).

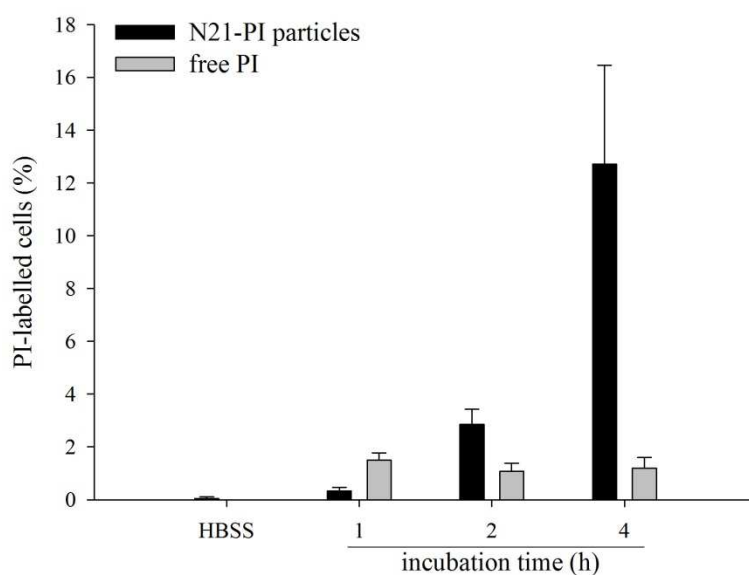


Figure 5.4: Cellular uptake of PI-labelled silica nanoparticles (N21-PI) and free PI in solution. Caco-2 cells were incubated with HBSS, N21-PI nanoparticles (100 $\mu\text{g/ml}$) or the corresponding concentration of free PI (0.727 ng/ml) for 1, 2 and 4 hours. Whole cells were analysed via flow cytometry. Results are the mean mean \pm SD of three independent experiments.

These fluorescence characteristics of PI could be rechecked via fluorescence measurements. Free PI as well as nanoparticle bound PI (N21-PI particles) was incubated for 30 minutes without cells or with intact or permeabilized Caco-2 cells. In comparison to the cell-free experiment, samples with intact cells showed no increase in fluorescence, whereas permeabilized cells demonstrated an increase in the emission. Permeabilized cells allowed a contact to DNA and RNA and consequently an alteration in the fluorescence signal (Table 5.4).

Table 5.4: Fluorescence characteristics of PI. Free PI as well as PI-labelled nanoparticles (N21-PI) were incubated for 30 minutes with intact and triton-X-permeabilized cells. Samples were analyzed using an emission filter of 617 nm and an excitation filter of 536 nm.

Sample	Without Cells	Intact Cells	Permeabilized Cells
Free PI	86	99	1072
PI-labelled nanoparticles (N21-PI)	83	72	434

5.4.3 Cellular uptake and localization of PI-labelled silica nanoparticles

The cellular uptake and also the localization of nanoparticles within the cell are of great interest. Within 4 hours, PI-labelled nanoparticles were able to enter Caco-2 cells. Flow cytometry analysis demonstrated that $12.7\% \pm 3.75$ of the cells and $3.6\% \pm 1.89$ of the nuclei exhibited a PI signal. Triton-X permeabilized cells served as a positive control. The triton-X-caused cell membrane damage allowed N21-PI particles free access to DNA or RNA within the cells. Therefore, the resulted fluorescence signal demonstrated the maximal fluorescence caused by PI-labelled nanoparticles (Figure 5.5).

To specify if internalized nanoparticles were localized in the cytoplasm or the cell nucleus, cells were pre-incubated with RNase A to enzymatically degrade the ribose backbone of the RNA and thereby eliminating RNA molecules. In contrast, DNA molecules were not influenced by this RNase treatment. As a result PI-labelled nanoparticles were not able to bind to the RNA anymore, but had the continuing ability to intercalate into DNA. DNA is predominantly located in the nucleus, whereas RNA is found in the cytoplasm. Thus, a fluorescence signal (e.g. via flow cytometry) generated after pre-incubation with RNase must be due to an association of PI molecules with DNA indicative for an uptake into the nucleus. After a 1-hour-pre-incubation with RNase and a subsequent 4-hour-incubation with N21-PI nanoparticles, $5.7\% \pm 2.92$ of Caco-2 cells were labelled with PI. In contrast, $12.7\% \pm 3.75$ of the cells were positive for a PI staining without any addition of RNase. These results demonstrated that about 6% of the analysed cells contained PI molecules which showed an association with DNA indicative for a nuclear uptake. A subsequent isolation of the nuclei evidenced these findings. Isolated nuclei did not show a significant difference to RNase pre-incubated whole cells. In RNase pre-incubated cells, RNA was eliminated enzymatically, whereas in isolated nuclei, the cytoplasm and its containing RNA-bound PI-labelled nanoparticles were removed mechanically. As a result, only DNA-associated and therefore nucleus-localized PI molecules could be detected (Figure 5.5).

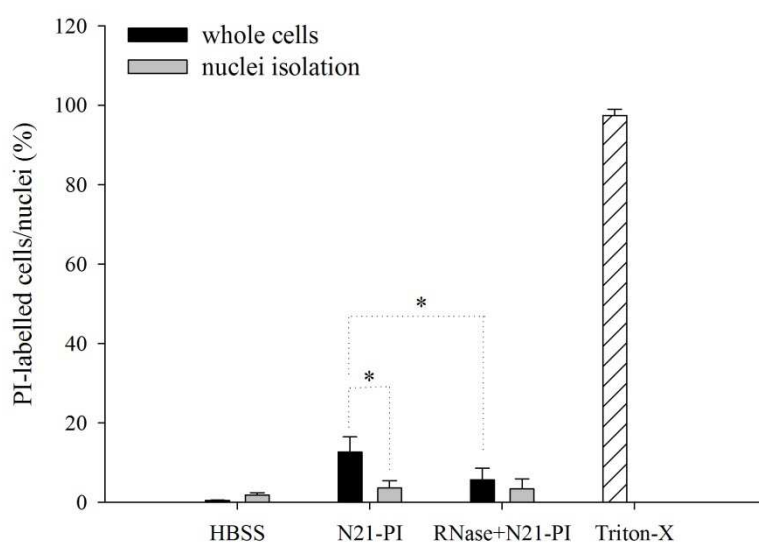


Figure 5.5: Cellular and nuclear uptake and localization of PI-labelled silica nanoparticles (N21-PI). Caco-2 cells were incubated with N21-PI nanoparticles in a concentration of 100 $\mu\text{g/ml}$ for 4 hours without or with pre-incubation of RNase. Whole cells as well as isolated nuclei were analysed via flow cytometry. As a positive control cells had been permeabilized with triton-X prior to nanoparticle incubation. HBSS served as negative control. Results are the mean \pm SD of three independent experiments. The asterisks depict significant differences between the different samples ($p \leq 0.05$ *).

The significant decrease in the emitted PI signal ($p \leq 0.02$) for whole cells after pre-incubation with RNase could be also detected via CLSM in a qualitative way (Figure 5.6). As a positive control permeabilized cells were stained with free PI in solution (0.727 ng/ml) (Figure 5.6 A) which resulted in a clear red staining of the inner cells. As a negative control Caco-2 cells were incubated for 1 minute with N21-PI nanoparticles. In this experiment no red staining could be detected (Figure 5.6 B), because nanoparticles did not enter the cell during this short incubation time. Furthermore, N21-PI nanoparticles were incubated for 4 hours without (Figure 5.6 C) or with a previous cellular incubation with RNase for 1 hour (Figure 5.6 D). Figure 5.6 C clearly shows a red staining inside the green-labelled cell membranes. The red signal inside the cells is an indication for PI-labelled nanoparticles taken up into the cells. This fluorescence signal was absent in cells pre-incubated with RNase, because PI could not bind to RNA anymore. Obviously, after 4 hours only a low amount of particles or PI molecules were able to enter the nucleus, insufficient to cause a detectable fluorescence signal.

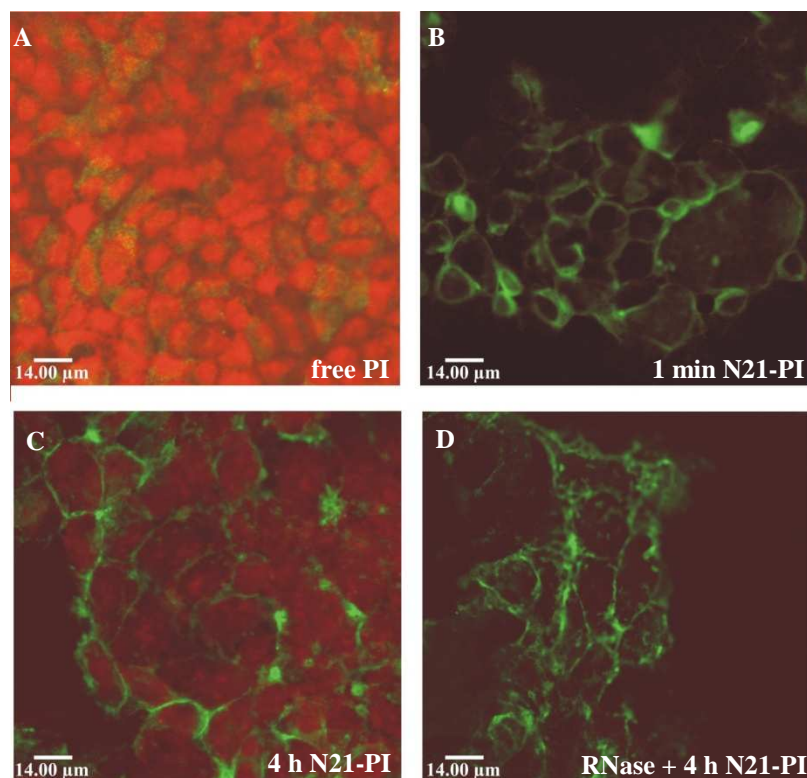


Figure 5.6: Cellular uptake and localization of PI-labelled silica nanoparticles. Caco-2 cells were plated on glass culture slides. Cells were incubated with (A) free PI (after fixation), (B) N21-PI particles for 1 minute, (C) N21-PI particles for 4 hours or (D) N21-PI particles for 4 hours with a pre-incubation of RNase. Membranes were stained with FITC-labelled WGA (green) followed by a cell fixation with 4% formalin. Analysis was performed via CLSM. Bars=14.00 µm.

5.4.4 Identification of the internalization mechanisms involved in the uptake of silica nanoparticles

To proof if nanoparticles were internalized in an active or a passive process, uptake experiments were conducted at a temperature of 37°C and a temperature of 4°C as well. For this purpose, Caco-2 cells were incubated with N21-PI, N34-PI or N84-PI nanoparticles for 4 hours under standard cell culture conditions or at a temperature of 4°C. For N21-PI and N34-PI particles no uptake inhibition at 4°C in comparison to the uptake rate at 37°C could be demonstrated. In contrast, N84-PI particles showed a significantly reduced cellular uptake of $49.49\% \pm 16.6$ when incubated at a temperature of 4°C (Figure 5.7).

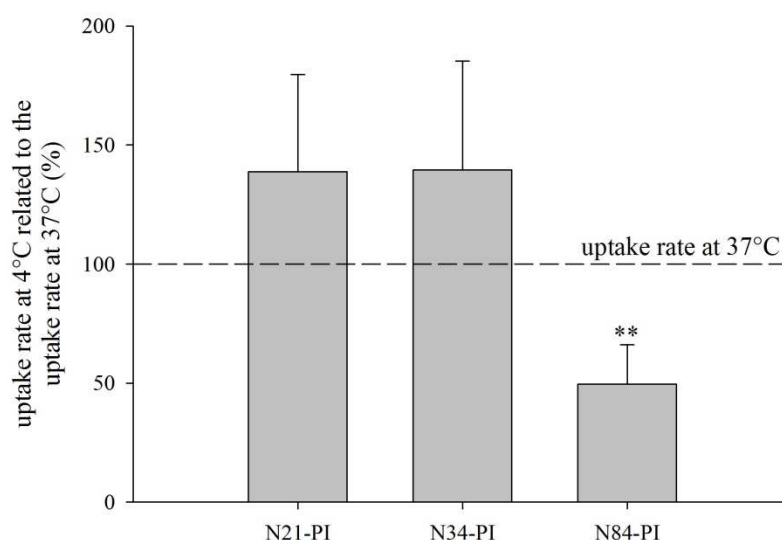


Figure 5.7: Temperature-dependent uptake of silica nanoparticles. Caco-2 cells were incubated for 4 hours with different silica nanoparticles (N21-PI, N34-PI and N84-PI) at a temperature of 37°C or 4°C. Cells were analysed via FACS. Data show the alteration in the uptake rate compared to control cells incubated at 37°C in HBSS. Results are the mean \pm SD of three independent experiments. The asterisks depict significant differences between cells incubated at 4°C and cells incubated at 37°C ($p \leq 0.01$ **).

For the clarification of the uptake mechanisms involved in the cellular uptake of nanoparticles, Caco-2 cells were incubated with different endocytosis inhibitors. Chlorpromazine (clathrin-dependent endocytosis) and nystatin (caveolae-dependent endocytosis) showed no inhibition in the uptake rate when compared to cells pre-incubated in HBSS instead of an inhibitor (Figure 5.8 A and B). In contrast, cytochalasin D (phagocytosis) and monensin (clathrin- and caveolae-independent pathways) demonstrated a concentration-dependent inhibition in the uptake of nanoparticles into Caco-2 cells (Figure 5.8 C and D).

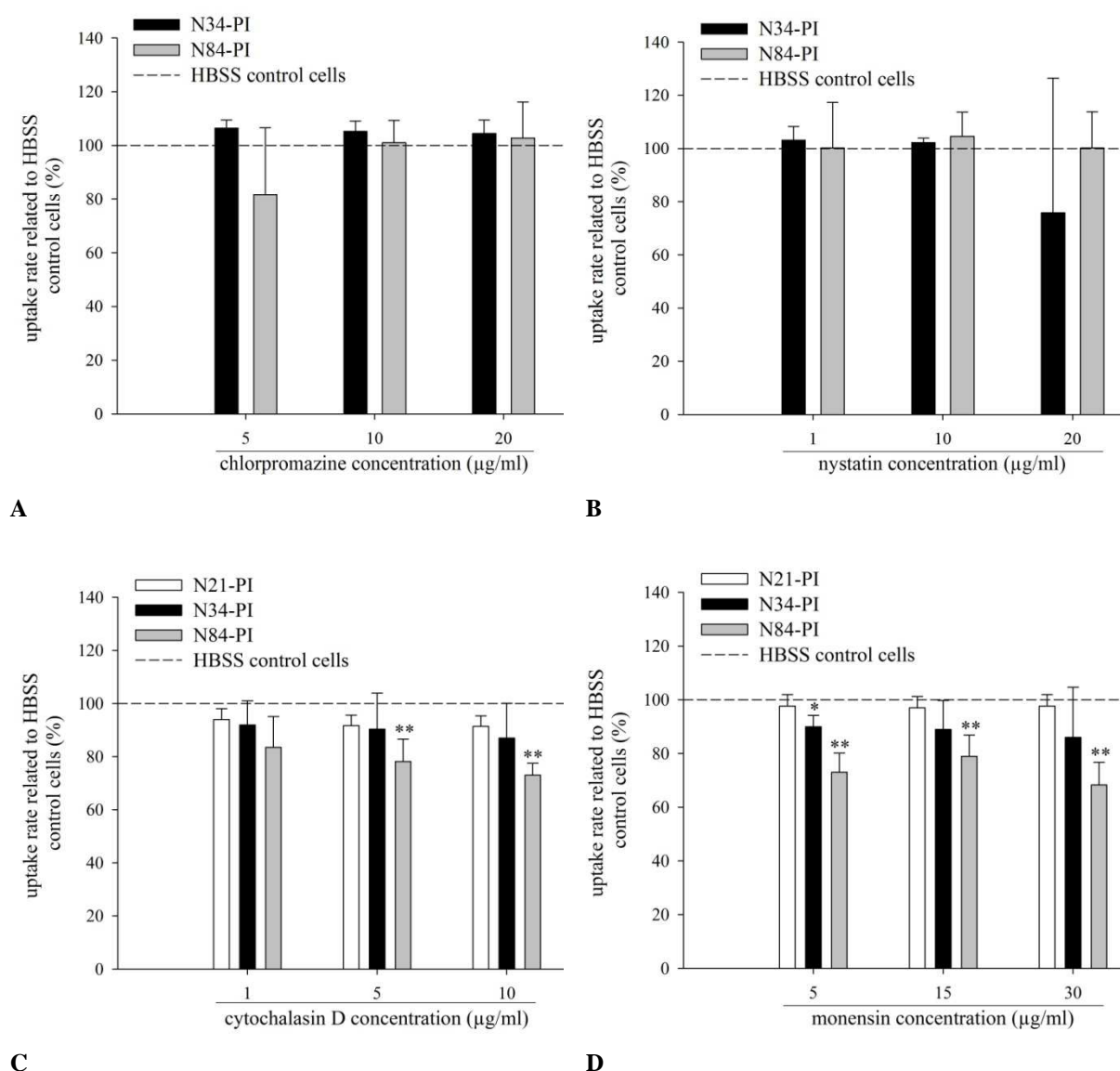


Figure 5.8: Identification of the internalization mechanisms involved in the uptake of silica nanoparticles. Caco-2 cells were pre-incubated for 2 hours with different endocytosis inhibitors: **(A)** Chlorpromazine, clathrin-dependent endocytosis **(B)** Nystatin, caveolae-dependent endocytosis. **(C)** Cytochalasin D, phagocytosis. **(D)** Monensin, caveolae- and clathrin-independent endocytosis. Afterwards, cells were incubated with N21-PI (only C and D), N34-PI and N84-PI nanoparticles for 4 hours. Cells were analysed via FACS. Data show the alteration in the uptake rate compared to control cells incubated in HBSS instead of an endocytosis inhibitor. The asterisks depict significant differences between inhibitor-incubated and control cells ($p \leq 0.05$ *, $p \leq 0.01$ **). Results are the mean mean \pm SD of three or two (chlorpromazine) independent experiments.

The inhibition of the nanoparticulate uptake by cytochalasin D and monensin was dependent on the used nanoparticle sizes. Nanoparticles with a size of 21 nm (N21-PI) were not influenced by these endocytosis inhibitors and exhibited no decreased uptake (Figure 5.8 C and D, white bars). In contrast, particles with a size of 34 nm (N34-PI) showed

a significantly reduced internalization after cellular pre-incubation with 5 $\mu\text{g/ml}$ monensin (Figure 5.8 C and D, black bars). The largest used nanoparticles with a size of 84 nm demonstrated the strongest influence by cytochalasin D or monensin. For cytochalasin D as well as for monensin a concentration-dependent decrease in the cellular uptake of these nanoparticles was documented (Figure 5.8 C and D, grey bars).

5.5 DISCUSSION

In this study, silica nanoparticles with adsorbed PI served as novel tools for the quantification of the cellular uptake. These particles promise a clear differentiation between particles associated with the outer cell membrane and particles taken up into the cell. Therefore, this nanoparticulate staining in combination with the new established flow cytometry assay, demonstrates a promising tool for the quantitative investigation of cellular uptake and localization. Especially, the cellular localization and the involved uptake mechanisms are essential parameters with regard to toxicity and the future application spectrum.

Silica nanoparticles present potential drug carriers for molecules with a low bioavailability or stability. In this study the membrane-impermeable fluorescent dye PI served as a model substance. It could be demonstrated that free PI molecules could not overcome intact cell membranes due to its chemical composition. In contrast, its binding to silica nanoparticles allowed a time-dependent internalization into the cells. This ability of nanoparticles could be very helpful in the oral application of cytostatics in cancer therapy. Most anticancer drugs are orally not or minimal bioavailable, e.g., the bioavailability of the cytostatic paclitaxel is less than 1%. Lipid based nanoparticles already improved the paclitaxel transport across Caco-2 cells (Roger et al., 2009). In addition, an *in vivo* study demonstrated an enhanced oral bioavailability of paclitaxel via paclitaxel-loaded lipid nanocapsules (Peltier et al., 2006).

As the cellular uptake of nanoparticles is strongly associated with an alteration in pH, a further experiment investigated the stability of the binding between PI molecules and silica nanoparticles in HBSS with different pH values. Hitherto, various uptake mechanisms had

been described as potential cell capture pathways for nanoparticles (Hillaireau & Couvreur, 2009). All these mechanisms are associated with several specific organelles such as endosomes or lysosomes. These organelles are involved in the sequential cellular passage of particles. ATP-dependent proton pumps are responsible for the generation of an internal acidic environment of these organelles. Thereby, the pH can reach from 5.0 to 6.5 (Mellman et al., 1986; Pantarotto et al., 2004; Yamashiro & Maxfield, 1984). Conducted experiments investigated the strength of the binding between PI molecules and silica nanoparticles, demonstrated a strong association between dye and nanoparticles at different pH values. Therefore, it could be suggested that the generated fluorescence signal was based on nanoparticle bound PI. In addition, it should be mentioned that e.g., lysosomes possess a specific enzymatic content including esterases and cathepsins (Mellman et al., 1986). The impact of these enzymes to the stability of the binding between fluorescence dyes and particles should clearly be kept in mind. Furthermore, due to mechanic forces during the internalization process, there could be a release of PI during nanoparticulate transport through the cell as well. Visualization techniques such as scanning electron microscopy could be used to clarify this question.

Besides the cellular uptake, also the localization of nanoparticles within the cell is of great interest. Especially, drug delivery to the nucleus is an increasing field as the nucleus is a promising target, because the cell and transcription machinery is localized there (Breunig et al., 2008; Tkachenko et al., 2003). Silica nanoparticles sized between 40 and 70 nm had already been reported to penetrate the nuclei of Hep-2 epithelial cells (Chen & Mikecz von, 2005). Furthermore, gold nanoparticles functionalized with a TAT protein-derived peptide sequence could be localized in the nucleus, whereas unfunctionalized nanoparticles were just present in the cytoplasm and showed no translocation into the nucleus (de la Fuente & Berry, 2005). The usage of RNase in combination with the PI-labelling of nanoparticles allowed more detailed insights in the cellular localization of these particles. RNase enzymatically eliminates RNA molecules, DNA molecules were not influenced by this RNase treatment. As a result, PI-labelled nanoparticles were not able to bind to RNA anymore but had the continuing ability to intercalate into DNA. DNA is predominantly located in the nuclei, whereas RNA is found in the form of mRNA and tRNA in the cytoplasm and furthermore in small quantities as pre-mRNA and snRNA in the nucleus (Barciszewski & Clark, 1999). Thus, a fluorescence signal (e.g. via flow cytometry) generated after pre-incubation with

RNase was due to an association of PI-molecules with DNA indicative for an uptake into the nucleus. Results demonstrated that about 6% of the analysed cells contained PI molecules which showed an association with DNA indicative for a nuclear uptake. A subsequent isolation of the nuclei evidenced these findings. However, the main amount of these particles was localized in the cytoplasm. A functionalization of these particles with ligands such as nucleus localization signals could increase their target delivery and entry into the nucleus.

Nevertheless, as used silica nanoparticles apparently were able to enter the cell nucleus, genotoxicity should be mentioned as well. Recent studies already demonstrated a strong association between genotoxic effects, the cellular uptake rate und the intracellular localization of silver nanoparticles (Ahamed et al., 2008). Carbon nanotubes showed the possibility to cause DNA damage due to their penetration into the cell nucleus (Tkachenko et al., 2003). Silica nanoparticles were described as well to enter the nucleus and influence the gene expression (Chen & Mikecz von, 2005). Silica nanoparticles with a size of 21 nm caused a decrease in cellular viability (compare to chapter 3). Hitherto, the reason of that cytotoxic effect could not be clarified. Thereby, a genotoxic effect due to the nuclear localization of these particles could not be excluded.

Hitherto, various uptake mechanisms have been described as potential cell capture pathways for nanoparticles (Hillaireau & Couvreur, 2009; Luhmann et al., 2008). In general, nanoparticles must cross one or more biological membranes before they diffuse across the plasma membrane to finally enter the target organelle. Depending on the drug characteristics, the chosen uptake pathway as well as the intracellular fate of the drug carrier is essential for the efficacy of the drug. Thereby, the release of the drug into the enzymatic environment of the lysosomes or the direct release in the cell cytoplasm will dramatically influence the pharmacological activity of a drug (Hillaireau & Couvreur, 2009). Mostly, the internalization of nanoparticles into macrophages via phagocytosis is documented. Phagocytosis as the involved mechanism is described for particles sized between 250 and 3000 nm (Conner & Schmid, 2003; Khalil et al., 2006; Mayor & Pagano, 2007). Whereas, nanoparticles smaller than 250 nm were less efficiently internalized via phagocytosis (Korn & Weisman, 1967). Phagocytosis is a process which occurs only in highly specialized cells such as macrophages. However, also for other cell types a phagocytosis-like mechanism could be demonstrated

during the uptake of large cationic-lipid-DNA complexes and PEI polyplexes (Kopatz et al., 2004; Matsui et al., 1997). Such a phagocytosis-like mechanism could also play a role in the conducted uptake experiments in this study. Silica nanoparticles with a size of 84 nm showed a significant concentration-dependent uptake reduction after pre-incubation with cytochalasin D, an inhibitor for phagocytosis. Even, if the size of the particles is not in the optimal range of phagocytosis, the inhibition of phagocytosis caused a clear reduction in the uptake of silica nanoparticles with a size of 84 nm. This uptake process starts with the interaction of particles with specific receptors such as opsonic receptors on the phagocyte. This causes an actin assembly and the formation of cell surface extensions that cover the particle to engulf it. Subsequently, the particle is internalized and the actin is shed from the phagosomes. The resulting phagosome transports the particle through the cytoplasm. Afterwards, a series of fusion and fission events begin, which result in the formation of mature phagolysosomes where internalized particles are degraded (Khalil et al., 2006). Phagocytosis has been traditionally referred to as “cell eating” whereas the non-phagocytic endocytosis pathways characterized as “cell drinking” based on their involvement in the uptake of fluids and solutes. However, this terminology is not relevant anymore when working with nanoparticles. Based on their small size, solid nanoparticles can be internalized via these non-phagocytotic pathways which are clathrin-dependent, caveolae-dependent and clathrin-/caveolae-independent endocytosis (Hillaireau & Couvreur, 2009). In general, the uptake of nanoparticles and the intracellular pathways are dependent on the analyzed cell type as well as on the particular size, shape, charge and chemistry of the particles. The uptake of poly-L-lysine-PEG-DNA nanocapsules (80-90 nm) in SV 40 transformed kidney cells was inhibited by wortmannin (inhibitor for macropinocytosis), genistein and methyl- β -cyclodextrin (inhibitor of caveolae-mediated endocytosis). Chlorpromazine (inhibitor of clathrin-dependent endocytosis) caused no reduction in the uptake of these particles (Luhmann et al., 2008). Thereby, various pathways seem to be involved in the uptake of one nanoparticle type and take place simultaneously. Via the use of different endocytosis inhibitors, it could be shown that, not only a single uptake pathway is involved, but various endocytosis processes interact. The uptake of silica nanoparticles was mediated via phagocytosis as well as a clathrin-/ caveolae-independent pathway as the internalization of nanoparticles with sizes of 34 and 84 nm were influenced by monensin, an inhibitor for this mechanism. A further study demonstrated strong differences in the uptake rate of polystyrene particles sized between 20 and 1010 nm in different cell lines. Polystyrene nanoparticles with

a size of 20 nm were internalized in a high amount by all used cell types. A murine squamous cell line took up particles with sizes of 93, 220- and 560 nm but not with a size of 1010 nm. Similar results could be demonstrated for human hepatocyte carcinoma cells and a mouse hepatoma cell line. These cells internalized the smaller particles but not the 590- and 1010-nm particles. In contrast, human bladder carcinoma cells and primary human umbilical vein endothelial cells took up all used particles (Zauner et al., 2001). However, the understanding of the role of endocytosis pathways in the internalization of drug delivery nanoparticles is a rising research field. The enzymatic content of these endocytotic organelles is a key issue for polymeric nanoparticles. Polymeric nanoparticles such as PLGA nanoparticles were degraded via a hydrolytic mechanism facilitated by low pH values (Shive & Anderson, 1997). This ensures a drug release and avoids a cellular accumulation of these particles which could lead to further toxicities (Hillaireau & Couvreur, 2009). In contrast, silica nanoparticles would resist such an acidic milieu, which would be important in oral drug delivery. Here, particles have to penetrate the intestinal barrier without damage or degradation to enter the blood circulation and reach their target tissues.

Endocytosis can be strongly inhibited by lowering the temperature from standard cell culture conditions of 37°C to 4°C. At a temperature of 37°C, poly-L-lysine-PEG-DNA nanocapsules were found in the cytoplasm, whereas they were located at the outer cell membrane when the experiment were performed at 4°C (Luhmann et al., 2008). Caco-2 cells as well as a rat gastrointestinal tissue demonstrated a higher internalization of PLGA particles with a size of 100 nm than for particles sized between 500 nm and 10 µm (Desai et al., 1996; Desai et al., 1997). Furthermore, the uptake of polystyrene particles with a size of 20 nm was not reduced in murine squamous carcinoma cells when incubated at 4°C. In contrast, larger particles (93-560 nm) showed a size-dependent reduction in the cellular uptake at 4°C. The uptake of 560 nm polystyrene particles was strongly reduced at 4°C. In contrast, the internalization of particles with a size of 93 nm was less reduced (Zauner et al., 2001). These results correlate with findings in this study, where a size-dependent reduction in the uptake of nanoparticles at a temperature of 4°C could be observed as well. The internalization of PI-labelled silica nanoparticles with a size of 21 and 34 nm was not or rather low influenced by endocytosis inhibitors. Furthermore, the uptake of these particles was not reduced when experiments were performed at a temperature of 4°C in contrast to experiments at 37°C. Silica nanoparticle

with a size of 84 nm exhibited a strong reduction of about 50% in their transport rate at 4°C. The cellular pre-incubation with inhibitors for phagocytosis (cytochalasin D) and clathrin- and caveolae-independent endocytosis (monensin) caused a concentration-dependent increase in the uptake of these nanoparticles. Therefore, it is suggested, that the uptake of nanoparticles with small sizes (~20-40 nm) is carried out via passive pathways. Larger particles seem to use active internalization processes to enter a cell.

5.6 CONCLUSION

In conclusion, the PI-labelling of nanoparticles in combination with flow cytometry studies is a promising tool for the quantification of cellular uptake and localization of nanoparticles *in vitro*. It allows a clear distinction between particles internalized into cells and particles adsorbed to the outer cell membrane. Quantitative data allow an easy comparison between different studies and facilitate the experimental approach.

PI-labelled nanoparticles with a size of 21 nm showed an uptake into the cell and were even able to generate a PI signal in the nucleus indicating a nuclear localization. This allows various pharmaceutical applications but should be considered critically as well, as silica nanoparticles localized in the nucleus could cause deleterious cellular damage. Further control experiments using high resolution visualization techniques such as scanning electron microscopy could provide further evidences for a nuclear localization of these particles.

Furthermore, it could be demonstrated that particles with such a small size were internalized via passive pathways rather than by endocytotic processes. Active uptake mechanisms such as phagocytosis and clathrin- and caveolae-independent pathways seemed to play a role in the uptake of larger silica nanoparticles (84 nm).

6

Summary

Nanomaterials are innovative tools in the field of oral drug delivery. The main obstacle of this application route is the overcoming of the intestinal barrier and the insistence against cells of the immune system. An overcoming or circumvention of these barriers would lead to an enhancement in the oral bioavailability. One delivery strategy is based on the encapsulation or adsorption of drugs and molecules in nanoparticles. Thereby, inorganic nanoparticles such as silica nanoparticles provide promising characteristics as novel drug carriers. The modification of the nanoparticle surface with poly ethylene glycol (PEG) could avoid a clearance via phagocytes and other immune cells. For the application in this field, cellular binding, association, uptake properties and localization of nanoparticles within the cell have to be investigated in detail. Especially, the quantification of cellular uptake is a scarcely explored topic, but is very important for the comparison of different studies and materials. Therefore, the aim of this study was to evaluate the cellular association, uptake and transport properties of fluorescently-labelled silica nanoparticles with different sizes and surface modifications in a quantitative way using flow cytometry. Furthermore, these particles had to be evaluated for their oxidative and cytotoxic potential.

Flow cytometry analysis demonstrated that rhodamine B-isothiocyanate (RITC)-labelled silica nanoparticles sized between 50 and 77 nm exhibited a clear association with Caco-2 cells. Thereby, nanoparticles with a size of 50 nm were associated with 86% of Caco-2 cells and with 31% of isolated nuclei. Nanoparticles with a size of 77 nm showed an association rate of 85% with whole cells and 17% with isolated nuclei. In contrast, larger particles with a size of 94 nm and PEG-modified nanoparticles with similar sizes showed no or a rather very low cellular interaction. Transport experiments correlated with these association studies, as a size- and time-dependent transport across a Caco-2 cell monolayer could be observed. Small

and unmodified nanoparticles (50 nm) showed the highest transport, whereas PEG-modified and larger unmodified nanoparticles (94 nm) were not or rather low transported.

However, the fluorescent labelling with RITC lacks the possibility to distinguish between particles internalized into the cell and particles adsorbed to the outer cell surface via flow cytometry. To allow a distinction between internalized and adsorbed particles as well as to obtain further information about the cellular localization, particles with adsorbed propidium iodide (PI) were prepared. These particles only give a fluorescence signal when associated with DNA or RNA. Consequently, particles adsorbed to the outer cell surface were not detected, whereas internalized particles exhibited a clear fluorescence signal. Flow cytometry measurements showed a time-dependent uptake of PI-labelled silica nanoparticles with a size of 21 nm. Further experiments with the additional usage of RNase exhibited that PI signals could be detected in the cytoplasm and less in the nucleus. RNase enzymatically eliminates RNA molecules which are predominantly located in the cytoplasm. As a result, PI-labelled nanoparticles were not able to bind to the RNA anymore but had the continuing ability to intercalate into DNA, predominantly located in the nuclei. Thus, a fluorescence signal generated after pre-incubation with RNase was due to an association of PI molecules with DNA indicative for an uptake into the nucleus. It could be shown that after a pre-incubation with RNase and a subsequent 4-hour-incubation with PI-labelled nanoparticles with a size of 21 nm, 6% of Caco-2 cells were labelled in PI indicative for a nuclear uptake. In contrast, 13% of the cells were positive for a PI staining without any addition of RNase.

The carrier function of silica nanoparticles could be demonstrated by comparing the cellular uptake of free PI and nanoparticle-bound PI. Free PI was not able to enter Caco-2 cells, whereas PI bound to silica nanoparticles showed a clear time-dependent internalization.

The nanoparticle labelling with PI further allowed the identification of the cellular endocytosis mechanisms involved in the uptake of nanoparticles in a quantitative way. Therefore, Caco-2 cells were incubated with different endocytosis inhibitors. Chlorpromazine (clathrin-dependent endocytosis) and nystatin (caveolae-dependent endocytosis) showed no inhibition in the uptake rate of nanoparticles when compared to cells pre-incubated without an inhibitor. Cytochalasin D (phagocytosis) and monensin (clathrin- and caveolae-independent pathways) demonstrated a concentration-dependent inhibition in the uptake of nanoparticles.

Furthermore, this inhibition was dependent on the used nanoparticle size. The uptake of silica nanoparticles with a size of 21 nm were not influenced by these endocytosis inhibitors, whereas nanoparticles with a size of 34 and 84 nm showed a strong influence by cytochalasin D or monensin. Uptake experiments at a temperature of 4°C further demonstrated, that smaller particles were internalized via passive processes, whereas particles with a size of 84 nm used active pathways to enter the cells.

As pharmaceutical or medical used silica nanoparticles come into a close contact with biological systems, it is essential to evaluate their oxidative and cytotoxic potential. Therefore, a novel method for the combined detection of oxidative stress and cytotoxicity was established. This assay is based on the automated non-invasive online monitoring of the oxygen concentration in solution (SensorDish[®] Reader). Cellular respiration is associated with a consumption of oxygen and therefore serves as an indicator for cytotoxicity and can be determined measuring the long-term cellular consumption of oxygen during cell incubation. An increase in air saturation caused by decreased cellular consumption of oxygen is a very early indication for cytotoxicity. The generation of reactive oxygen species could be analysed via the increase in molecular oxygen due to the involvement of antioxidant defence enzymes. Silica nanoparticles with different sizes and surface modifications were investigated with this novel method concerning their oxidative and cytotoxic potential. Thereby, size, time, concentration as well as surface modification of nanoparticles affected the cellular viability but not oxidative stress levels. Results of this cytotoxicity studies correlate with performed cell association and uptake experiments. RITC-labelled silica nanoparticles with a size of 50 nm caused a clear decrease in cellular viability over time and had been also described to enter Caco-2 cells time-dependently. In contrast, nanoparticles which showed no association with cells exhibited no cytotoxic potential. Similar results could be demonstrated for PI-labelled nanoparticles, where the uptake rate showed a high correlation with the observed cytotoxic effect of these particles. Furthermore, it could be shown that the occurred cytotoxicity was not reversible within 72 hours.

Outlook

Results of this thesis show that silica nanoparticles have a potential as oral drug carriers. Dependent on their size and surface modification, silica nanoparticles exhibit a strong association with epithelial cells and can be internalized and finally transported across a cell monolayer. Especially, the transport across a cellular barrier is essential in the oral administration of these carriers. Nanoparticles have to cross the intestinal epithelium to reach their target site somewhere else in the body. The manner of the nanoparticulate overcoming of such a barrier is therefore an important research topic. Hitherto, it is known, that the transport across the intestinal epithelial barrier is not mainly occurring in enterocytes but in the intestinal M cell and the follicle associated epithelium. A recent study already introduced a novel *in vitro* model for the human intestinal follicle associated epithelium which could help investigating the passage of nanoparticles across the intestinal barrier more detailed (des Rieux et al., 2005). The uptake of nanoparticles becomes important once particles have reached the target tissue or cells of e.g. a tumour. Thereby, it could be shown that a surface modification with PEG is not the best solution because nanoparticles could not bind to cells anymore and therefore could not be internalized. In contrast, once reaching the blood circulation, the characteristics of PEG are essential. A surface modification with PEG avoids a clearance by macrophages and other cells of the immune system and therefore, prolongs the retention time of nanoparticles in the blood. Thus, the improvement of the nanoparticulate surface modification is a necessary task. An indication could be the functionalization of the particle surface with markers or antibodies adequate to specialized cells. M-cells of the gut e.g. produce GP2 proteins as receptors on their surface that bind E. coli or salmonella bacteria (Terahara et al., 2008). Tumour genes are widely explored and collected in data bases. Prominent examples are the human epidermal growth factor receptor 2 (HER-2) in breast cancer and the Wilms' tumour gene 1 (WT-1) which is overexpressed in 70-90 % of acute

leukaemias (Olayioye, 2001; Boublikova et al., 2006). The intelligent combination of all these surface modifications would allow a targeted and efficient transport of nanoparticles.

The loading of nanoparticles with drugs would be the next step in research. This thesis investigates silica nanoparticles as a carrier system loaded with fluorescence dyes. Thereby, these labellings were core-loaded (RITC) or adsorbed to the particle surface (PI). Drug molecules would be bound to nanoparticles in a similar manner. Experiments with PI-labelled nanoparticles already showed that silica nanoparticles served as carriers to facilitate the cellular uptake of the membrane-impermeable dye PI.

Spherical silica nanoparticles had been already loaded with the poorly, water soluble drug telmisartan (Zhang et al., 2010). A further study described an oral delivery system for indomethacin engineered from cationic lipid emulsions and silica nanoparticles (Simovic et al., 2010). Mesoporous silica nanoparticles (MSN) have been demonstrated to be able to deliver kinds of model substances such as fluorescein, Texas Red and rhodamine B. The loading was in the order of hundred milligrams per gram of nanoparticles (Slowing et al., 2008). A MSN-based system was also used to deliver genes in cells. Therefore, the delivery system was complexed with a plasmid DNA that encodes for an enhanced green fluorescence protein (GFP). Furthermore, this material allows membrane-impermeable molecules, such as pharmaceutical drugs and fluorescent dyes, to be encapsulated inside the MSN channels (Radu et al., 2004). Other studies showed a release of drugs such as ibuprofen, erythromycin and alendronate from MSN as well using different strategies to modify the control of drug release (Balas et al., 2006; Lu et al., 2004; Vallet-Regi et al., 2006). A silica-lipid hybrid microcapsule system was used for the encapsulation of celecoxib classified as a BCS Class II drug (poor solubility, high permeability) that is practically insoluble at gastrointestinal pH (Tan et al., 2009). More complex delivery systems allow e.g. a glucose-responsive controlled release of insulin and cyclic AMP (Zhao et al., 2009).

The important question concerning all these applications is still, where silica nanoparticles remain after administration. Hitherto, there is a lack of publications dealing with the fate of silica nanoparticles. A study of Wu et al. described the biodegradation of amorphous silica shells merged with superparamagnetic iron oxide nanoparticles. After injection into mice, nanoparticles were cleared from the kidney within 2 hours followed by an accumulation in the

liver and spleen (Wu et al., 2008). However, the findings about fate and behaviour in the body are essential and require intensive research in the future.

References

- Ahamed M, Karns M, Goodson M, Rowe J, Hussain SM, Schlager JJ, Hong Y. 2008. DNA damage response to different surface chemistry of silver nanoparticles in mammalian cells. *Toxicol. Appl. Pharmacol.*
- Ajani JA, Takiuchi H. 1999. Recent developments in oral chemotherapy options for gastric carcinoma. *Drugs* 58 Suppl 3 85-90.
- Allen TM, Cullis PR. 2004. Drug delivery systems: entering the mainstream. *Science* 303 (5665) 1818-22.
- Allouche J, Boissière M, Hélary C, Livage J, Coradin T. 2006. Biomimetic core-shell gelatine/silica nanoparticles: a new example of biopolymer-based nanocomposites. *Journal of Materials Chemistry* 16 (30) 3120-1325.
- Artursson P, Palm K, Luthman K. 1997. Intestinal drug absorption and metabolism in cell cultures: Caco-2 and beyond. *Pharm. Res.* 14 (12) 1655-8.
- Artursson P, Palm K, Luthman K. 2001. Caco-2 monolayers in experimental and theoretical predictions of drug transport. *Adv. Drug Deliv. Rev* 46 (1-3) 27-43.
- Avalos I, Chung CP, Oeser A, Milne GL, Morrow JD, Gebretsadik T, Shintani A, Yu C, Stein CM. 2007. Oxidative stress in systemic lupus erythematosus: relationship to disease activity and symptoms. *Lupus* 16 (3) 195-200.
- Baier J, Maisch T, Maier M, Landthaler M, Baumler W. 2007. Direct detection of singlet oxygen generated by UVA irradiation in human cells and skin. *J. Invest. Dermatol.* 127 (6) 1498-506.
- Balas F, Manzano M, Horcajada P, Vallet-Regi M. 2006. Confinement and controlled release of bisphosphonates on ordered mesoporous silica-based materials. *J. Am. Chem. Soc.* 128 (25) 8116-7.
- Barbé C, Bartlett J, Kong L, Finnie K, Lin HQ, Larkin M, Calleja S, Bush A, Calleja G. 2004. Silica particles: A Novel Drug-Delivery System. *Adv. Mater.* 16 (21) 1959-66.
- Barciszewski J, Clark BFC. 1999. *RNA Biochemistry and Biotechnology*

- Barr J, Sharma CS, Sarkar S, Wise K, Dong L, Periyakaruppan A, Ramesh GT. 2007. Nicotine induces oxidative stress and activates nuclear transcription factor kappa B in rat mesencephalic cells. *Mol. Cell. Biochem.* 297 (1-2) 93-9.
- Basu SK, Goldstein JL, Anderson RG, Brown MS. 1981. Monensin interrupts the recycling of low density lipoprotein receptors in human fibroblasts. *Cell* 24 (2) 493-502.
- Beckers S, Noor F, Muller-Vieira U, Mayer M, Strigun A, Heinzle E. 2009. High throughput, non-invasive and dynamic toxicity screening on adherent cells using respiratory measurements. *Toxicol. In Vitro.*
- Behrens I, Pena AI, Alonso MJ, Kissel T. 2002. Comparative uptake studies of bioadhesive and non-bioadhesive nanoparticles in human intestinal cell lines and rats: the effect of mucus on particle adsorption and transport. *Pharm. Res.* 19 (8) 1185-93.
- Beisner J, Dong M, Taetz S, Nafee N, Griesse EU, Schaefer U, Lehr CM, Klotz U, Mordt TE. 2009. Nanoparticle mediated delivery of 2'-O-methyl-RNA leads to efficient telomerase inhibition and telomere shortening in human lung cancer cells. *Lung Cancer.*
- Bertram C, Hass R. 2008. Cellular responses to reactive oxygen species-induced DNA damage and aging. *Biol. Chem.* 389 (3) 211-20.
- Bharali DJ, Klejbor I, Stachowiak EK, Dutta P, Roy I, Kaur N, Bergey EJ, Prasad PN, Stachowiak MK. 2005. Organically modified silica nanoparticles: a nonviral vector for in vivo gene delivery and expression in the brain. *Proc. Natl. Acad. Sci. U. S. A.* 102 (32) 11539-44.
- Bogdanska JJ, Todorova B, Labudovic D, Atanasovska E. 2007. Effect of clofibrate on the enzymes associated with oxidative stress in Wistar rat liver. *Bratisl. Lek. Listy* 108 (2) 56-64.
- Bose Girigoswami K, Bhaumik G, Ghosh R. 2005. Induced resistance in cells exposed to repeated low doses of H₂O₂ involves enhanced activity of antioxidant enzymes. *Cell Biol. Int.* 29 (9) 761-7.
- Bottomley A. 2002. The cancer patient and quality of life. *Oncologist* 7 (2) 120-5.
- Boublikova L, Kalinova M, Ryan J, Quinn F, O'Marcaigh A, Smith O, Browne P, Stary J, McCann SR, Trka J, Lawler M. 2006. Wilms' tumor gene 1 (WT1) expression in childhood acute lymphoblastic leukemia: a wide range of WT1 expression levels, its impact on prognosis and minimal residual disease monitoring. *Leukemia* 20 (2) 254-63.
- Brandt R, Keston AS. 1965. Synthesis of diacetyldichlorofluorescein: a stable reagent for fluorometric analysis *Anal. Biochem.* 11 6-9.
- Brannon-Peppas L, Blanchette JO. 2004. Nanoparticle and targeted systems for cancer therapy. *Adv. Drug. Deliv. Rev.* 56 (11) 1649-59.
- Breunig M, Bauer S, Goepferich A. 2008. Polymers and nanoparticles: intelligent tools for intracellular targeting? *Eur. J. Pharm. Biopharm.* 68 (1) 112-28.

- Cedervall T, Lynch I, Foy M, Berggard T, Donnelly SC, Cagney G, Linse S, Dawson KA. 2007. Detailed identification of plasma proteins adsorbed on copolymer nanoparticles. *Angew. Chem. Int. Ed. Engl.* 46 (30) 5754-6.
- Chen M, Mikecz von A. 2005. Formation of nucleoplasmic protein aggregates impairs nuclear function in response to SiO₂ nanoparticles. *Exp. Cell Res.* 305 (1) 51-62.
- Chen WC, Tang F, Horie K, Borchardt RT. 2002. Caco-2 cell monolayers as a model for studies of drug transport across human intestinal epithelium. In: Lehr CM, editor. *Cell Culture Models of biological barriers*: Taylor & Francis. pp. 143-63.
- Chung TH, Wu SH, Yao M, Lu CW, Lin YS, Hung Y, Mou CY, Chen YC, Huang DM. 2007. The effect of surface charge on the uptake and biological function of mesoporous silica nanoparticles in 3T3-L1 cells and human mesenchymal stem cells. *Biomaterials* 28 (19) 2959-66.
- Clark MA, Jepson MA, Hirst BH. 2001. Exploiting M cells for drug and vaccine delivery. *Adv. Drug Deliv. Rev.* 50 (1-2) 81-106.
- Collnot EM, Baldes C, Wempe MF, Hyatt J, Navarro L, Edgar KJ, Schaefer UF, Lehr CM. 2006. Influence of vitamin E TPGS poly(ethylene glycol) chain length on apical efflux transporters in Caco-2 cell monolayers. *J. Control. Release* 111 (1-2) 35-40.
- Conner SD, Schmid SL. 2003. Regulated portals of entry into the cell. *Nature* 422 (6927) 37-44.
- Conti M, Tazzari V, Baccini C, Pertici G, Serino LP, De Giorgi U. 2006. Anticancer drug delivery with nanoparticles. In *Vivo* 20 (6A) 697-701.
- Danson S, Ferry D, Alakhov V, Margison J, Kerr D, Jowle D, Brampton M, Halbert G, Ranson M. 2004. Phase I dose escalation and pharmacokinetic study of pluronic polymer-bound doxorubicin (SP1049C) in patients with advanced cancer. *Br J Cancer* 90 (11) 2085-91.
- Daum N, Neumeyer A, Wahl B, Bur M, Lehr CM. 2009. In vitro systems for studying epithelial transport of macromolecules. In: Belting M, editor. *Methods Mol. Biol.*: Humana Press. pp. 151-64.
- de la Fuente JM, Berry CC. 2005. Tat peptide as an efficient molecule to translocate gold nanoparticles into the cell nucleus. *Bioconjug. Chem.* 16 (5) 1176-80.
- DeMario MD, Ratain MJ, Vogelzang NJ, Mani S, Vokes EE, Fleming GF, Melton K, Johnson S, Benner S, Lebwohl D. 1999. A phase I study of oral uracil/ftorafur (UFT) plus leucovorin and bis-acetato-ammine-dichloro-cyclohexylamine-platinum IV (JM-216) each given over 14 days every 28 days. *Cancer Chemother. Pharmacol.* 43 (5) 385-8.
- des Rieux A, Fievez V, Garinot M, Schneider YJ, Pr  at V. 2006. Nanoparticles as potential oral delivery systems of proteins and vaccines: A mechanistic approach. *J. Control. Release* 116 1.

- des Rieux A, Ragnarsson EG, Gullberg E, Preat V, Schneider YJ, Artursson P. 2005. Transport of nanoparticles across an in vitro model of the human intestinal follicle associated epithelium. *Eur. J. Pharm. Sci.* 25 (4-5) 455-65.
- Desai MP, Labhasetwar V, Amidon GL, Levy RJ. 1996. Gastrointestinal uptake of biodegradable microparticles: effect of particle size. *Pharm. Res.* 13 (12) 1838-45.
- Desai MP, Labhasetwar V, Walter E, Levy RJ, Amidon GL. 1997. The mechanism of uptake of biodegradable microparticles in Caco-2 cells is size dependent. *Pharm. Res.* 14 (11) 1568-73.
- Deschaume O, Shafran KL, Perry CC. 2006. Interactions of bovine serum albumin with aluminum polyoxocations and aluminum hydroxide. *Langmuir* 22 (24) 10078-88.
- Deshpande RR, Wittmann C, Heinzle E. 2004. Microplates with integrated oxygen sensing for medium optimization in animal cell culture. *Cytotechnology* 46 (1) 1-8.
- Diaz-Moscoso A, Vercauteren D, Rejman J, Benito JM, Ortiz Mellet C, De Smedt SC, Fernandez JM. 2010. Insights in cellular uptake mechanisms of pDNA-polycationic amphiphilic cyclodextrin nanoparticles (CDplexes). *J. Control. Release* 143 (3) 318-25.
- Dong X, Mattingly CA, Tseng MT, Cho MJ, Liu Y, Adams VR, Mumper RJ. 2009. Doxorubicin and paclitaxel-loaded lipid-based nanoparticles overcome multidrug resistance by inhibiting P-glycoprotein and depleting ATP. *Cancer Res.* 69 (9) 3918-26.
- Drazkiewicz M, Skozynska-Polit E, Wanke M, Swiezewska E. 2003. The activity of antioxidant enzymes in *Arabidopsis thaliana* exposed to colchicine and H₂O₂. *Cell. Mol. Biol. Lett.* 8 (3) 777-81.
- EFSA. 2009. Scientific opinion: The potential risks arising from nanoscience and nanotechnologies on food and feed safety. *EFSA Journal* 958 1-39.
- Eom HJ, Choi J. 2009. Oxidative stress of silica nanoparticles in human bronchial epithelial cell, Beas-2B. *Toxicol. In Vitro*.
- Farokhzad OC, Langer R. 2006. Nanomedicine: developing smarter therapeutic and diagnostic modalities. *Adv Drug Deliv Rev* 58 (14) 1456-9.
- Feng SS. 2004. Nanoparticles of biodegradable polymers for new-concept chemotherapy. *Expert Rev. Med. Devices* 1 (1) 115-25.
- Fernandez-Checa JC, Garcia-Ruiz C, Colell A, Morales A, Mari M, Miranda M, Ardite E. 1998. Oxidative stress: role of mitochondria and protection by glutathione. *Biofactors* 8 (1-2) 7-11.
- Fischer D, Bieber T, Li Y, Elsasser HP, Kissel T. 1999. A novel non-viral vector for DNA delivery based on low molecular weight, branched polyethylenimine: effect of molecular weight on transfection efficiency and cytotoxicity. *Pharm. Res.* 16 (8) 1273-9.
- Florence AT. 2005. Nanoparticle uptake by the oral route: Fulfilling its potential? *Drug Disc T* 2 (1) 75-81.

- Fotakis G, Timbrell JA. 2006. In vitro cytotoxicity assays: comparison of LDH, neutral red, MTT and protein assay in hepatoma cell lines following exposure to cadmium chloride. *Toxicol. Lett.* 160 (2) 171-7.
- Frey A, Neutra MR. 1997. Targeting of mucosal vaccines to Peyer's patch M cells. *Behring Inst. Mitt.* (98) 376-89.
- Fuller JE, Zugates GT, Ferreira LS, Ow HS, Nguyen NN, Wiesner UB, Langer RS. 2008. Intracellular delivery of core-shell fluorescent silica nanoparticles. *Biomaterials* 29 (10) 1526-32.
- Gabizon AA, Shmeeda H, Zalipsky S. 2006. Pros and cons of the liposome platform in cancer drug targeting. *J. Liposome Res.* 16 (3) 175-83.
- Gabor F, Trimmel K, Ratzinger G, Kerleta V, Fillafer C, Wirth M. 2008. Characterisation of binding and uptake of biomimetic nanoparticles by flow cytometry. *J. Drug Del. Sci. Tech.* 18 (1) 1-8.
- Gemeinhart RA, Luo D, Saltzman WM. 2005. Cellular fate of a modular DNA delivery system mediated by silica nanoparticles. *Biotechnol. Prog.* 21 (2) 532-7.
- Gonsette RE. 2008. Review: Oxidative stress and excitotoxicity: a therapeutic issue in multiple sclerosis? *Mult. Scler.* 14 (1) 22-34.
- Gottesman MM, Ambudkar SV. 2001. Overview: ABC transporters and human disease. *J. Bioenerg. Biomembr.* 33 (6) 453-8.
- Gradishar WJ. 2006. Albumin-bound paclitaxel: a next-generation taxane. *Expert Opin Pharmacother* 7 (8) 1041-53.
- Green M, Howman E. 2005. Semiconductor quantum dots and free radical induced DNA nicking. *Chem. Commun. (Camb.)* (1) 121-3.
- Gref R, Couvreur P, Barratt G, Mysiakine E. 2003. Surface-engineered nanoparticles for multiple ligand coupling. *Biomaterials* 24 (24) 4529-37.
- Gref R, Minamitake Y, Peracchia MT, Trubetskoy V, Torchilin V, Langer R. 1994. Biodegradable long-circulating polymeric nanospheres. *Science* 263 (5153) 1600-3.
- Grzelak A, Rychlik B, Bartosz G. 2000. Reactive oxygen species are formed in cell culture media. *Acta Biochim. Pol.* 47 (4) 1197-8.
- Grzelak A, Rychlik B, Bartosz G. 2001. Light-dependent generation of reactive oxygen species in cell culture media. *Free Radic. Biol. Med.* 30 (12) 1418-25.
- Gu YJ, Cheng J, Lin CC, Lam YW, Cheng SH, Wong WT. 2009. Nuclear penetration of surface functionalized gold nanoparticles. *Toxicol. Appl. Pharmacol.* 237 (2) 196-204.
- Hamman JH, Enslin GM, Kotze AF. 2005. Oral delivery of peptide drugs: barriers and developments. *BioDrugs* 19 (3) 165-77.

- Hidalgo IJ, Kato A, Borchard RT. 1989. Binding of epidermal growth factor by human colon carcinoma cell (Caco-2) monolayers. *Biochem. Biophys. Res. Commun.* 160 (1) 317-34.
- Hidalgo IJ, Raub TJ, Borchardt RT. 1989. Characterization of the human colon carcinoma cell line (Caco-2) as a model system for intestinal epithelial permeability. *Gastroenterology* 96 (3) 736-49.
- Hilgers AR, Conradi RA, Burton PS. 1990. Caco-2 cell monolayers as a model for drug transport across the intestinal mucosa. *Pharm. Res.* 7 (9) 902-10.
- Hillaireau H, Couvreur P. 2009. Nanocarriers' entry into the cell: relevance to drug delivery. *Cell. Mol. Life Sci.* 66 (17) 2873-96.
- Hillery AM, Florence AT. 1996. The effect of absorbed poloxamer 188 and 407 surfactants on the intestinal uptake of 60-nm polystyrene particles after oral administration in the rats. *Int. J. Pharm.* 132 123-30.
- Hirsch LR, Stafford RJ, Bankson JA, Sershen SR, Rivera B, Price RE, Hazle JD, Halas NJ, West JL. 2003. Nanoshell-mediated near-infrared thermal therapy of tumors under magnetic resonance guidance. *Proc. Natl. Acad. Sci. U. S. A.* 100 (23) 13549-54.
- Huang M, Khor E, Lim LY. 2004. Uptake and cytotoxicity of chitosan molecules and nanoparticles: effects of molecular weight and degree of deacetylation. *Pharm. Res.* 21 (2) 344-53.
- Hughes TE, Sasak WV, Ordovas JM, Forte TM, Lamon-Fava S, Schaefer EJ. 1987. A novel cell line (Caco-2) for the study of intestinal lipoprotein synthesis. *J. Biol. Chem.* 262 (8) 3762-7.
- Hunter J, Jepson MA, Tsuruo T, Simmons NL, Hirst BH. 1993. Functional expression of P-glycoprotein in apical membranes of human intestinal Caco-2 cells. Kinetics of vinblastine secretion and interaction with modulators. *J Biol Chem.* 1993 Jul 15;268(20):14991-7 268 (20) 14991-7.
- Huo Q, Liu J, Wang LQ, Jiang Y, Lambert TN, Fang E. 2006. A new class of silica cross-linked micellar core-shell nanoparticles. *J. Am. Chem. Soc.* 128 (19) 6447-53.
- Hussain SM, Hess KL, Gearhart JM, Geiss KT, Schlager JJ. 2005. In vitro toxicity of nanoparticles in BRL 3A rat liver cells. *Toxicol. In Vitro* 19 (7) 975-83.
- Jain TK, Roy I, De TK, Maitra A. 1998. Nanometer Silica Particles Encapsulating Active Compounds: A Novel Ceramic Drug Carrier. *J. Am. Chem. Soc.* 120 11092-5.
- Johnson F, Giulivi C. 2005. Superoxide dismutases and their impact upon human health. *Mol. Aspects Med.* 26 (4-5) 340-52.
- Kawasaki ES, Player A. 2005. Nanotechnology, nanomedicine, and the development of new, effective therapies for cancer. *Nanomed.* 1 (2) 101-9.

- Kensy F, John GT, Hofmann B, Buchs J. 2005. Characterisation of operation conditions and online monitoring of physiological culture parameters in shaken 24-well microtiter plates. *Bioprocess Biosyst. Eng.* 28 (2) 75-81.
- Khalil IA, Kogure K, Akita H, Harashima H. 2006. Uptake pathways and subsequent intracellular trafficking in nonviral gene delivery. *Pharmacol. Rev.* 58 (1) 32-45.
- Kneuer C, Sameti M, Bakowsky U, Schiestel T, Schirra H, Schmidt H, Lehr CM. 2000. A nonviral DNA delivery system based on surface modified silica-nanoparticles can efficiently transfect cells in vitro. *Bioconjug. Chem.* 11 (6) 926-32.
- Kneuer C, Sameti M, Haltner EG, Schiestel T, Schirra H, Schmidt H, Lehr CM. 2000. Silica nanoparticles modified with aminosilanes as carriers for plasmid DNA. *Int. J. Pharm.* 196 (2) 257-61.
- Kocincova AS, Nagl S, Arain S, Krause C, Borisov SM, Arnold M, Wolfbeis OS. 2008. Multiplex bacterial growth monitoring in 24-well microplates using a dual optical sensor for dissolved oxygen and pH. *Biotechnol. Bioeng.* 100 (3) 430-8.
- Kopatz I, Remy JS, Behr JP. 2004. A model for non-viral gene delivery: through syndecan adhesion molecules and powered by actin. *J. Gene Med.* 6 (7) 769-76.
- Korn ED, Weisman RA. 1967. Phagocytosis of latex beads by *Acanthamoeba*. II. Electron microscopic study of the initial events. *J. Cell Biol.* 34 (1) 219-27.
- Kortesuo P, Ahola M, Karlsson S, Kangasniemi I, Yli-Urpo A, Kiesvaara J. 2000. Silica xerogel as an implantable carrier for controlled drug delivery--evaluation of drug distribution and tissue effects after implantation. *Biomaterials* 21 (2) 193-8.
- Kraehenbuhl JP, Neutra MR. 2000. Epithelial M cells: differentiation and function. *Annu. Rev. Cell Dev. Biol.* 16 301-32.
- Laaksonen T, Santos H, Vihola H, Salonen J, Riikonen J, Heikkilä T, Peltonen L, Kumar N, Murzin DY, Lehto VP, Hirvonen J. 2007. Failure of MTT as a toxicity testing agent for mesoporous silicon microparticles. *Chem. Res. Toxicol.* 20 (12) 1913-8.
- Lamaze C, Schmid SL. 1995. Recruitment of epidermal growth factor receptors into coated pits requires their activated tyrosine kinase. *J. Cell Biol.* 129 (1) 47-54.
- Lamprecht A, Schäfer U, Lehr CM. 2001. Size-dependent bioadhesion of micro- and nanoparticulate carriers to the inflamed colonic mucosa. *Pharm. Res.* 18 (6) 788-93.
- Lamprecht A, Ubrich N, Yamamoto H, Schaefer U, Takeuchi H, Maincent P, Kawashima Y, Lehr CM. 2001. Biodegradable Nanoparticles for Targeted Drug Delivery in Treatment of Inflammatory Bowel Disease. *J. Pharmacol. Exp. Ther.* 299 (2) 775-81.
- Lavrovsky Y, Chatterjee B, Clark RA, Roy AK. 2000. Role of redox-regulated transcription factors in inflammation, aging and age-related diseases. *Exp. Gerontol.* 35 (5) 521-32.

- LeFevre ME, Olivo R, Vanderhoff JW, Joel DD. 1978. Accumulation of latex in Peyer's patches and its subsequent appearance in villi and mesenteric lymph nodes. *Proc. Soc. Exp. Biol. Med.* 159 (2) 298-302.
- Lehr CM, Bouwstra JA, Schacht EH, Junginger HE. 1991. In vitro evaluation of mucoadhesive properties of chitosan and some other natural polymers *Int. J. Pharm.* 78 43-8.
- Limbach LK, Li Y, Grass RN, Brunner TJ, Hintermann MA, Muller M, Gunther D, Stark WJ. 2005. Oxide nanoparticle uptake in human lung fibroblasts: effects of particle size, agglomeration, and diffusion at low concentrations. *Environ. Sci. Technol.* 39 (23) 9370-6.
- Limbach LK, Wick P, Manser P, Grass RN, Bruinink A, Stark WJ. 2007. Exposure of engineered nanoparticles to human lung epithelial cells: Influence of chemical composition and catalytic activity on oxidative stress. *Environ. Sci. Technol.* 41 4158-63.
- Lin YH, Mi FL, Chen CT, Chang WC, Peng SF, Liang HF, Sung HW. 2007. Preparation and characterization of nanoparticles shelled with chitosan for oral insulin delivery. *Biomacromolecules* 8 (1) 146-52.
- Liu Y, Miyoshi H, Nakamura M. 2007. Nanomedicine for drug delivery and imaging: a promising avenue for cancer therapy and diagnosis using targeted functional nanoparticles. *Int. J. Cancer* 120 (12) 2527-37.
- Lu J, Liong M, Zink JJ, Tamanoi F. 2007. Mesoporous silica nanoparticles as a delivery system for hydrophobic anticancer drugs. *Small* 3 (8) 1341-6.
- Lucocq JM, Baschong W. 1986. Preparation of protein colloidal gold complexes in the presence of commonly used buffers. *Eur. J. Cell Biol.* 42 (2) 332-7.
- Luhmann T, Rimann M, Bittermann AG, Hall H. 2008. Cellular uptake and intracellular pathways of PLL-g-PEG-DNA nanoparticles. *Bioconjug. Chem.* 19 (9) 1907-16.
- Ma Z, Lim LY. 2003. Uptake of chitosan and associated insulin in Caco-2 cell monolayers: a comparison between chitosan molecules and chitosan nanoparticles. *Pharm. Res.* 20 (11) 1812-9.
- Maier CM, Chan PH. 2002. Role of superoxide dismutases in oxidative damage and neurodegenerative disorders. *Neuroscientist* 8 (4) 323-34.
- Malstrom B, Andreasson L, Reinhammer B. 1975. *The Enzymes*. New York: Academic Press.
- Malvern. Dynamic Light Scattering: An introduction in 30 Minutes. DLS technical note, Malvern Instruments MRK656-01 1-8.
- Malvern. Zeta Potential: An introduction in 30 minutes. Zetasizer Nano series technical note, Malvern Instruments MRK654-01 1-6.
- Manzano M, Colilla M, Vallet-Regi M. 2009. Drug delivery from ordered mesoporous matrices. *Expert Opin. Drug Deliv.* 6 (12) 1383-400.

- Marklund S. 1980. Distribution of CuZn superoxide dismutase and Mn superoxide dismutase in human tissues and extracellular fluids. *Acta Physiol. Scand. Suppl.* 492 19-23.
- Matsui H, Johnson LG, Randell SH, Boucher RC. 1997. Loss of binding and entry of liposome-DNA complexes decreases transfection efficiency in differentiated airway epithelial cells. *J. Biol. Chem.* 272 (2) 1117-26.
- May JA, Ratan H, Glenn JR, Losche W, Spangenberg P, Heptinstall S. 1998. GPIIb-IIIa antagonists cause rapid disaggregation of platelets pre-treated with cytochalasin D. Evidence that the stability of platelet aggregates depends on normal cytoskeletal assembly. *Platelets* 9 (3-4) 227-32.
- Mayor S, Pagano RE. 2007. Pathways of clathrin-independent endocytosis. *Nat. Rev. Mol. Cell Biol.* 8 (8) 603-12.
- Meerum-Terwogt JM, Beijnen JH, ten Bokkel-Huinink WW, Rosing H, Schellens JH. 1998. Co-administration of cyclosporin enables oral therapy with paclitaxel. *Lancet* 352 (9124) 285.
- Mellman I, Fuchs R, Helenius A. 1986. Acidification of the endocytic and exocytic pathways. *Annu. Rev. Biochem.* 55 663-700.
- Mollenhauer HH, Morre DJ, Rowe LD. 1990. Alteration of intracellular traffic by monensin; mechanism, specificity and relationship to toxicity. *Biochim. Biophys. Acta* 1031 (2) 225-46.
- Moulari B, Pertuit D, Pellequer Y, Lamprecht A. 2008. The targeting of surface modified silica nanoparticles to inflamed tissue in experimental colitis. *Biomaterials* 29 (34) 4554-60.
- Mustata G, Dinh SM. 2006. Approaches to oral drug delivery for challenging molecules. *Crit. Rev. Ther. Drug Carrier Syst.* 23 (2) 111-35.
- Nagy K, Pasti G, Bene L, Nagy I. 1995. Involvement of Fenton reaction products in differentiation induction of K562 human leukemia cells. *Leuk. Res.* 19 (3) 203-12.
- Nakase H, Okazaki K, Tabata Y, Uose S, Ohana M, Uchida K, Matsushima Y, Kawanami C, Oshima C, Ikada Y, Chiba T. 2000. Development of an oral drug delivery system targeting immune-regulating cells in experimental inflammatory bowel disease: a new therapeutic strategy. *J. Pharmacol. Exp. Ther.* 292 (1) 15-21.
- Nakase H, Okazaki K, Tabata Y, Uose S, Ohana M, Uchida K, Nishi T, Debreceni A, Itoh T, Kawanami C, Iwano M, Ikada Y, Chiba T. 2001. An oral drug delivery system targeting immune-regulating cells ameliorates mucosal injury in trinitrobenzene sulfonic acid-induced colitis. *J. Pharmacol. Exp. Ther.* 297 (3) 1122-8.
- Napierska D, Thomassen LC, Rabolli V, Lison D, Gonzalez L, Kirsch-Volders M, Martens JA, Hoet PH. 2009. Size-dependent cytotoxicity of monodisperse silica nanoparticles in human endothelial cells. *Small* 5 (7) 846-53.
- Noor F, Niklas J, Muller-Vieira U, Heinzle E. 2009. An integrated approach to improved toxicity prediction for the safety assessment during preclinical drug development using Hep G2 cells. *Toxicol. Appl. Pharmacol.* 237 (2) 221-31.

- Oberdorster G, Oberdorster E, Oberdorster J. 2005. Nanotoxicology: an emerging discipline evolving from studies of ultrafine particles. *Environ. Health Perspect.* 113 (7) 823-39.
- Olayioye MA. 2001. Update on HER-2 as a target for cancer therapy: intracellular signaling pathways of ErbB2/HER-2 and family members. *Breast Cancer Res.* 3 (6) 385-9.
- Owens DE, 3rd, Peppas NA. 2006. Opsonization, biodistribution, and pharmacokinetics of polymeric nanoparticles. *Int. J. Pharm.* 307 (1) 93-102.
- Pan Y, Neuss S, Leifert A, Fischler M, Wen F, Simon U, Schmid G, Brandau W, Jahnen-Dechent W. 2007. Size-dependent cytotoxicity of gold nanoparticles. *Small* 3 (11) 1941-9.
- Pantarotto D, Briand JP, Prato M, Bianco A. 2004. Translocation of bioactive peptides across cell membranes by carbon nanotubes. *Chem. Commun. (Camb.)* (1) 16-7.
- Park EJ, Choi J, Park YK, Park K. 2008. Oxidative stress induced by cerium oxide nanoparticles in cultured BEAS-2B cells. *Toxicology* 245 (1-2) 90-100.
- Park EJ, Park K. 2009. Oxidative stress and pro-inflammatory responses induced by silica nanoparticles in vivo and in vitro. *Toxicol. Lett.* 184 (1) 18-25.
- Parton RG, Joggerst B, Simons K. 1994. Regulated internalization of caveolae. *J. Cell Biol.* 127 (5) 1199-215.
- Patil S, Sandberg A, Heckert E, Self W, Seal S. 2007. Protein adsorption and cellular uptake of cerium oxide nanoparticles as a function of zeta potential. *Biomaterials* 28 (31) 4600-7.
- Peltier S, Oger JM, Lagarce F, Couet W, Benoit JP. 2006. Enhanced oral paclitaxel bioavailability after administration of paclitaxel-loaded lipid nanocapsules. *Pharm. Res.* 23 (6) 1243-50.
- Peng J, He X, Wang K, Tan W, Li H, Xing X, Wang Y. 2006. An antisense oligonucleotide carrier based on amino silica nanoparticles for antisense inhibition of cancer cells. *Nanomed.* 2 (2) 113-20.
- Peracchia MT, Fattal E, Desmaele D, Besnard M, Noel JP, Gomis JM, Appel M, d'Angelo J, Couvreur P. 1999. Stealth PEGylated polycyanoacrylate nanoparticles for intravenous administration and splenic targeting. *J. Control. Release* 60 (1) 121-8.
- Peracchia MT, Harnisch S, Pinto-Alphandary H, Gulik A, Dedieu JC, Desmaele D, d'Angelo J, Muller RH, Couvreur P. 1999. Visualization of in vitro protein-rejecting properties of PEGylated stealth polycyanoacrylate nanoparticles. *Biomaterials* 20 (14) 1269-75.
- Qu B, Li QT, Wong KP, Tan TM, Halliwell B. 2001. Mechanism of clofibrate hepatotoxicity: mitochondrial damage and oxidative stress in hepatocytes. *Free Radic. Biol. Med.* 31 (5) 659-69.
- Rabinovitch M. 1995. Professional and non-professional phagocytes: an introduction. *Trends Cell Biol.* 5 (3) 85-7.

- Radu DR, Lai CY, Jeftinija K, Rowe EW, Jeftinija S, Lin VS. 2004. A polyamidoamine dendrimer-capped mesoporous silica nanosphere-based gene transfection reagent. *J. Am. Chem. Soc.* 126 (41) 13216-7.
- Rice-Evans C, Burdon R. 1993. Free radical-lipid interactions and their pathological consequences. *Prog. Lipid Res.* 32 (1) 71-110.
- Roberts MJ, Bentley MD, Harris JM. 2002. Chemistry for peptide and protein PEGylation. *Adv. Drug Deliv. Rev.* 54 (4) 459-76.
- Roger E, Lagarce F, Garcion E, Benoit JP. 2009. Lipid nanocarriers improve paclitaxel transport throughout human intestinal epithelial cells by using vesicle-mediated transcytosis. *J. Control. Release* 140 (2) 174-81.
- Rosenholm JM, Peuhu E, Bate-Eya LT, Eriksson JE, Sahlgren C, Linden M. Cancer-cell-specific induction of apoptosis using mesoporous silica nanoparticles as drug-delivery vectors. *Small* 6 (11) 1234-41.
- Rosenkranz AR, Schmaldienst S, Stuhlmeier KM, Chen W, Knapp W, Zlabinger GJ. 1992. A microplate assay for the detection of oxidative products using 2',7'-dichlorofluorescein-diacetate. *J. Immunol. Methods* 156 (1) 39-45.
- Rossi LM, Shi L, Quina FH, Rosenzweig Z. 2005. Stober synthesis of monodispersed luminescent silica nanoparticles for bioanalytical assays. *Langmuir* 21 (10) 4277-80.
- Rothberg KG, Ying YS, Kamen BA, Anderson RG. 1990. Cholesterol controls the clustering of the glycopospholipid-anchored membrane receptor for 5-methyltetrahydrofolate. *J. Cell Biol.* 111 (6 Pt 2) 2931-8.
- Roy I, Ohulchanskyy TY, Bharali DJ, Pudavar HE, Mistretta RA, Kaur N, Prasad PN. 2005. Optical tracking of organically modified silica nanoparticles as DNA carriers: a nonviral, nanomedicine approach for gene delivery. *Proc. Natl. Acad. Sci. U. S. A.* 102 (2) 279-84.
- Rugo RE, Schiestl RH. 2004. Increases in oxidative stress in the progeny of X-irradiated cells. *Radiat. Res.* 162 (4) 416-25.
- Sahlin S, Hed J, Rundquist I. 1983. Differentiation between attached and ingested immune complexes by a fluorescence quenching cytofluorometric assay. *J. Immunol. Methods* 60 (1-2) 115-24.
- Sanders E, Ashworth CT. 1961. A study of particulate intestinal absorption and hepatocellular uptake. Use of polystyrene latex particles. *Exp. Cell Res.* 22 137-45.
- Sanganwar GP, Gupta RB. 2008. Dissolution-rate enhancement of fenofibrate by adsorption onto silica using supercritical carbon dioxide. *Int. J. Pharm.* 360 (1-2) 213-8.
- Sayes CM, Gobin AM, Ausman KD, Mendez J, West JL, Colvin VL. 2005. Nano-C60 cytotoxicity is due to lipid peroxidation. *Biomaterials* 26 (36) 7587-95.
- Sayre LM, Perry G, Smith MA. 2008. Oxidative stress and neurotoxicity. *Chem. Res. Toxicol.* 21 (1) 172-88.

SCCP. 2007. Opinion on safety of nanomaterials in cosmetic products 1-63.

Schulze C, Kroll A, Lehr CM, Schaefer UF, Becker K, Schnekenburger J, Schulze-Isfort C, Landsiedel R, Wohlleben W. 2008. Not ready to use-overcoming pitfalls when dispersing nanoparticles in physiological media. *Nanotoxicology* 2 (2) 51-61.

Shive MS, Anderson JM. 1997. Biodegradation and biocompatibility of PLA and PLGA microspheres. *Adv. Drug Deliv. Rev.* 28 (1) 5-24.

Shvedova AA, Castranova V, Kisin ER, Schwegler-Berry D, Murray AR, Gandelsman VZ, Maynard A, Baron P. 2003. Exposure to carbon nanotube material: assessment of nanotube cytotoxicity using human keratinocyte cells. *J. Toxicol. Environ. Health A* 66 (20) 1909-26.

Sies H. 1986. Biochemistry of oxidative Stress. *Angew. Chem. Int. Ed. Engl.* 25 1058-71.

Sies H. 1993. Strategies of antioxidant defense. *Eur. J. Biochem.* 215 (2) 213-9.

Simovic S, Hui H, Song Y, Davey AK, Rades T, Prestidge CA. 2010. An oral delivery system for indomethacin engineered from cationic lipid emulsions and silica nanoparticles. *J Control Release* 143 (3) 367-73.

Slowing I, Trewyn BG, Lin VS. 2006. Effect of surface functionalization of MCM-41-type mesoporous silica nanoparticles on the endocytosis by human cancer cells. *Journal of the American Chemical Society* 128 (46) 14792-3.

Slowing, II, Vivero-Escoto JL, Wu CW, Lin VS. 2008. Mesoporous silica nanoparticles as controlled release drug delivery and gene transfection carriers. *Adv. Drug Deliv. Rev.* 60 (11) 1278-88.

Soltero R, Ekwuribe N. 2005. The oral delivery of protein and peptide drugs. *Innov. Pharm. Tech.* 106-10.

Sparreboom A, van Asperen J, Mayer U, Schinkel AH, Smit JW, Meijer DK, Borst P, Nooijen WJ, Beijnen JH, van Tellingen O. 1997. Limited oral bioavailability and active epithelial excretion of paclitaxel (Taxol) caused by P-glycoprotein in the intestine. *Proc. Natl. Acad. Sci. U. S. A.* 94 (5) 2031-5.

Stöber W, Fink A. 1968. Controlled growth of monodisperse silica spheres in the micron size range. *J. Colloid Interface Sci.* 26 62-9.

Taetz S, Nafee N, Beisner J, Piotrowska K, Baldes C, Murdter TE, Huwer H, Schneider M, Schaefer UF, Klotz U, Lehr CM. 2009. The influence of chitosan content in cationic chitosan/PLGA nanoparticles on the delivery efficiency of antisense 2'-O-methyl-RNA directed against telomerase in lung cancer cells. *Eur. J. Pharm. Biopharm.* 72 (2) 358-69.

Tan A, Simovic S, Davey AK, Rades T, Prestidge CA. 2009. Silica-lipid hybrid (SLH) microcapsules: a novel oral delivery system for poorly soluble drugs. *J. Control. Release* 134 (1) 62-70.

- Tan A, Simovic S, Davey AK, Rades T, Boyd BJ, Prestidge CA. 2010. Silica nanoparticles to control the lipase-mediated digestion of lipid-based oral delivery systems. *Mol. Pharm.* 7 (2) 522-32.
- Tao Z, Morrow MP, Asefa T, Sharma KK, Duncan C, Anan A, Penefsky HS, Goodisman J, Souid AK. 2008. Mesoporous silica nanoparticles inhibit cellular respiration. *Nano Lett.* 8 (5) 1517-26.
- Tao Z, Toms BB, Goodisman J, Asefa T. 2009. Mesoporosity and functional group dependent endocytosis and cytotoxicity of silica nanomaterials. *Chem. Res. Toxicol.* 22 (11) 1869-80.
- Terahara K, Yoshida M, Igarashi O, Nochi T, Pontes GS, Hase K, Ohno H, Kurokawa S, Mejima M, Takayama N, Yuki Y, Lowe AW, Kiyono H. 2008. Comprehensive gene expression profiling of Peyer's patch M cells, villous M-like cells, and intestinal epithelial cells. *J. Immunol.* 180 (12) 7840-6.
- Tkachenko AG, Xie H, Coleman D, Glomm W, Ryan J, Anderson MF, Franzen S, Feldheim DL. 2003. Multifunctional gold nanoparticle-peptide complexes for nuclear targeting. *J. Am. Chem. Soc.* 125 (16) 4700-1.
- Tobio M, Sanchez A, Vila A, Soriano II, Evora C, Vila-Jato JL, Alonso MJ. 2000. The role of PEG on the stability in digestive fluids and in vivo fate of PEG-PLA nanoparticles following oral administration. *Colloids Surf.* 18 (3-4) 315-23.
- Trush MA, Kensler TW. 1991. An overview of the relationship between oxidative stress and chemical carcinogenesis. *Free Radic. Biol. Med.* 10 (3-4) 201-9.
- Ulukaya E, Ozdikicioglu F, Oral AY, Demirci M. 2008. The MTT assay yields a relatively lower result of growth inhibition than the ATP assay depending on the chemotherapeutic drugs tested. *Toxicol. In Vitro* 22 (1) 232-9.
- Valle JW, Armstrong A, Newman C, Alakhov V, Pietrzynski G, Brewer J, Campbell S, Corrie P, Rowinsky EK, Ranson M. 2010. A phase 2 study of SP1049C, doxorubicin in P-glycoprotein-targeting pluronics, in patients with advanced adenocarcinoma of the esophagus and gastroesophageal junction. *Invest. New Drugs.*
- Vallet-Regi M. 2006. Ordered mesoporous materials in the context of drug delivery systems and bone tissue engineering. *Chemistry (Weinheim an der Bergstrasse, Germany)* 12 (23) 5934-43.
- Vallhov H, Gabrielsson S, Stromme M, Scheynius A, Garcia-Bennett AE. 2007. Mesoporous silica particles induce size dependent effects on human dendritic cells. *Nano Lett.* 7 (12) 3576-82.
- Vauthier C, Couvreur P. 2007. Developing nanoparticle drug carriers. *Pharm tech* 35-42.
- Venkatesan N, Yoshimitsu J, Ito Y, Shibata N, Takada K. 2005. Liquid filled nanoparticles as a drug delivery tool for protein therapeutics. *Biomaterials.* (34) 7154-63.

- Wahl B, Daum N, Ohrem HL, Lehr CM. 2008. Novel luminescence assay offers new possibilities for the risk assessment of silica nanoparticles. *Nanotoxicology* 2 (4) 243-51.
- Wang F, Gao F, Lan M, Yuan H, Huang Y, Liu J. 2009. Oxidative stress contributes to silica nanoparticle-induced cytotoxicity in human embryonic kidney cells. *Toxicol. In Vitro* 23 (5) 808-15.
- Wang H, Joseph JA. 1999. Quantifying cellular oxidative stress by dichlorofluorescein assay using microplate reader. *Free Radic. Biol. Med.* 27 (5-6) 612-6.
- Wang J, Wang S, Manzer R, McConville G, Mason RJ. 2006. Ozone induces oxidative stress in rat alveolar type II and type I-like cells. *Free Radic. Biol. Med.* 40 (11) 1914-28.
- Wang LH, Rothberg KG, Anderson RG. 1993. Mis-assembly of clathrin lattices on endosomes reveals a regulatory switch for coated pit formation. *J. Cell Biol.* 123 (5) 1107-17.
- Weyermann J, Lochmann D, Zimmer A. 2005. A practical note on the use of cytotoxicity assays. *Int. J. Pharm.* 288 (2) 369-76.
- Win KY, Feng SS. 2005. Effects of particle size and surface coating on cellular uptake of polymeric nanoparticles for oral delivery of anticancer drugs. *Biomaterials* 26 (15) 2713-22.
- Worle-Knirsch JM, Pulskamp K, Krug HF. 2006. Oops they did it again! Carbon nanotubes hoax scientists in viability assays. *Nano Lett.* 6 (6) 1261-8.
- Wu SH, Lin YS, Hung Y, Chou YH, Hsu YH, Chang C, Mou CY. 2008. Multifunctional mesoporous silica nanoparticles for intracellular labeling and animal magnetic resonance imaging studies. *Chembiochem.* 9 (1) 53-7.
- Xia T, Kovochich M, Liong M, Meng H, Kabehie S, George S, Zink JJ, Nel AE. 2009. Polyethyleneimine coating enhances the cellular uptake of mesoporous silica nanoparticles and allows safe delivery of siRNA and DNA constructs. *ACS Nano* 3 (10) 3273-86.
- Yamashiro DJ, Maxfield FR. 1984. Acidification of endocytic compartments and the intracellular pathways of ligands and receptors. *J. Cell. Biochem.* 26 (4) 231-46.
- Yang H, Liu C, Yang D, Zhang H, Xi Z. 2009. Comparative study of cytotoxicity, oxidative stress and genotoxicity induced by four typical nanomaterials: the role of particle size, shape and composition. *J. Appl. Toxicol.* 29 (1) 69-78.
- Yin H, Too HP, Chow GM. 2005. The effects of particle size and surface coating on the cytotoxicity of nickel ferrite. *Biomaterials* 26 (29) 5818-26.
- Zauner W, Farrow NA, Haines AM. 2001. In vitro uptake of polystyrene microspheres: effect of particle size, cell line and cell density. *J. Control. Release* 71 (1) 39-51.
- Zhang L, Gu FX, Chan JM, Wang AZ, Langer RS, Farokhzad OC. 2008. Nanoparticles in medicine: therapeutic applications and developments. *Clin. Pharmacol. Ther.* 83 (5) 761-9.
- Zhang Y, Chen Y, Westerhoff P, Crittenden J. 2009. Impact of natural organic matter and divalent cations on the stability of aqueous nanoparticles. *Water Res.* 43 (17) 4249-57.

Zhang Y, Zhi Z, Jiang T, Zhang J, Wang Z, Wang S. 2010. Spherical mesoporous silica nanoparticles for loading and release of the poorly water-soluble drug telmisartan. *J. Control. Release.*

Zhao Y, Trewyn BG, Slowing, II, Lin VS. 2009. Mesoporous silica nanoparticle-based double drug delivery system for glucose-responsive controlled release of insulin and cyclic AMP. *J. Am. Chem. Soc.* 131 (24) 8398-400.

9

Publications

Journal articles:

1. A. Neumeyer, C.-M. Lehr & N. Daum. Novel method for the non-invasive determination of reactive oxygen species *in vitro*. Submitted to Toxicology in Vitro
2. A. Neumeyer, M. Bukowski, M. Veith, C.-M. Lehr & N. Daum. PI-labelling of nanoparticles as novel tool for the quantification of cellular binding and uptake. Submitted to Nanomedicine: Nanotechnology, Biology and Medicine

Book chapter:

N. Daum, A. Neumeyer, B. Wahl, M. Bur & C.M. Lehr. *In vitro* systems for studying epithelial transport of macromolecules. M. Belting (Ed.), Methods Mol. Biol., Vol. 480, Humana Press, 2009, pp. 151-164.

Oral presentation:

Quantification of the cellular uptake and localization of silica nanoparticles in Caco-2 cells.
2nd NanoImpactNet Conference, March, 9th-12th 2010, Lausanne, Switzerland

Poster presentations:

1. Novel method for the non-destructive detection of oxidative stress caused by nanoparticles.
Nanotoxicology, September, 7th-10th 2008, Zürich, Switzerland

2. Propidium iodide (PI)-labelled nanoparticles as a novel tool for the quantification of their cellular uptake and localization. 8th International Conference and Workshop on Biological Barrier 2010, March, 21st–April, 1st 2010, Saarbrücken, Germany
3. Quantification of the cellular binding, uptake and localization of propidium iodide labelled nanoparticles. Nanotoxicology, June, 2nd-4th 2010, Edinburgh, Great Britain
4. Quantification of the cellular binding, uptake and localization of propidium iodide-labelled nanoparticles. 37th Annual Meeting & Exposition of the Controlled Release Society (CRS), July, 10th-14th 2010, Portland, USA

10

Abbreviations

5ASA	5-Amino salicylic acid
BCS	Biopharmaceutic classification system
BSA	Bovine serum albumin
CLSM	Confocal laser scanning microscopy
DAPI	4',6'-diamidino-2-phenylindole
DCF	dichlorofluorescein
DCF-DA	2',7'-dichlorofluorescein diacetate
DDC	Sodium diethyldithiocarbamate trihydrate
DIAMO	Amino-ethyl-3-aminopropyl-trimethoxysilan
DLS	Dynamic light scattering
DMEM	Dulbecco's modified eagle medium
DNA	Deoxyribonucleic acid
ELS	Electrophoretic light scattering
EVOM	Epithelial voltohmmeter
FACS	Fluorescence activated cell sorting
FCS	Fetal calf serum
FITC	Fluorescein isothiocyanate
FSC	Forward scatter
GFP	Green fluorescence protein
H ₂ O ₂	Hydrogen peroxide
HBSS	Hank's balanced salt solution
HER-2	Human epidermal growth factor receptor 2
IBD	Inflammatory bowel disease
LDH	Lactate dehydrogenase

MSN	Mesoporous silica nanoparticles
MTT	Thiazolyl blue tetrazolium bromide
PBS	Phosphate buffered saline
PEG	Poly ethylene glycol
PEI	Polyethylenimine
P-gp	P-glycoprotein
PI	Propidium iodide
RITC	Rhodamine B-isothiocyanate
RNA	Ribonucleic acid
RNase	Ribonuclease
ROS	Reactive oxygen species
SD	Standard derivation
SDR	SensorDish [®] Reader
SOD	Superoxide dismutase
SSC	Sideward scatter
TEER	Transepithelial electrical resistance
TEM	Transmission electron microscopy
TEOS	Tetraethylorthosilicate
WGA	wheat germ agglutinin
WT-1	Wilms' tumour gene 1
ζ	Zeta

Acknowledgement

Herrn Prof. Dr. Claus-Michael Lehr möchte ich für die Aufnahme in sein Institut, die Überlassung des interessanten Arbeitsthemas sowie die Unterstützung während meiner Arbeit danken.

Desweiteren danke ich Herrn Prof. Dr. Ingolf Bernhardt für die freundliche Übernahme des Zweitgutachtens.

Meiner Betreuerin Frau Dr. Nicole Daum möchte ich an dieser Stelle für die gute Betreuungsarbeit und die ständige Diskussionsbereitschaft danken. Außerdem danke ich ihr für das Korrekturlesen dieser Arbeit und jeglicher Manuskripte.

Bedanken möchte ich mich auch beim Institut für Neue Materialien und besonders bei Herrn Dr. Mirko Bukowski, der mich während der drei Jahre meiner Promotion mit Nanopartikeln versorgt hat und TEM-Aufnahmen für mich angefertigt hat.

Herzlichen Dank an alle Mitglieder der Arbeitsgruppe Biopharmazie und pharmazeutische Technologie für die gute Arbeitsatmosphäre und die Hilfsbereitschaft untereinander. Ein besonderes Dankeschön gilt an meinen „Mittagstrupp“ und meine Bürokollegen, die mir so manchen Arbeitstag erträglicher gemacht haben.

Meinem Freund Johannes Heck möchte ich für seine Geduld mit mir während der Promotion danken. Er war mir immer eine große Unterstützung und hat mich immer wieder motiviert.

Curriculum vitae

Personal data

Name	Andrea Neumeyer
Address	Rehstr. 15, 66663 Merzig
Date of birth	29 th September 1980
Place of birth	Trier
Nationality	German

phD studies

01/2007-05/2010	phD thesis in the Department of Biopharmaceutics and Pharmaceutical Technology, Saarland University, Saarbrücken, Germany
-----------------	---

Academic studies

11/2006	Diploma in Biology (Dipl. Biol.)
03/2006-11/2006	Diploma project: „Effects of eugenol and isoeugenol on cell cycle regulation in a human cell system”, Department of Ecotoxicology and Toxicology, University of Trier, Germany
12/2005-02/2006	Final Diploma exams
03/2004-12/2005	Main studies of Biology at the University of Technology Kaiserslautern, Germany
09/3003	Intermediate degree in Biology
10/2001-09/2003	Basic studies in Biology at the Heinrich-Heine University of Düsseldorf, Germany

Schooling

06/2000	Abitur at the Auguste-Viktoria-Gymnasium of Trier, Germany
---------	--